ADHESION PROPERTIES AND PHASE TRANSFORMATIONS OF URIC ACID CRYSTALS

A Dissertation
submitted to the Faculty of the
Graduate School of Arts and Sciences
of Georgetown University
in partial fulfillment of the requirements for the
degree of
Doctor of Philosophy
in Chemistry

By

Janeth B. Presores, M.S.

Washington, DC
April 24, 2012

ProQuest LLC.
789 East Eisenhower Parkway
P.O. Box 1346
Ann Arbor, MI 48106 - 1346

ADHESION PROPERTIES AND PHASE TRANSFORMATIONS OF URIC ACID CRYSTALS

Janeth B. Presores, M.S.

Thesis Advisor: Jennifer A. Swift, Ph.D.

ABSTRACT

Uric acid, a product of protein metabolism, is the most abundant organic component in human kidney stones. At least six different crystalline phases of uric acid have been identified in kidney stones. Anhydrous uric acid (UA) and uric acid dihydrate (UAD) are the most common. We characterize these crystals to understand crystal nucleation, growth, aggregation and adhesion phenomena related to stone formation.

Chemical force microscopy was used to investigate the adhesion on the largest plate face of UA single crystals. The adhesion forces between UA (100) and atomic force microscopy tips modified with hydrophobic, hydrophilic, and charged groups were quantified in model aqueous solutions and model urine solutions. The highest adhesion was found between UA (100) and cationic tips in both solutions. This highlights a major difference between molecular crystal surfaces (in this case a weak acid) and most other inorganic biominerals. Solution parameters such as ionic strength and pH were influential in the magnitude of adhesion force obtained.

Solution-mediated phase transformation of UAD to UA may be important in the physiologic deposition of kidney stones, since compositional analysis of numerous kidney stones reveals that UAD is rarely found in the absence of UA. Using a combination of X-ray, thermal and optical techniques, the kinetics of the transformation of pure UAD and doped UAD crystals were studied in model aqueous solutions and model urine solutions. UAD transformed to UA via a 2-

step process; metastable UAD undergoes dissolution followed by nucleation and growth of the stable UA. Pure UAD transformed to UA within 48 hours at 37^{o}C, but UAD doped with molecular dyes and physiologically relevant ions transformed more slowly. The presence of trace amounts of impurities appear to stabilize the UAD more than it affects the growth of UA. This *in vitro* study provides insight into how UAD may be stablilized in physiologic solution and demonstrates that the UAD to UA transformation kinetics occur on a time scale that may be relevant to kidney stone formation.

ACKNOWLEDGMENTS

I would first like to thank my advisor, Prof. Jennifer Swift for giving me a great project to work on. Without her scholarly guidance, her valuable suggestions, encouragement, patience and understanding, this dissertation would not have been possible.

I would also like to thank the past and present members of the Swift group: Rupa Hiremath, Christina Capacci-Daniel, Shoaleh Dehghan, Amanuel Zellelow, Clare Perrin, Ilana Goldberg, and Jessica Urbelis for their friendship, help and support all these years. I am grateful to Ryan Sours for his pioneering work on uric acid crystal growth and to Richard Abendan who taught me the CFM technique.

My gratitude extends to Prof. Bahram Moasser, Prof. J. Faye Rubinson, and Prof. Sarah Stoll for serving on my committee. Their constructive comments and suggestions are invaluable to me.

I had the privilege of working with three undergraduates Katherine Cromer, Alexandra Gorab, and Anne Duckles and with a high school senior Dan Park. I am grateful for their contributions to the uric acid crystal growth projects.

As for the staff in the Department of Chemistry: Kay Bayne, Travis Hall, Dr. Steve Hannum, Dr. Mo Itani, Inez Traylor, and Yen Miller, I thank them for their time and for all their help especially on the paperwork necessary for completing my graduate studies. I also appreciate the staff in the Department of Physics GNuLab: Paul Goldey and Dr. Jasper Nijdam for their help with chemical vapor deposition and SEM experiments.

Thank you also to many of my fellow graduate students who have helped me with various instruments. Many thanks go to the Filipino community for their constant support and friendship. I especially thank Michele Pablico-Lansigan for always being there for me and for being a great roommate for the past six years.

To all my friends in the US, thank you for welcoming me into your homes. Special thanks to the Ramos' family (Sir Ed, Ma'am Dolly, Hazel, Bryan, and Cheryl) in Los Angeles, California for their generosity all these years.

I would also like to express my appreciation to Xavier University-Ateneo de Cagayan, especially the Chemistry Department for their encouragements and support of my professional endeavors.

Most especially, I would like to express my deepest gratitude to my mother, my brother and his family, my sister and her family, and my relatives in the Philippines. I would not be where I am today without their understanding, unwavering love, and support.

This dissertation is dedicated to my entire family and to the loving memory of my father.

TABLE OF CONTENTS

LIST OF FIGURES

FIGURE NO. **PAGE**

LIST OF TABLES

TABLE NO. **PAGE**

LIST OF ABBREVIATIONS

AAS	Atomic absorption spectrophotometry
AES	Atomic emission spectrophotometry
AFM	Atomic force microscopy
BBY	Bismarck brown Y
$CaU_2 \cdot 6H_2O$	Calcium urate hexahydrate
CFM	Chemical force microscopy
CG	Chrysoidin G
COD	Calcium oxalate dihydrate
COM	Calcium oxalate monohydrate
DD	1-Dodecanethiol
DSC	Differential scanning calorimetry
$[Dye]_{soln}$	Concentration of dye in solution
HAP	Hydroxyapatite
HSM	Hot Stage Microscopy
IS	Ionic strength
MA	4-Mercaptoaniline
MBA	4-Mercaptobenzoic acid
MEG	Mercaptoethylguanidine
MP	4-Mercaptophenol
MSU	Monosodium urate monohydrate

MU	11-Mercapto-1-undecanol
MUA	11-Mercaptoundecanoic acid
PXRD	Powder X-ray diffraction
SAMs	Self-assembled monolayers
SEM	Scanning electron microscopy
EDS	Energy dispersive spectroscopy
SPIP	Scanning probe image processor
TGA	Thermogravimetric analysis
UA	Anhydrous uric acid
UAD	Uric acid dihydrate
UAD-salt	Uric acid dihydrate grown in the presence of salts
UAD-urine	Uric acid dihydrate grown from artificial urine solutions
UAD-dye	Uric acid dihydrate grown in the presence of dyes
UAM	Uric acid monohydrate
UV-VIS	UV-Visible

CHAPTER 1 BACKGROUND OF STUDY

Uric acid was discovered in 1776 by Karl Wilhelm Scheele in urinary calculi.[1] The isolated substance was first called lithic acid and was renamed to uric acid by George Pearson in 1795.[2] A century later, the first total synthesis of uric acid was reported by the 1902 Nobel laureate Emil Fisher.[3] Uric acid, 7,9-dihydro-1H-purine-2,6,8(3H)-trione, has a molecular formula of $C_5H_4N_4O_3$ and a molecular structure as shown in Figure 1.1.

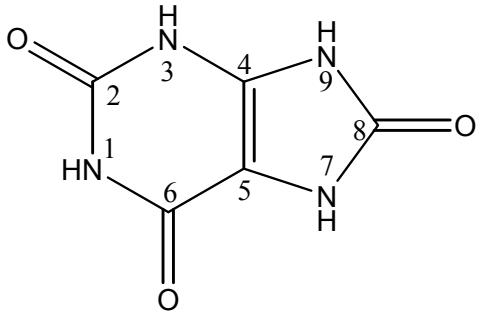

Figure 1.1. Molecular structure of uric acid, $C_5H_4N_4O_3$, numbered according to Fischer.[3]

Uric acid is the final product of purine metabolism in humans, formed from the conversion of xanthine to uric acid by xanthine oxidase.[4] Two-thirds of uric acid elimination is handled by the kidneys, with approximately 300-400 mg/day excreted under normal circumstances.[5] Overproduction of uric acid can be a consequence of high consumption of purine-rich[6-8] foods such as fish, meat, and poultry, or chemotherapy[9] and can lead to crystallization of uric acid in the joints or in the kidneys.

1.1 Pathological Crystallization

Crystal formation within living organisms is a process known as biomineralization. Biomineralized material is typically composed of at least two parts: the precipitating crystalline phase(s) and a supporting structure, called matrix, containing small amounts of proteins and polysaccharides.[10, 11] Biological organisms form hard minerals by design (i.e. cartilage, teeth, shells, and bones) for support, defense, and feeding.[10] Pathological crystallization, on the other hand, happens when unwanted crystallization occurs in living organisms.

Pathological crystallization results in painful or even life threatening conditions such as gallstones, kidney stones, gout, osteoarthritis, atherosclerosis and tissue calcification associated with cancer.[12] It is often difficult to understand the mechanism of their formation due to the complex nature of the biological solution from which they deposit. Factors that lead to crystallization of a phase in a complex biological system include supersaturation, complexation of ions, solution pH, crystal growth inhibitors, and the structure and properties of the supporting matrix.[10] For instance, a high supersaturation of uric acid in the serum and in urine can contribute to the formation of gout and kidney stones, respectively.

1.1.1 Gout

Gout is an inflammatory arthritis caused by the crystallization of monosodium urate monohydrate (MSU) in joints, most commonly the big toes, ankles, knees, wrists, fingers, and elbows.[13, 14] Urate, the ionized form of uric acid, has a limited solubility under physiological conditions, and its saturation level in the plasma at pH 7.4 is 6.8 mg/dl (408 μmol/l).[15, 16] The risk of developing gout is often related to hyperuricemia. Hyperuricemia is usually defined as a serum urate level of >7 mg/dL, the approximate level at which urate is supersaturated in the plasma.[17] Dietary risk factors that contribute to hyperuricemia include high alcohol intake and consumption of purine-rich foods, such as red meat or seafood.[18, 19] Other known risk factors for gout are obesity, fructose consumption,[20] hypertension, and use of diuretic drugs.[21]

A recent study on the prevalence of gout and hyperuricemia in adults in the US showed that the prevalence of gout is 5.9 % (6.1 million) in men and 2.0 % (2.2 million) in women, while hyperuricemia (serum level > 7 mg/dl) is 21.2% and 5.7 % in men and women, respectively.[22] The prevalence of hyperuricemia increases with age, with 31.4 % among individuals ages 65 and older.

Acute gout attacks may be sudden and are manifested by a red, tender, swollen joint that is very painful. Gout if untreated may progress to a chronic disease characterized by joint destruction, bone erosion, secondary osteoarthritis, disability, and deforming deposits of urate crystals (tophi).[23, 24] The long-term treatment of gout is to lower the serum urate levels which are achieved by the use of non-steroidal anti-inflammatory drugs, colchicines, febuxostat,[23, 25] and allopurinol.[25-28]

1.1.2 Kidney Stones

The function of the human kidney is to excrete metabolic waste products, maintain normal composition and volume of body fluids, and to concentrate the urine to preserve water and essential nutrients. Approximately 180 L of blood is filtered daily, only 1 to 1.5 L of which is excreted as urine.[29] Urine is a complex mixture composed of water, a variety of ionic salts, macromolecules, and waste products such as urea, uric acid and ammonium ions that are filtered out of the blood system. When high levels of slightly soluble waste salts are present in urine, these salts can precipitate to form kidney stones. Most precipitates will move through the urinary tract and pass by themselves. Small stones (≤ 5 mm) have a greater chance of passing, but larger stones (≥10 mm) usually must be removed through certain procedures as lithotripsy and percutaneous nephrolithotomy.[29, 30]

Kidney stones are aggregates of micron-sized crystals that are commonly held together by an organic matrix. The matrix in human renal stones accounts for 1-3 % of the total stone weight and consists mainly of a mixture of proteins, carbohydrates, glycosaminoglycans, lipids, and organic ash.[31] Over 200 different crystalline species have been identified in stones.[32] The most common inorganic crystalline components are calcium oxalate monohydrate ($CaC_2O_4 \cdot H_2O$), calcium oxalate dihydrate ($CaC_2O_4 \cdot 2H_2O$), apatite $Ca_5(PO_4)_3(OH)$, brushite ($CaHPO_4 \cdot 2H_2O$), and struvite ($MgNH_4PO_4 \cdot 6H_2O$). Organic components include L-cystine ($-SCH_2CHNH_2COOH)_2$ and uric acid. Anhydrous uric acid ($C_5H_4N_4O_3$) is the most abundant organic crystalline phase, having been identified as the major component in ~13 % of stones.[33] Several other phases of uric acid including the dihydrate ($C_5H_4N_4O_3 \cdot 2H_2O$),[34] monohydrate ($C_5H_4N_4O_3 \cdot H_2O$),[35] and various urate salts (i.e. $NaC_5H_3N_4O_3 \cdot H_2O$, $NH_4C_5H_3N_4O_3$)[33, 36-39] have also been identified in human

kidney stones, though typically as minor components. The frequency of occurrence of major kidney stone components is listed in Table 1.1. The composition of kidney stones varies between countries which are attributed to climatic, dietary, and ethnic differences.

Table 1.1. % Frequency occurrence of major kidney stones components from different countries.[33, 38, 40]

Component	**Berlin, 1982[40]**	**US, 1989[33]**	**Morocco, 2006[38]**
Calcium oxalate monohydrate	24.9	55.4	78.9
Apatite	1.1	26.9	33.9
Calcium oxalate dihydrate	0.6	34.6	24
Anhydrous uric acid	2.4	12.6	19.2
Uric acid dihydrate	-	3.9	-
Ammonium hydrogen urate	-	-	7
Struvite	0.3	12.6	4.8
Cystine	0.2	0.5	1
Brushite	0.4	1.7	< 1

The worldwide incidence and prevalence of kidney stones across race, gender and age is increasing. Urolithiasis studies in the past 20 years were reported in a number of countries such as Italy,[41] Turkey,[42] Japan,[43] Iceland,[44] Spain,[45] Germany,[46] Greece,[47] and in the US.[48] Two studies in the Unites States, one in 1976 to 1980 and the other in 1988 to 1994 showed that overall prevalence of kidney stones increased from 3.2 % (±0.21) to 5.2 % (±0.34).[48] A higher overall rate of kidney stone disease was observed for men (4.9±0.42 % to 6.3±0.56%) than for women (2.8±0.17 % to 4.1±0.27%) between 1976 to 1980 and 1988 to 1994. Recent estimates suggest that 8-12% of men (4-6 % of women) in the US[48] and UK[49] will develop kidney stones at some time in their lives.

Three underlying factors are responsible for uric acid nephrolithiasis: low urine pH, hyperuricosuria, and low urine volume.[50, 51] Urinary pH is a principal determinant of uric acid solubility in urine.[4, 52] Uric acid precipitation and stone formation has been correlated with very acidic urine.[4, 53] The urine pH of uric acid stone formers demonstrates variability, but their urine remains acidic throughout the day and is generally lower than non-stone formers.[54] A low urine pH is often encountered in patients with type 2 diabetes which predisposes them to uric acid stone formation.[55] High consumption of purine-rich foods, impaired renal function and advanced age are additional factors associated with low urine pH.[8, 56, 57]

Hyperuricosuria (elevated urine uric acid) is defined as urinary uric acid excretion of more than 700 mg in 24 hours.[58] It is associated with diet, malignancy and chemotherapy, and uricosuric drugs and is a contributor to uric acid stone formation.[4, 50, 59] Dehydration and low urine volume are also risk factors to uric acid stone formation since they increases uric acid supersaturation. A higher risk of uric acid stones has been reported in workers chronically exposed to high temperature surroundings.[60] General measures to prevent uric acid stone formation is to maintain a daily urine output of greater than 2 L and to reduce intake of purine-rich food.[51, 61, 62] In addition, alkalinization of urine with potassium citrate is effective in preventing the recurrence of kidney stones.[51, 61] The goal is to increase the pH, but no higher than ~6.5 as this increases the risk of calcium phosphate stone formation.[5]

Urinary calculi formation is a complex process. Apart from nucleation and crystal growth, the concept of aggregation in which crystal nuclei bind to each other to form larger particles is important in the stone formation process. Various components of kidney stones can act as effective substrates for the heterogeneous nucleation of other components. Guan *et al.*

demonstrated that brushite crystals serve as a substrate for calcium oxalate monohydrate by heterogeneously nucleating or aggregating calcium oxalate on or near the surface of brushite.[63] In another study, Grases *et al.* reported that uric acid was a heterogeneous nucleant of calcium oxalate.[64] Crystal nucleation, growth, and aggregation will not always result in stone formation if the nucleated crystals are passed along with the urine flow.[65] Therefore, crystal retention is a key factor in urinary stone formation. The kidneys of stone formers must have crystal binding sites that allow crystals to settle, grow, and aggregate into a stone.[29] Crystal retention can be caused by adhesion of crystals with the epithelial cells in the renal tubules. Koka *et al.* studied the adhesion of uric acid crystals to the surface of renal epithelial cells.[66] The authors concluded that hydrogen bonding and hydrophobic interactions play a major role in the uric acid crystal-cell interactions under conditions where uric acid is electrically neutral.

1.2 Uric Acid Solution and Crystal Properties

1.2.1 Dissociation

Uric acid is a weak diprotic acid capable of losing two protons at the N3 and N9 positions in its ring system.[67] Spectrophotometric titrations of N-methyl derivatives of uric acid indicated that the proton at N3 is more acidic than the proton at N9 (Figure 1.2). Crystal structures of uric acid salts of sodium,[68] magnesium,[69] lead,[70] and calcium (described in Chapter 6) further prove that the dissociation to the singly ionized form of uric acid is a result of deprotonation at N3. The second dissociable proton at N9 occurs at pH values not physiologically relevant.

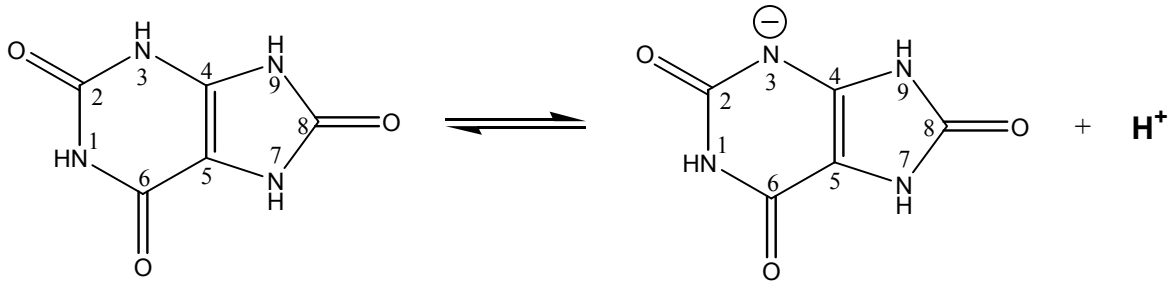

Figure 1.2. Dissociation of uric acid to a singly ionized form. Loss of a proton occurs at the N3 position.

In aqueous solutions at physiologically relevant pH, the dissociation of uric acid is given by Equations 1.1 and 1.2 where uric acid is denoted as $[H_2U]$, urate as $[HU^-]$, and K_a is the dissociation constant.

(1.1) $$H_2U_{(aq)} \rightleftharpoons HU^-_{(aq)} + H^+_{(aq)}$$

(1.2) $$K_a = \frac{[HU^-_{(aq)}]\,[H^+_{(aq)}]}{[H_2U_{(aq)}]}$$

The first pK_a of uric acid is 5.5.[67] Above this value, urate is the predominant species in the solution (Figure 1.3). The changing relative abundance of different species (i.e. protonated uric acid or urate) with pH is an important factor in the kidneys. The kidneys concentrate the urine to preserve water and essential nutrients, and the pH of the fluid that passes through the renal systems gradually decreases. The pH of typical urine ranges from 4.78-7.41[71] with the protonated uric acid being the predominant form at the lower pH end. High uric acid concentration, low urine volume, and acidic urinary environments promote uric acid precipitation and potential stone formation.

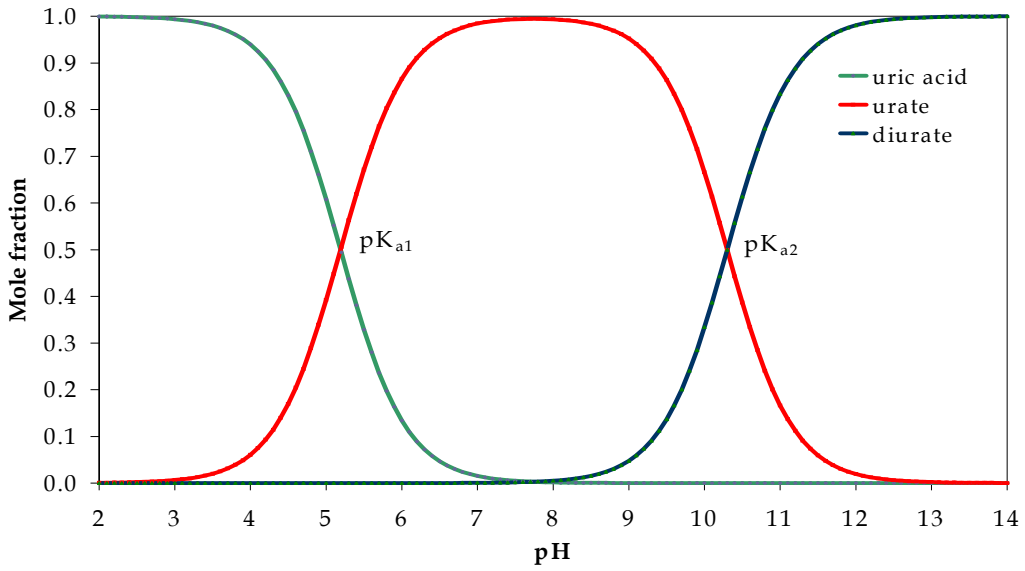

Figure 1.3. Fractional composition diagram of uric acid-urate-diurate system as a function of solution pH.

1.2.2 Solubility

The solubility of uric acid has been the subject of extensive study in order to elucidate the process of uric acid stone formation as well as to understand oral therapy to dissolve the crystals. Uric acid is only slightly soluble in aqueous solutions. Its solubility equilibrium and solubility product constant are given by Equation 1.3 and Equation 1.4 respectively.

(1.3) $$H_2U_{(s)} \rightleftharpoons H_2U_{(aq)}$$

(1.4) $$K_s = [H_2U_{(aq)}]$$

The solubility product constant (pK_s) for uric acid has been determined at several temperatures.[72] A plot of the evaluated pK_s values against temperature generates straight lines

for both anhydrous uric acid (UA) and uric acid dihydrate (UAD) with intercepts of 4.28 for UA and 4.24 for UAD. As K_s is directly proportional to the concentration of uric acid, the solubility of UA and UAD at a specific temperature (^{o} C) can be calculated using Equation 1.5 and Equation 1.6 for UA and UAD, respectively.[72, 73]

(1.5) $$[UA_{(aq)}] = 10^{(0.021\,T - 4.28)}$$

(1.6) $$[UAD_{(aq)}] = 10^{(0.028\,T - 4.24)}$$

The solubility of UA and UAD at different temperatures are shown in Figure 1.4. At all temperatures, UAD is more soluble than UA. At 37° C, for example, the solubility of UAD (0.63 mM) is about twice that of UA (0.31 mM).

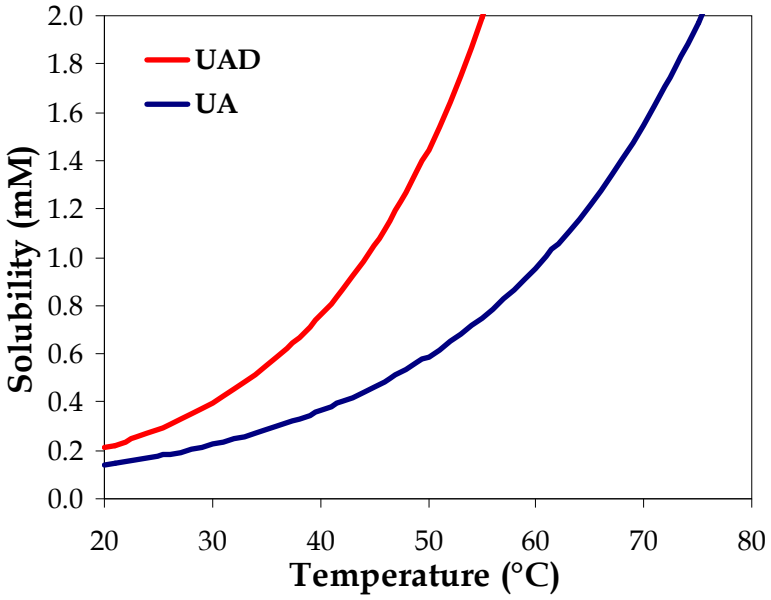

Figure 1.4. Solubility of UA and UAD as a function of temperature.[72]

The aqueous solubilities of UA and UAD are independent of pH at pH ≤ 3. At an ionic strength range of 0.15 - 0.30 M, the solubility of uric acid is constant regardless of the nature and concentration of the inorganic components of urine, and/or the presence of organic substances like creatine and urea.[74] The same solubility was also cited in standard reference artificial urine.[74] At higher solution pH, uric acid dissociates to an ionized urate form. To account for the contribution of the urate formed in solution, the total concentration is calculated using the following modified equation:

$$[U]_{tot} = K_s \left(1 + \frac{K'_1}{H^+}\right) \tag{1.7}$$

where $[U]_{tot}$ is the sum of the concentration of uric acid and urate in solution. The contribution of diurate is negligible. The plot of concentration of UA or UAD, urate, and their combined total as a function of pH at 37^o C is shown in Figure 1.5.

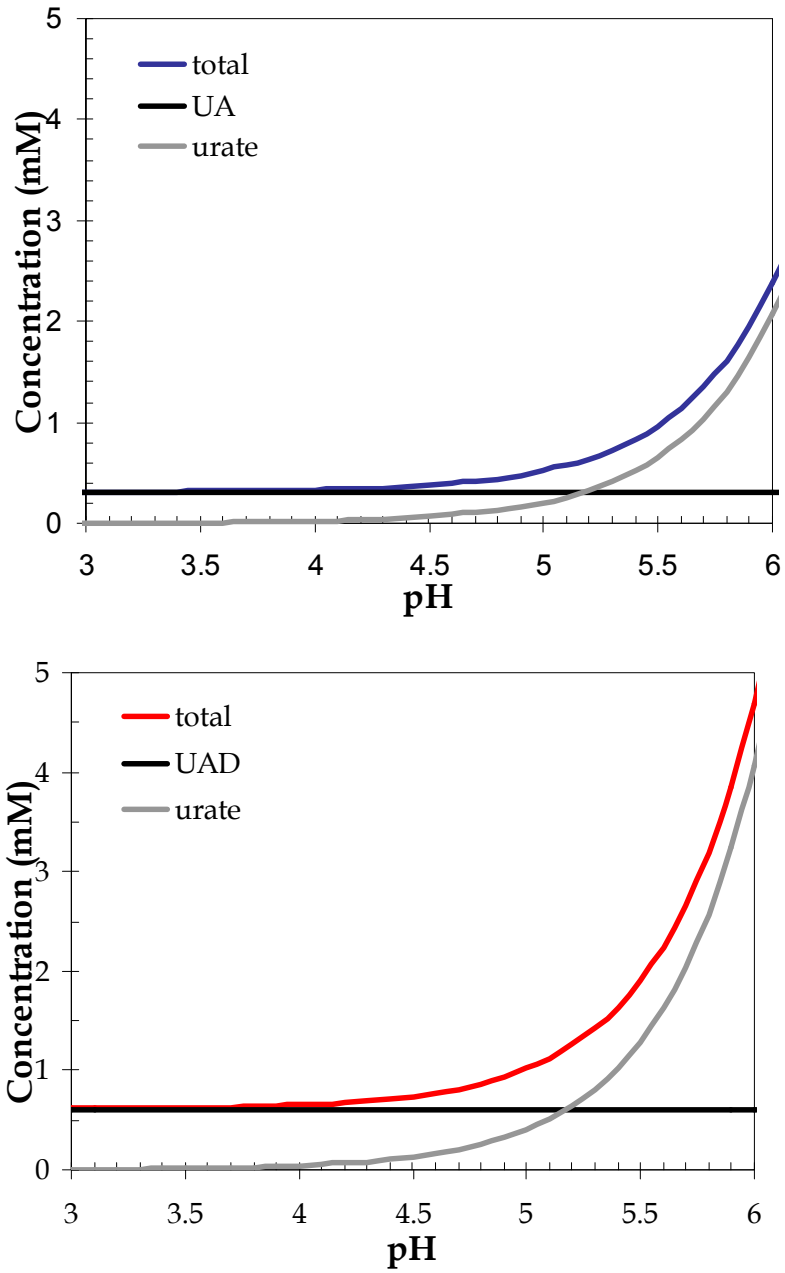

Figure 1.5. (Top) The concentration of UA, urate, and their combined total as a function of pH at 37° C. (Bottom) The concentration of UAD, urate, and their combined total as a function of pH at 37° C. Data based on Königsberger and Königsberger.[72]

1.2.3 Growth of UA and UAD Crystals

In this thesis, UA and UAD crystals were grown under a variety of conditions. Our standard practice involved dissolving 180-200 mg of uric acid (1-1.2 mM) in 1 L boiling distilled water. The pH of the solution was buffered to 4.0 with sodium acetate and acetic acid and kept at either 25° C or 37° C for 2 days. UAD crystals formed at 25° C while UA formed at 37° C. Crystals were vacuum-filtered through Whatman #1 filter paper and air-dried. UA and UAD crystals were colorless rectangular plates between 100 and 300 μm in size in the largest dimension. Water used was purified by passage through two Barnstead deionizing cartridges followed by distillation. All chemical reagents were used as received and without further purification. Modified growth conditions are described in Chapter 3 and Chapter 5.

1.2.4 Crystal Structure

UA crystallizes in a monoclinic crystal system with a $P2_1/a$ space group and four molecules per unit cell. The unit cell dimensions are a = 14.464(3), b = 7.403(2), c = 6.208(1) Å, and β = 65.10(5)°.[75] The layers in the UA motif are spaced 6.56 Å apart (Figure 1.6). Each layer consists of parallel ribbons of uric acid molecules hydrogen-bonded head-to-head (O_2···H-N_1: 1.826 Å, 175.0°) and tail-to-tail (O_8···H-N_7: 1.734 Å, 155.8°), with the ribbon plane perpendicular to the (100) surface and no hydrogen bonding between ribbons within a layer.

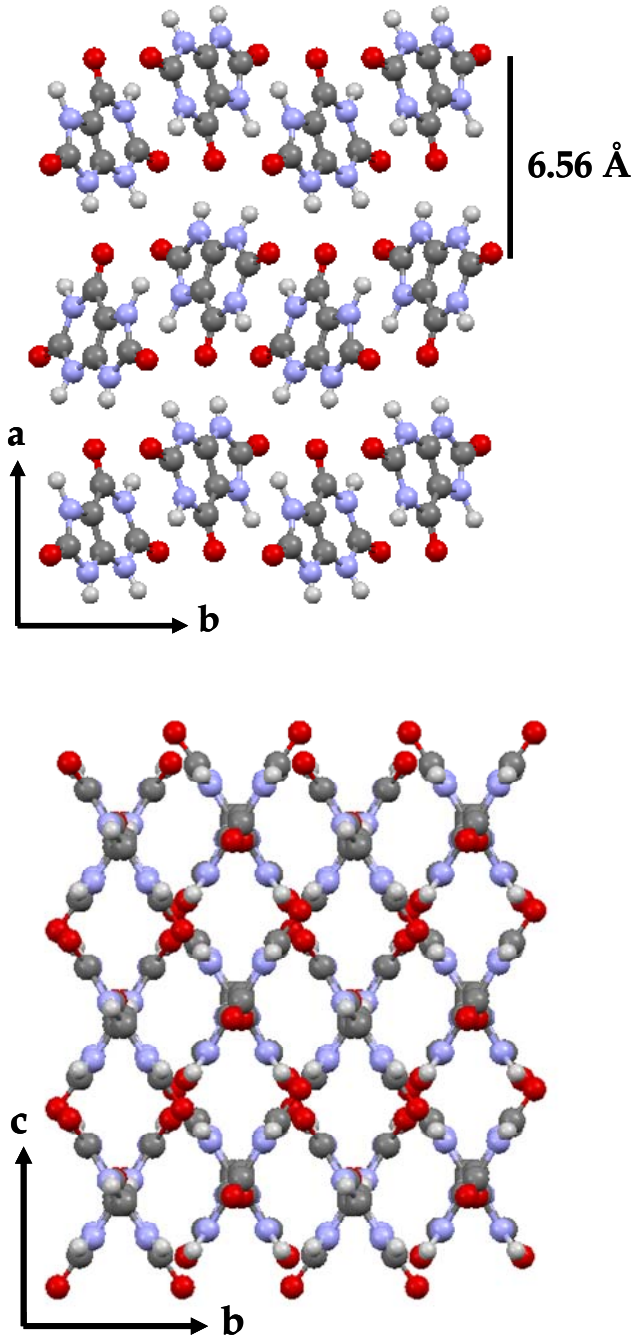

Figure 1.6. (Top) Crystal packing diagram of anhydrous uric acid (UA) viewed along *c*, and (Bottom) viewed along *a*, constructed from fractional coordinates in refcode: URICAC.[75]

Several structural determinations of UAD have been reported in the past. The first complete crystal structure of UAD obtained from human urinary sediments was orthorhombic *Pnab* (*a* = 7.409 (1), *b* = 17.549 (3), *c* = 6.332 (1) Å) as reported by Artioli *et al.* in 1997.[76] However, this structure had reflections that should have been systematically absent based on an orthorhombic cell. This means crystallographically, it is not entirely correct. A crystal structure of a synthetic UAD crystal was later described by Parkin and Hope as having a disordered monoclinic unit cell, with a $P2_1/c$ space group and cell parameters *a* = 7.237 (3) Å, b = 6.363 (4) Å, *c* = 17.449 (11) Å, and β=90.51 (1)°.[77] Despite the different cell conventions, the orthorhombic and monoclinic UAD structures are nearly identical when examined side by side.

The obvious difference in the structure between UA and UAD is that in UAD, ribbons form planes separated by water. The addition of water molecules increases the spacing between layers to 8.73 Å. Water molecules are hydrogen-bonded to uric acid molecules at both N2 and N4, and to all three oxygen atoms of the uric acid molecules. O1 and O3 form a single hydrogen bond (to either water depending on the disorder component), whereas O2 coordinates to both. We refer to Parkin and Hope's cell parameters in all subsequent discussion (Figure 1.7).

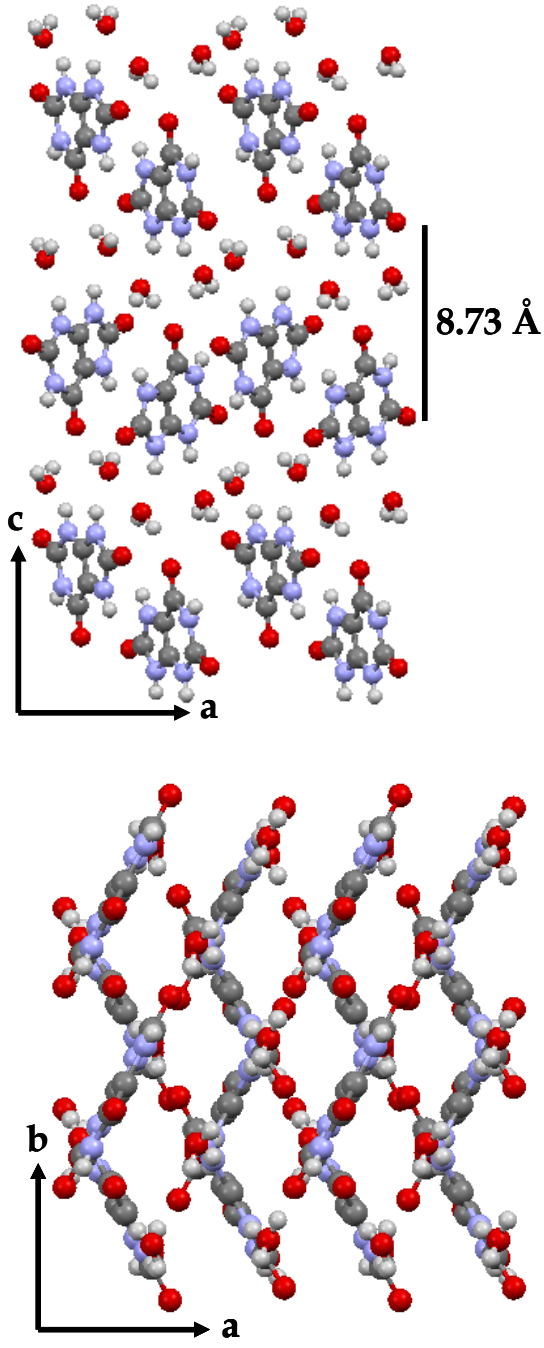

Figure 1.7. (Top) Packing diagram of UAD viewed along *b*, and (Bottom) viewed along *c*, constructed from fractional coordinates in refcode: ZZZPPI02.[77]

1.2.5 Crystal Morphology

Synthetic crystals of UA grown from buffered or unbuffered distilled water deposit as clear, colorless rectangular plates with large (100) faces bounded by (210), (201), (001), and sometimes (121) faces (Figure 1.8).[78] Crystals are typically ~200-300 μm in the largest dimension. UAD crystals are also colorless rectangular plates but the largest face is (001) bounded by (102) and (011) side faces.[78]

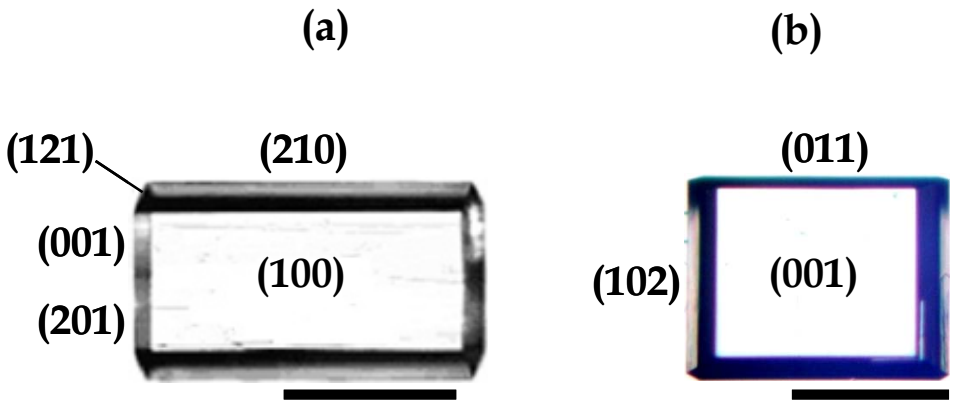

Figure 1.8. Photomicrographs of (a) UA and (b) UAD with various faces labeled. Scale bars = 100 μm.

Naturally-derived uric acid crystals are colored (i.e. yellow orange to brown) and can have more variable morphologies (i.e. tabular, prismatic, equant, columnar, and sphenoidal). The dark colored cores of the crystals are due to the small amount of organic matrix in the crystals.[79] Adsorbed uricine (a bilirubin breakdown pigment) also give uric acid stones their characteristic reddish-orange color.[80, 81] Figure 1.9 shows examples of pathologically deposited uric acid crystals.

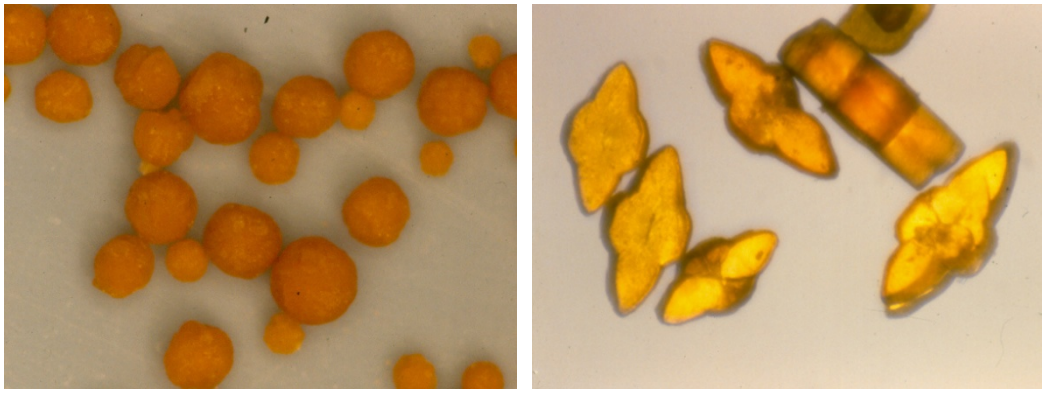

Figure 1.9. Micrographs of pathologically deposited uric acid crystals. Courtesy of Louis C. Herring Lab (Orlando, Florida).[32]

1.2.6 Optical Properties

While the morphologies of UA and UAD have similar characteristics, they can be unambiguously distinguished through their conoscopic light interference patterns. An Olympus BX-50 polarizing microscope with a 505 nm narrow bandpass filter was used to collect conoscopic images of UA and UAD single crystals.

Both UA and UAD are monoclinic and are optically biaxial which means that they each have two principal refractive indices.[82, 83] In UA crystals, the indices of refractions are n_α = 1.588 (3) parallel to *b*, while n_β = 1.739 (3) and n_γ = 1.898 (3) are offset by 45.6° from *a** and *c*.[82, 83] In UAD crystals, the indices of refractions are n_α = 1.508 (3) parallel to *a*, n_β = 1.691 (3) parallel to *c*, and n_γ = 1.728 (3) parallel to *b*.[73, 82, 83] Hence, the optic plane in UA is tilted 45.6° through the large (100) plate face, while UAD exhibit a characteristic pattern with the optic plane perpendicular to the large (001) plate face. The conoscopic interference patterns of UA and UAD are shown in Figure 1.10. Due to the high optic angles in both UA and UAD, the melatopes for

these crystals are not observable. However, the obvious differences in their patterns allow us to easily distinguish UA from UAD.

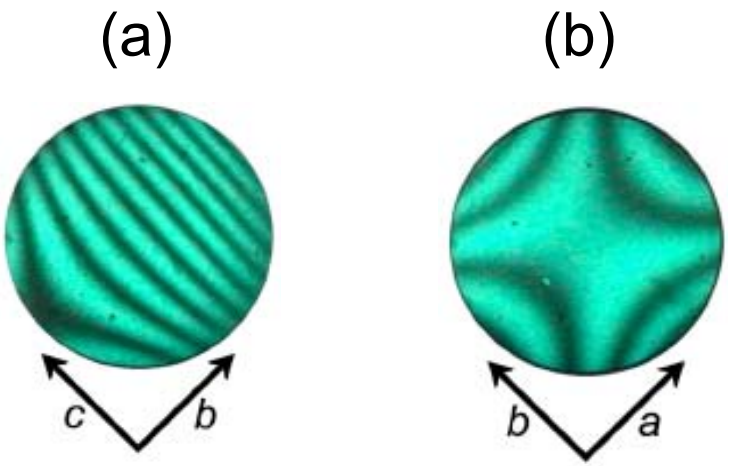

Figure 1.10. Conoscopic interference pattern of (a) UA and (b) UAD. Relevant crystallographic directions are indicated.

Other techniques that we use to differentiate UA and UAD crystals are infrared spectroscopy, single crystal X-ray diffraction, and powder X-ray diffraction. Infrared spectroscopy distinguishes UAD from UA by the strong water absorption band at ~3440 cm^{-1}.[73] Powder X-ray diffraction which we frequently use differentiates UA and UAD through their distinct diffraction patterns (Figure 1.11). The characteristic diffraction lines for UAD are (002), (011), (102), (004), (112), (210), and (21-1) while that of UA are (200), (001), (210), (11-1), (121), and (021).

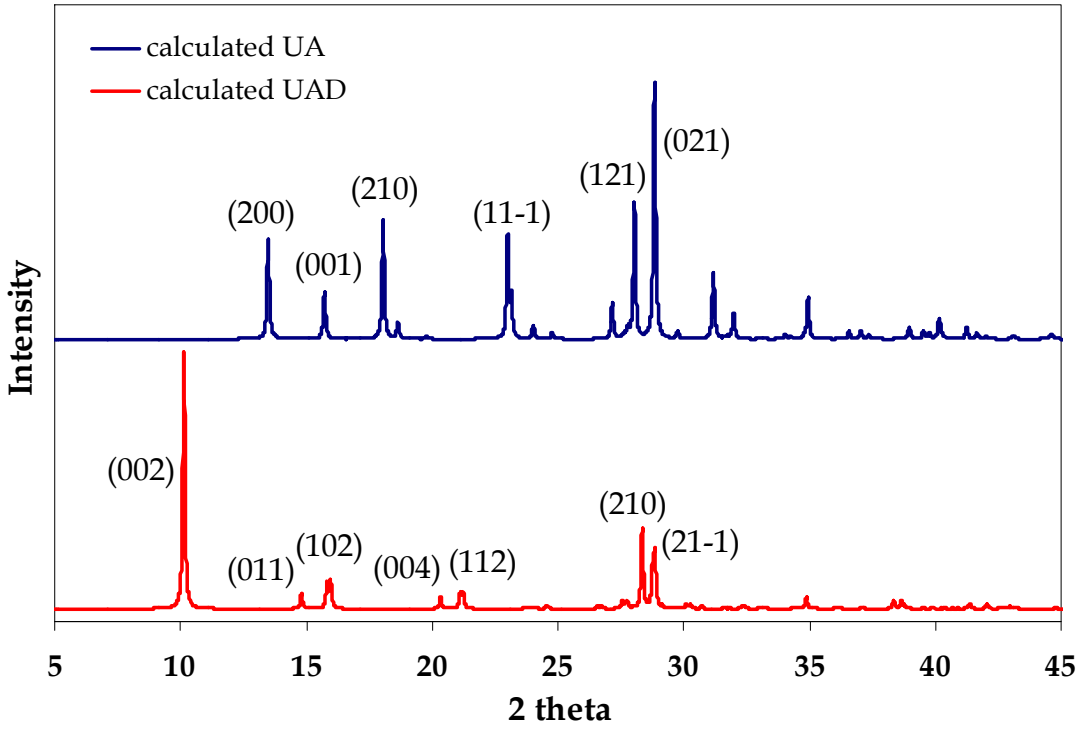

Figure 1.11. PXRD calculated patterns for UA (blue) and UAD (red) crystals from refcode URICAC and ZZZPPI02, respectively. Their characteristic diffraction lines are indicated.

1.3 Phase Transformation and Epitaxial Nucleation

Any solid may exist in different forms (i.e. hydrates, solvates, and polymorphs). Sometimes several phases can coexist under the same conditions. The relative thermodynamic stability of the various solid phases is determined by the Gibbs free energy and is given by:

(1.8) $$G = H - TS$$

where H is the enthalpy, T is absolute temperature and S is the entropy. The phase with the lowest free energy at a given temperature is the stable phase. According to Oswald's Rule of Stages,[84] a less stable phase lying nearest in free energy to the original state initially forms. This is not necessarily the most stable phase with the lowest free energy. Figure 1.12 illustrates an energy diagram for the nucleation of a two-phase system.

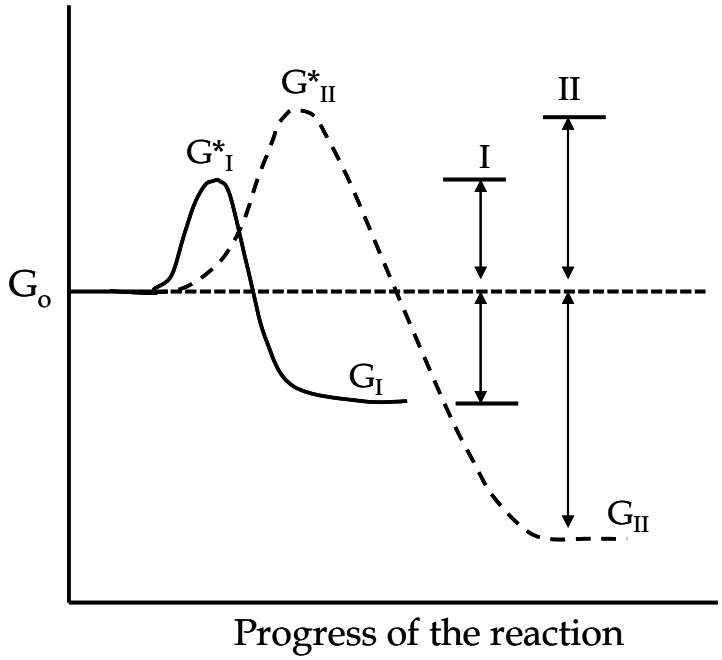

Figure 1.12. Schematic diagram for the nucleation of a two-phase system showing the energy barriers for the formation of phase I and II. Adapted from Rodriguez-Spong *et al*.[85]

As illustrated in Figure 1.12, the transition from the initial state G_o to phase I or II depends on the energy barrier for the formation of the two phases. Phase I is the metastable phase and II is the stable phase. The energy barrier for the nucleation of I ($G^*_I - G_o$) is lower than that for II (G^*_{II}

– G_o).[85, 86] Since the nucleation rate is related to the energy barrier, the metastable phase will nucleate at a faster rate than the stable phase, as it has a lower energy barrier to overcome.[86] The metastable phase can subsequently transform into the stable phase over time.

Phase transformation of a metastable phase to a stable phase can occur both in the solid state and in solution. In the former, the metastable phase undergoes molecular rearrangement to allow formation of the stable phase.[87] In the latter, the transformation occurs by the dissolution of the metastable phase and crystallization of the stable phase from solution.[88] This transformation is driven by the solubility difference between the metastable form and stable form, and the rate limiting step in the overall kinetics can depend on either dissolution of the metastable form or growth of the stable form. Factors such as crystal size,[89] temperature,[90] impurities,[91] and stirring[89] affect the transformation process. The kinetics of transformation are determined by measuring the solution concentration or fractional concentration of the crystals in contact with the solution. An important feature of this transformation process is that the surface of a phase existing in solution can facilitate the nucleation of a second phase.

Epitaxial nucleation is a specific case of heterogeneous nucleation described by an oriented growth of a second phase on a crystalline substrate.[92] Close values of crystal lattice parameters between two phases are a prerequisite for epitaxial nucleation. The energy for nucleation is lowered and the nucleation is considered two-dimensional rather than three-dimensional.[85, 92] Boistelle and Rinaudo demonstrated an epitaxial nucleation between UA and UAD phases.[78] By manipulating supersaturation, each phase could be made to act as a nucleation substrate for the other. Epitaxial nucleation of UAD occurs on the UA (100) face, while the growth of UA on UAD occurs on some unspecified lateral faces of UAD. An illustration of epitaxial growth of UA

on UAD in our present study is depicted in Figure 1.13. During the transformation process, UAD crystals become opaque and UA crystals were observed to grow epitaxially on the UAD crystal surfaces.

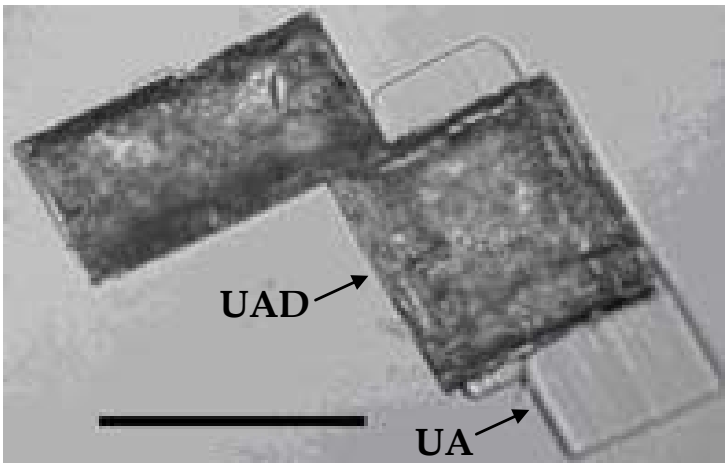

Figure 1.13. Photomicrograph showing epitaxial growth of UA (colorless and smooth) on UAD (opaque). Scale bar is 100 μm.

The epitaxial relationship between UA and UAD has been observed in kidney stones.[93, 94] Frincu *et al.* calculated the epitaxial relationships between UA and UAD as well as between the two forms of uric acid and various other minerals found in kidney stones.[95] Epitaxial matches between various faces of UA and UAD indicated a near perfect commensurate relationship between UAD (001) and UA (100). Forty one matches between UAD and various mineral surfaces showed the best matches with brushite and struvite. Of the 52 identified matches between UA surfaces and assorted minerals, the best matches were shown for calcium oxalate dihydrate, brushite, struvite, and newberyite. In a complex physiologic environment, it is not obvious how matrix might mediate these epitaxial relationships.

1.4 Overview of the Study

As mentioned earlier, uric acid can adopt different crystal forms. Central to this thesis is the study of two forms: anhydrous uric acid (UA) and uric acid dihydrate (UAD). Both forms have been identified in kidney stones, with UA in higher abundance than UAD. We characterize these crystals in order to understand crystal nucleation, growth, aggregation and adhesion related to stone formation. The adhesion properties of UA surfaces are clearly important in both the attachment of crystals to renal epithelial cells and their aggregation to other crystals and/or matrix en route to stone formation. The adhesion properties of UA crystal surfaces were measured using chemical force microscopy and are detailed in Chapter 2.

In Chapter 3, the crystal growth of UAD from different solutions and its characterization is presented. Compositional analysis of numerous kidney stones showed that when UAD is present, it is generally associated with UA.[34] This suggests that phase transformation may occur in these natural materials though the rate at which this process occurs was unknown. Previous work by Zellelow *et al.*[87] reported the phase transformation of UAD in air, and Chapter 4 and 5 investigates this transformation in solution. Solution-mediated transformation of UAD to UA may be important in the physiologic deposition of kidney stones, since UAD is metastable and rarely found in the absence of UA. The transformation process of UAD in both model aqueous solutions with known ionic strengths and pH, as well as model urine solutions is discussed in Chapter 4. Synthetic UAD crystals are known to be less stable than natural crystals.[96, 97] The stability of natural crystals is presumably due to the incorporation of impurities during its crystallization.[97] Chapter 5 describes the effect of impurities on the kinetics of the UAD to UA transformation.

Finally, various urate salts have been identified as minor components in kidney stones.[33, 36-39] Understanding the interaction of metal ions with urates can help elucidate the role of metals in the pathological deposition of kidney stones. Chapter 6 describes the crystal growth, characterization, and the first single crystal structure of a calcium urate salt.

1.5 References

1. Scheele, K., "Investigations of bladder stones (Swed)." *Kongl. Vetenskaps. Acad. Handl.* **1776,** 37, 327-332.

2. Pearson, G., "Experiments and observations, tending to show the composition and properties of urinary concretions." *Phil. Trans. Roy. Soc. London* **1798,** 88, 15-46.

3. Fisher, E., "Ueber die Constitution des Caffeins, Xanthins, Hypoxanthins und Verwandeter Basen." *Ber. Dtsch. Chem. Ges.* **1897,** 30, 549-559.

4. Asplin, J. R., "Uric Acid Stones." *Seminars in Nephrology* **1996,** 16, (5), 412-424.

5. Knudsen, B. E.; Beiko, D. T.; Denstedt, J. D., Uric Acid Urolithiasis. In *Urinary Stone Disease: A Practical Guide to Medical and Surgical Management*, Stoller, M. L.; Meng, M. V., Eds. Humana Press: New Jersey, 2007; pp 299-308.

6. Fellström, B.; Danielson, B. G.; Karlström, B.; Lithell, H.; Ljunghall, S.; Vessby, B., "The influence of a high dietary intake of purine-rich animal protein on urinary urate excretion and supersaturation in renal stone disease." *Clin. Sci.* **1983,** 64, 339-405.

7. Robertson, W. G.; Peacock, M.; Hodgkinson, A., "Dietary changes and the incidence of urinary calculi in the U.K. between 1958 and 1976." *J. Chron. Dis.* **1979,** 32, 469-476.

8. Sabry, Z. I.; Shadarevian, S. B.; Cowan, J. W.; Campbell, J. A., "Relationship of dietary intake of sulphur amino-acids to urinary excretion of inorganic sulphate in man." *Nature* **1965,** 206, 931-933.

9. McCREA, L. E., "Formation of uric acid calculi during chemotherapy for leukemia." *J. Urol.* **1955,** 73, (1), 29-34.

10. Sangwal, K., Mineralization in Natural and Artificial Systems. In *Additives and Crystallization Processes: From Fundamental to Applications*, John Wiley & Sons, Ltd: England, 2007; pp 205-264.

11. Estroff, L., "Introduction: Biomineralization." *Chem. Rev.* **2008,** 108, 4329-4331.

12. Königsberger, E.; Königsberger, L.-C., Solubility Phenomena Related to Normal and Pathological Biomineralization Processes. In *Biomineralization: Medical Aspects and Solubility*, Königsberger, E.; Königsberger, L.-C., Eds. John Wiley & Sons, Ltd: 2006; pp 1-37.

13. Martinon, F.; Glimcher, L. H., "Gout: new insights into an old disease." *J. Clin. Invest.* **2006,** 8, (116), 2073-2075.

14. Underwood, M., "Diagnosis and management of gout." *BMJ* **2006,** 332, 1315-1319.

15. Masseoud, D.; Rott, K.; Liu-Bryan, R.; Agudelo, C., "Overview of Hyperuricemia and Gout." *Curr. Pharm. Des.* **2005,** 11, 4117-4124.

16. Doherty, M., "New insights into the epidemiology of gout." *Rheumatology* **2009,** 48, ii2-ii8.

17. Luk, A. J.; Simkin, P. A., "Epidemiology of Hyperuricemia and Gout." *Am J Manag Care* **2005,** 11, S435-S442.

18. Choi, H. K.; Atkinson, K.; Karlson, E. W.; Willett, W.; Curhan, G. C., "Alcohol intake and risk of incident gout in men: a prospective study." *Lancet* **2004,** 363, 1277-1281.

19. Choi, A.; Atkinson, K.; Karlson, E. W.; Willett, W.; Curhan, G. C., "Purine-rich foods, dairy protein intake and the risk of gout in men." *N. Engl. J. Med.* **2004,** 350, 1093-1103.

20. Rhoo, Y. H.; Zhu, Y.; Choi, H. K., "The Epidemiology of Uric Acid and Fructose." *Seminars in Nephology* **2011,** 31, (5), 410-419.

21. Saag, K. G.; Choi, H., "Epidemiology, risk factors, and lifestyle modifications for gout." *Arthritis. Res. Ther.* **2006,** 8 (Suppl 1):S2.

22. Zhu, Y.; Pandya, B. J.; Choi, H. K., "Prevalence of Gout and Hyperuricemia in the US General Population." *Arthritis Rheum* **2011,** 63, (10), 3136-3141.

23. Schumacher, H. R. J.; Becker, M. A.; Lloyd, E.; MacDonald, P. A.; Lademacher, C., "Febuxostat in the treatment of gout: 5-yr findings of the FOCUS efficacy and safety study." *Rheumatology* **2009,** 48, 188-194.

24. Nuki, "Gout." *Medicine* **2006,** 34, (10), 417-423.

25. Edwards, N. L., "Febuxostat: a new treatment in gout." *Rheumatology* **2009,** 48, ii15-ii19.

26. Bieber, J. D.; Terkeltaub, R. A., "Gout: On the Brink of Novel Therapeutic Options for an Ancient Disease." *Arthritis Rheum* **2004,** 50, (8), 2400-2414.

27. Chohan, S.; Becker, M. A., "Update on emerging urate-lowering therapies." *Curr. Opin. Rheumatol.* **2009,** 21, 143-149.

28. Singh, J. A.; Hodges, J. S.; Asch, S. M., "Opportunities for improving medication use and monitoring in gout." *Ann. Rheum. Dis.* **2009,** 68, 1265-1270.

29. Verkoelen, C. F., "Crystal Retention in Renal Stone Disease: A Crucial Role for the Glycosaminoglycan Hyaluronan?" *J. Am. Soc. Nephrol.* **2006,** 17, 1673-1687.

30. Ancheta, M.; Swangard, D., Anesthetic Considerations for Extracorporeal Shocwave Lithotripsy, Percutaneous Nephrolithotomy, and Laser Lithotripsy. In *Urinary Stone Disease: The Practical Guide to Medical and Surgical Management*, Stoller, M. L.; Meng, M. V., Eds. Humana Press: New Jersey, 2007; pp 495-509.

31. Boyce, W. H., "Organic Matrix in Human Urinary Concretions." *Am. J. Med.* **1968,** 45, 673-683.

32. Herring, L. C., *http://www.herringlab.com/a.html*.

33. Mandel, N. S.; Mandel, G. S., "Urinary Tract Stone Disease in the United States Veteran Population. II. Geographical Analysis of Variations in Composition." *J. Urol.* **1989,** 142, 1516-1521.

34. Lonsdale, K.; Mason, P., "Uric Acid, Uric Acid Dihydrate, and Urates in Urinary Calculi, Ancient and Modern." *Science* **1966,** 152, 1511-1512.

35. Schubert, G.; Reck, G.; Jancke, H.; Kraus, W.; Patzelt, C., "Uric acid monohydrate - a new urinary calculus phase." *Urol. Res.* **2005,** 33, 231-238.

36. Herring, L. C., "Observation on the analysis of ten thousand urinary calculi." *J. Urol.* **1962,** 88, 545-565.

37. Delatte, L. C.; Bellanato, J.; Santos, M.; Rodriguez-Miñon, J. L., "Monosodium urate in urinary calculi." *Eur. Urol.* **1978,** 4, (6), 441-447.

38. Benramdane, L.; Bouatia, M.; Idrissi, M. O. B.; Draoui, M., "Infrared Analysis of Urinary Stones, Using a Single Reflection Accessory and a KBr Pellet Transmission." *Spectrosc. Lett.* **2008,** 41, 72-80.

39. Pichette, V.; Bonnardeaux, A.; Cardinal, J.; Houde, M.; Nolin, L.; Boucher, A.; Ouimet, D., "Ammonium Acid Urate Crystal Formation in Adult North American Stone-Formers." *Am. J. Kidney Diseases* **1997,** 30, (2), 237-242.

40. Brien, G.; Schubert, G.; Bick, C., "10,000 analyses of urinary calculi using x-ray diffraction and polarizing microscopy." *Eur. Urol.* **1982,** 8, 251-256.

41. Trinchieri, A.; Coppi, F.; Montanari, E.; Del Nero, A.; Zanetti, G.; Pisani, E., "Increase in the Prevalence of Symptomatic Upper Urinary Tract Stones during the Last Ten Years." *Eur. Urol.* **2000,** 37, 23-25.

42. Akinci, M.; Esen, T.; Tellaloğlu, S., "Urinary Stone Disease in Turkey: An Updated Epidemiological Study." *Eur. Urol.* **1991,** 20, 200-203.

43. Yasuia, T.; Iguchi, M.; Suzuki, S.; Kohria, K., "Prevalence and Epidemiological Characteristics of Urolithiasis in Japan: National Trends Between 1965 and 2005." *Urology* **2008,** 71, (2), 209-213.

44. Indridson, O. S.; Birgisson, S. J.; Edvardsson, V. O.; Sigvaldason, H.; Sigfusson, N.; Palsson, R., "Epidemiology of kidney stones in Iceland A population-based study." *Scand. J. Urol. Nephrol.* **2006,** 40, 215-220.

45. Sánchez-Martin, F. M.; Millán Rodríguez, F.; Esquena Fernández, S.; Segarra Thomás, J.; F., R. B.; Martínez-Rodríguez, R.; H., V. M., "Incidence and prevalence of published studies about urolithiasis in Spain. A review." *Actas. Urol. Esp.* **2007,** 31, (5), 511-520.

46. Hesse, A.; Brändle, E.; Wilbert, D.; Köhrmann, K.-U.; Alken, P., "Study on the Prevalence and Incidence of Urolithiasis in Germany Comparing Years 1979 vs. 2000." *Eur. Urol.* **2003,** 44, 709-713.

47. Stamatiou, K. N.; Karanasiou, V. I.; Lacroix, R. E.; Kavouras, N. G.; Papadimitrious, V. T.; Chlopsios, C.; Lebren, F. A.; Sofras, F., "Prevalence of urolithiasis in rural Thebes, Greece." *Rural and Remote Health* **2006,** 6:610.

48. Stamatelou, K. K.; Francis, M. E.; Jones, C. A.; Nyberg, L. M. J.; Curhan, G., "Time trends in reported prevalence of kidney stones in the United States: 1976-1994." *Kidney Intl.* **2003,** 63, 1817-1823.

49. Ajayi, L.; Jaeger, P.; Robertson, W.; Unwin, R., "Renal stone disease." *Medicine* **2007,** 35, (8), 415-419.

50. Sakhaee, K., "Uric Acid Metabolism and Uric Acid Stones." *Urinary Tract Stone Disease* **2011**, 185-193.

51. Ngo, T. C.; Assimos, D. G., "Uric Acid Nephrolithiasis: Recent Progess and Future Directions." *Reviews in Urology* **2007,** 9, (1), 7-27.

52. Maalouf, N. M.; Cameron, M. A.; Sakhaee, K., "Novel insights into the pathogenesis of uric acid nephrolithiasis." *Curr. Opin. Nephrol. Hypertens.* **2004,** 13, 181-189.

53. Sakhaee, K.; Adams-Huet, B.; Moe, O. W.; Pak, C. Y., "Pathophysiologic basis for normouricosuric uric acid nephrolithiasis." *Kidney. Intl.* **2002,** 62, 971-979.

54. Cameron, M. A.; Maalouf, N. M.; Poindexter, J.; Adams-Huet, B.; Sakhaee, K.; Moe, O. W., "The diurnal variation in urine acidification differs between normal individuals and uric acid stone formers." *Kid. Interl.* **2012**, 1-8.

55. Cameron, M. A.; Maalouf, N. M.; Adams-Huet, B.; Moe, O. W.; Sakhaee, K., "Urine composition in type 2 diabetes: Predisposition to uric acid nephrolithiasis." *J. Am. Soc. Nephrol.* **2006,** 17, 1422-1428.

56. Agarwal, B. N.; Cabebe, F. G., "Renal acidification in elderly subjects." *Nephron.* **1980,** 26, 291-295.

57. Coe, F. L.; Moran, E.; Kavalich, A. G., "The contribution of dietary purine over-consumption to hyperuricosuria in calcium oxalate stone formers." *J. Chron. Dis.* **1976,** 29, 793-800.

58. Shekarriz, B.; Stoller, M. L.; Eisner, B. H. Hyperuricosuria and Gouty Diathesis. http://emedicine.medscape.com/article/444866-overview

59. Kenny, J. S.; Goldfarb, D. S., "Update on the Pathophysiology and Management of Uric Acid Renal Stones." *Curr. Rheumatol. Rep.* **2010,** 12, 125-129.

60. Borghi, L.; Meschi, T.; Amato, F.; Novarini, A.; Romanelli, A.; Cigala, F., "Hot occupation and nephrolithiasis." *J. Urol.* **1993,** 150, (6), 1757-60.

61. Bihl, G.; Meyers, A., "Recurrent renal stone disease—advances in pathogenesis and clinical management." *The Lancet* **2001,** 358, 651-656.

62. Taylor, E. N.; Curhan, G. C., "Diet and fluid prescription in stone disease." *Kidney Intl.* **2006,** 70, 835-839.

63. Guan, X.; Wang, L.; Dosen, A.; Tang, R.; Giese, R. F.; Giocondi, J. L.; Orme, C. A.; Hoyer, J. R.; Nancollas, G. H., "An Understanding of Renal Stone Development in a Mixed Oxalate-Phosphate System." *Langmuir* **2008,** 24, 7058-7060.

64. Grases, F.; Costa-Bauzá, A.; March, J. G.; Masárová, L., "Glycosaminoglycans, uric acid and calcium oxalate urolithiasis." *Urol. Res.* **1991,** 19, (6), 375-380.

65. Chung, H.-J.; Abrahams, H. M.; Meng, M. V.; Stoller, M. L., Theories of Stone Formation. In *Urinary Stone Disease: The Practical Guide to Medical and Surgical Management*, Stoller, M. L.; Meng, M. V., Eds. Humana Press: New Jersey, 2007; pp 55-68.

66. Koka, R. M.; Huang, E.; Lieske, J. C., "Adhesion of Uric Acid Crystals to the Surface of Renal Epithelial Cells." *Am. J. Physiol. Renal Physiol.* **2000**, F989-F998.

67. Smith, R. C.; Gore, J. Z.; McKee, M.; Howard, H., "The First Dissociation Constant of Uric Acid." *Microchem. J.* **1988,** 38, 118-124.

68. Mandel, N. S.; Mandel, G. S., "Monosodium Urate Monohydrate, the Gout Culprit." *J. Am. Chem. Soc.* **1976,** 98, 2319-2323.

69. Dubler, R.; Jameson, G. B.; Kopajtić, Z., "Uric Acid Salts of Magnesium: Crystal and Molecular Structures and Thermal Analysis of Two Phases of $Mg(C_5H_3N_4O_3)_2 \cdot 8H_2O$." *J. Inorg. Biochem.* **1986,** 26, 1-21.

70. Sattar, S.; Carroll, M. J.; Sargeant, A. A.; Swift, J. A., "Structure of a lead urate complex and its effect on the nucleation of monosodium urate monohydrate." *CrystEngComm* **2008,** 10, 155-157.

71. Elliot, J. S.; Sharp, R. F.; Lewis, L., "Urinary pH." *J. Urol.* **1959,** 81, 339-343.

72. Königsberger, E.; Königsberger, L.-C., "Thermodynamic Modeling of Crystal Deposition in Humans." *Pure Appl. Chem.* **2001,** 73, (5), 785-797.

73. Sours, R. E. Uric Acid Crystal Growth. Georgetown University, Washington, DC, 2004.

74. Königsberger, E.; Wang, Z., "Solubility of Uric Acid in Salt Solutions." *Monatsh. Chem.* **1999,** 130, 1067-1073.

75. Ringertz, H., "The Molecular and Crystal Structure of Uric Acid." *Acta Cryst.* **1966,** 20, 397-403.

76. Artioli, G.; Masciocchi, N.; Galli, E., "The Elusive Crystal Structure of Uric Acid Dihydrate: Implication for Epitaxial Growth During Biomineralization." *Acta Cryst.* **1997,** B53, 498-503.

77. Parkin, S.; Hope, H., "Uric Acid Dihydrate Revisited." *Acta Cryst.* **1998,** B54, 339-344.

78. Boistelle, R.; Rinaudo, C., "Phase transition and epitaxies between hydrated orthorhombic and anhydrous monoclinic uric acid crystals." *J. Cryst. Growth* **1981,** 53, 1-9.

79. Kim, K. M., "The stones." *Scanning Electron Microscopy* **1982,** 4, 1635-1660.

80. Coe, F. L.; Evan, A.; Worcester, E., "Kidney stone disease." *J. Clin. Invest.* **2005,** 115, 2598-2608.

81. Pinto, B.; Rocha, E.; Ruiz-Marcellan, F. J., "Isolation and characterization of uricine from uric acid stones." *Kid. Interl.* **1976,** 10, 437-443.

82. Ringertz, H., "Optical and crystallographic data of uric acid and its dihydrate." *Acta Cryst.* **1965,** 19, 286-287.

83. Shirley, R., "Uric Acid Dihydrate: Crystallography and Identification." *Science* **1966,** 152, 1512-1513.

84. Ostwald, W., "Ostwald, Studien ü ber die bildung und umwandlung fester körper." *Z. Phys. Chem.* **1897**, 289-330.

85. Rodríguez-Spong, B.; Price, C. P.; Jayasankar, A.; Matzger, A. J.; Rodríguez-Hornedo, N., "General principles of pharmaceutical solid polymorphism: a supramolecular perspective." *Adv. Drug. Deliv.* **2004,** 56, 241-274.

86. Bernstein, J., *Polymorphism in Molecular Crystals*. Clarendon Press: Oxford, 2002.

87. Zellelow, A. Z.; Kim, K.-H.; Sours, R. E.; Swift, J. A., "Solid-State Dehydration of Uric Acid Dihydrate." *Cryst. Growth. Des.* **2010,** 10, 418-425.

88. Cardew, P. T.; Davey, R. J., "The kinetics of solvent-mediated phase transformation." *Proc. R. Soc. Lond.* **1985,** 398, 415-428.

89. Liu, W.; Wei, H.; Black, S., "An Investigation of the Transformation of Carbamazepine from Anhydrate to Hydrate Using in Situ FBRM and PVM." *Or. Process Res. Dev.* **2009,** 13, 494-500.

90. Qu, H.; Louhi-Kultanen, M.; Rantanen, J.; Kallas, J., "Solvent-Mediated Phase Transformation Kinetics of an Anhydrate/Hydrate System." *Cryst. Growth. Des.* **2006,** 6, (9), 2053-2060.

91. Mukuta, T.; Lee, A. Y.; Kawakami, T.; Myerson, A. S., "Influence of Impurities on the Solution-Mediated Phase Transformation of an Active Pharmaceutical Ingredient." *Cryst. Growth. Des.* **2005,** 5, (4), 1429-1436.

92. Croker, D.; Hodnett, B. K., "Mechanistic Features of Polymorphic Transformations: The Role of Surfaces." *Cryst. Growth. Des.* **2010,** 10, 2806-2816.

93. Lonsdale, K., "Epitaxy as a Growth Factor in Urinary Calculi and Gallstones." *Nature* **1968,** 217, 56-58.

94. Lonsdale, K.; Sutor, D. J., "Crystallographic Studies of Urinary and Biliary Calculi." *Soviet Physics - Crystallography* **1972,** 16, (9), 1060-1068.

95. Frincu, M. C.; Fogarty, C. E.; Swift, J. A., "Epitaxial Relationships between Uric Acid Crystals and Mineral Surfaces: A Factor in Urinary Stone Formation." *Langmuir* **2004,** 20, 6524.

96. Kleeberg, J.; Kedar, G. S.; Dobler, M., "Studies on the Morphology of Human Uric Acid Stones." *Urol. Res.* **1981,** 9, 259-261.

97. Hesse, A.; Schneider, H.-J.; Berg, W.; Heinzsch, E., "Uric acid dihydrate as urinary calculus component." *Invest. Urol.* **1975,** 12, (5), 405-409.

CHAPTER 2 ADHESION PROPERTIES OF URIC ACID CRYSTAL SURFACES

2.1 Introduction

Recent estimates suggest that 8-12% of men (4-6 % of women) in the US[1] and UK[2] will develop kidney stones at some time in their lives. Kidney stones vary in their composition and size, but in general can be characterized as heterogeneous aggregates of micron-sized crystals held together by a small amount of organic matrix. The assembly of these macroscopic entities is not well understood but must include several key steps including crystal nucleation, growth, aggregation and attachment to renal tissue. Approaching the problem of kidney stone formation from a physical-chemical perspective requires detailed knowledge of the surface structure(s) of the individual crystalline building blocks and their adhesion properties in relation to other species present in the physiological fluid.

Over 200 different inorganic and organic crystalline phases have been identified in human kidney stones.[3] Anhydrous uric acid (UA) is the most abundant organic crystalline phase, having been identified as the major component in ~13 % of stones.[1] High incidence rates of uric acid

stones have been correlated with metabolic syndrome[4-7] and with chemotherapy treatment,[8] but can also occur in otherwise healthy groups. Several other phases of uric acid including the dihydrate,[9] monohydrate,[10] and various urate salts[11-14] have also been identified in human kidney stones, though typically as minor components.

The crystal structure of UA was first determined in the 1960s - space group $P2_1/a$ and unit cell dimensions a = 14.464(3), b = 7.403(2), c = 6.208(1) Å, and β = 65.10(5)°.[15] UA crystals grown from pure aqueous solution deposit as clear, colorless rectangular plates with large (100) faces bounded by (210), (201), (001), and sometimes (121) faces (Figure 2.1).[16] Crystal sizes typically do not exceed ~200-300 μm in the largest dimension. Physiologically derived crystals can have more varied morphologies, but typically are also plate-like. Micron sized crystals are handled effectively by properly functioning renal systems, however, macroscopic aggregates above a certain size (≥5 mm)[17] become problematic. The adhesion properties of UA surfaces are therefore clearly important in both the attachment of crystals to renal epithelial cells and their aggregation to other crystals and/or matrix en route to stone formation.

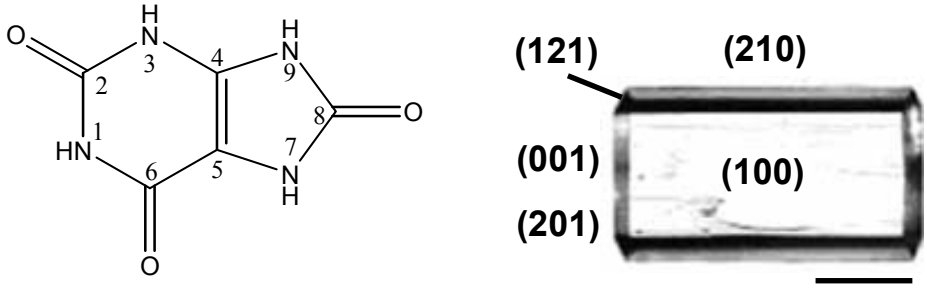

Figure 2.1. Molecular structure and typical plate-like morphology of anhydrous uric acid (UA) crystals grown from acidic aqueous solutions. Scale bar = 100 μm.

2.2 Principles of Atomic Force Microscopy

Atomic force microscopy (AFM)[18] is a technique used to study surfaces at the nanoscale based on interactions between a scanning probe and a surface (Figure 2.2). AFM employs an ultrasmall tip, usually silicon or silicon nitride, located at the end of a cantilever, which is raster-scanned over the surface of the sample that is mounted on a piezo-scanner. As the tip moves up and down with the contours of the surface, the cantilever deflects. The deflections are measured by a laser beam reflected off the back of the cantilever into a position sensitive photodiode detector. The measured deflections are used to generate the topographical image of the sample.

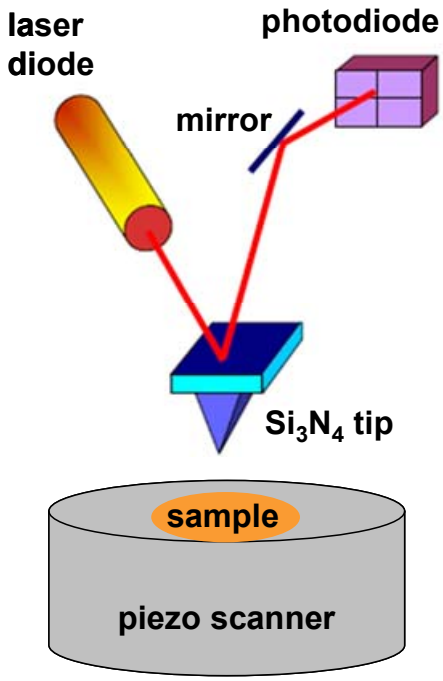

Figure 2.2. Simplified schematic diagram of an atomic force microscope.

AFM has been used in imaging and real time *in-situ* crystal growth of organic compounds[19-26] including UA.[27] The surface topography and real time growth kinetics of UA (100) single crystal

surfaces were examined as a function of supersaturation and pH.[27] Step velocities at various physiologically relevant pH values were found to linearly increase with uric acid supersaturation on UA (100). Recently, Perrin *et al.*[24, 25] measured the growth kinetics of monosodium urate monohydrate (MSU) for both (010) and (1-10) faces. Step velocities for monolayers and multiple layers displayed a second order polynomial dependence on urate supersaturation on MSU (010) and (1-10). Rimer *et al*. used AFM to study L-cystine, also a component of kidney stones and suggests that rational design of crystal growth inhibitors could lead to the prevention of L-cystine stones.[26]

2.3 Principles of Chemical Force Microscopy

Chemical force microscopy (CFM), a variation of atomic force microscopy, is used to measure the adhesion properties of surfaces.[28] In this technique, the AFM tips (Figure 2.3) are modified by controlled deposition of chromium and gold, followed by immersion of the tip in a solution of organic thiol. Chemisorption of the thiol (S-H) head groups onto a gold surface forms a self-assembled monolayer (SAM). Interactions between the specific functional groups at the far end of the thiol and the sample are used to discern the adhesion properties of the surface.

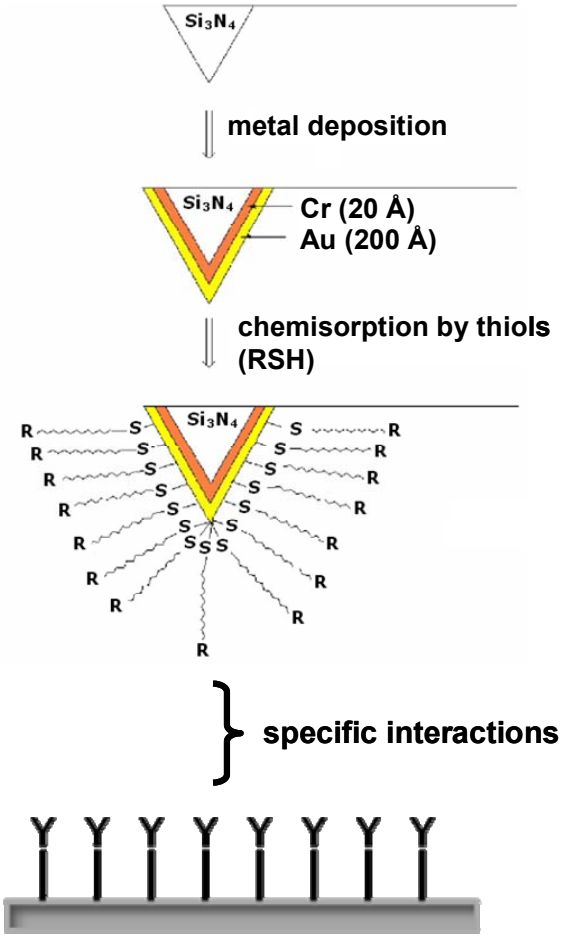

Figure 2.3. Schematic diagram of a modified AFM tip showing functional groups R that interact with the functional groups Y on the sample surface.

The adhesion between the modified tip and the surface is quantified using force curve measurements. This technique consists of an approach-retract cycle between the tip and sample during which the cantilever deflection is measured. A typical force curve is depicted in Figure 2.4.

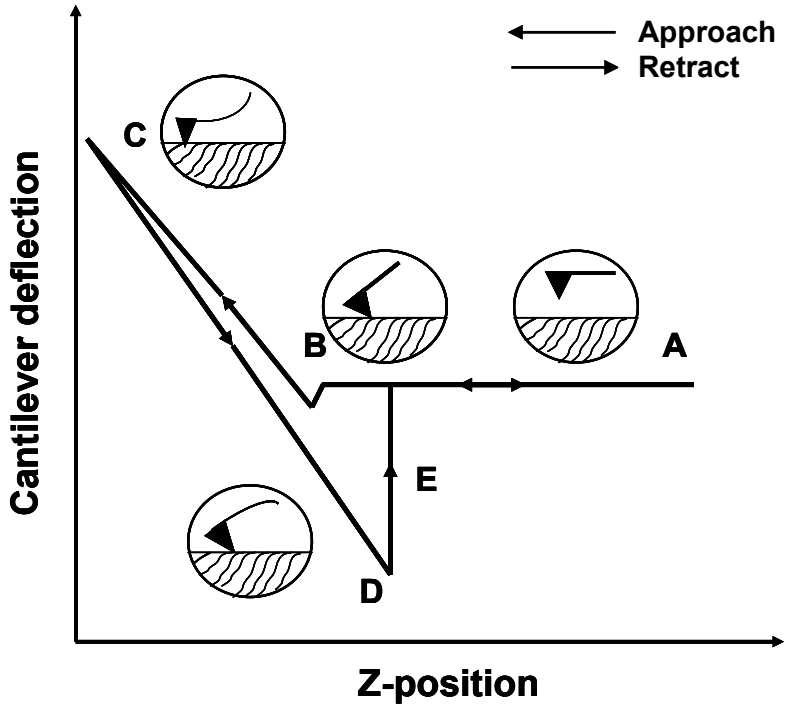

Figure 2.4. A schematic diagram of a typical force measurement cycle. (A) The tip approaches the surface, (B) "jumps" to contact the surface, (C) further approaches the surface, (D) is retracted from the surface, (E) is released back to its original state. Adapted from Barattin and Voyer.[29]

In a force measurement cycle, the tip (A) is brought close to the surface, then "jumps" to contact the surface (B). After contact, the tip is pressed onto the surface of the sample (C). As the tip is retracted from the surface, the curve shows some hysteresis due to adhesion between functional groups on the tip and the surface (D). When the adhesion is broken, the tip is released back to its original equilibrium state (E). The cantilever deflection measured in the force-curve cycle is converted to force, F, using Hooke's law: $F = -kx$ with knowledge of the cantilever spring constant, k, and the maximum negative deflection, x (deflection between A and D).

2.3.1 Previous Chemical Force Microscopy Studies on Crystal Surfaces

CFM has been used to study the adhesion properties of a broad range of materials, though the number of molecular crystal surfaces probed by CFM have to date been somewhat limited.[30-40] Chemical functionality of molecular crystals such as aspirin[30] and cholesterol[31] single crystal surfaces were assessed using various AFM probe tips. Utilizing hydrophobic and hydrophilic probe tips, Danesh *et al.*[30] demonstrated the difference in the surface chemical structure of aspirin single crystal planes (001) and (100). The data obtained from surface chemistry characterization have provided insight into the dissolution velocity of the two crystal planes. Abendan *et al.*[31] characterized both the surface structure and the chemical composition of cholesterol monohydrate single crystals under very different but well-defined solution conditions. This study demonstrated that the functionality of the crystal surface can be altered by changes in the solution composition. The 3-hydroxyl end of cholesterol molecules is presented on the plate face in aqueous media, while alkyl tail groups terminate the surface in organic solutions.

Smith *et al*.[39] utilized AFM tips functionalized with amine and carboxyl groups to map the distribution of surface charge on natural hydroxyapatite (HAP) crystals derived from enamel samples. It was found that apatite crystals comprise large areas of positive charge, interrupted by smaller domains of negative charge. Additionally, Robinson *et al*.[40] investigated the behavior and appearance of HAP crystal surfaces at various pH values. These studies lead to a better understanding of the binding of matrix proteins to the mineral surface.

Studies by Sheng *et al.*[32-34, 37] and Wesson *et al.*[37] measured the adhesion forces on calcium oxalate monohydrate (COM) and calcium oxalate dihydrate (COD). Tips with ionic terminal

groups had a significantly higher adhesion to the most prominent (100) face of COM than all COD surfaces.[32, 33] This observation was consistent with the greater propensity for COM to form stones. Adhesion studies in the presence of citrate and other urinary species further supported the role of urinary macromolecules in face-specific binding to COM surfaces.[33]

The present study uses CFM to investigate adhesion on the largest plate face of UA single crystals under well-defined aqueous conditions and in model urine solutions. The adhesion forces between UA (100) and tips modified with various hydrophobic, hydrophilic, and charged groups were assessed in an effort to elucidate the most significant types of surface interactions that can occur under simulated physiologic conditions and how crystal aggregation, which is mediated by matrix, occurs *in vivo*.

2.4 Experimental Methods and Materials

2.4.1 Materials

Water was purified by passage through two Barnstead deionizing cartridges followed by distillation. McIlvaine buffers[41] with controlled pH and ionic strength were prepared from $C_6H_8O_7 \cdot H_2O$ (99.0%, EMD), Na_2HPO_4 (99.5%, Fisher), and KCl (99.0%, Sigma). Artificial urine solution[42] was prepared from Na_2SO_4 (99.9%, Sigma), KCl (99.0%, Sigma), NH_4Cl (99.8%, EM Science), $MgSO_4 \cdot 7H_2O$ (98-102%, EM Science), Na_2HPO_4 (99.5%, Fisher), $Na_2HPO_4 \cdot H_2O$ (99.1%, Fisher), NaCl (99%, EM Science), $Na_3C_6H_5O_7 \cdot 2H_2O$ (Certified, Fisher Chemical), and urea (Certified ACS, Fisher Chemical).

1-Dodecanethiol (DD) (≥98%, Aldrich), 11-mercapto-1-undecanol (MU) (97%, Aldrich), 11-mercaptoundecanoic acid (MUA) (95%, Aldrich), 4-mercaptobenzoic acid (MBA) (97%,

Aldrich), 4-mercaptophenol (MP) (97%, Aldrich), 4-mercaptoaniline (MA) (97%, Aldrich), and mercaptoethylguanidine (MEG) (≥98%, Sigma) were used in the preparation of chemically modified AFM tips. All chemical reagents were used as received without further purification.

2.4.2 Uric Acid Sample Preparation

Uric acid (UA) single crystals were grown by dissolving 18-20 mg of uric acid (>99%, Sigma) in 100 mL boiling distilled water.[43] The solution was buffered to pH = 4.0 with sodium acetate (99%, EMD) and acetic acid (99.7%, EMD) and placed in a 37^{o} C (± 0.1^{o}) water-bath for 48 hours. UA crystals deposited as rectangular plates typically ~200-300 μm in their longest dimension with large (100) faces (Figure 2.1).

UA crystals were mounted on 15-mm diameter coverslips with Loctite 5-minute epoxy (Henkel Corp). The quality and orientation of the crystal were established using conoscopy[44] on an Olympus BX-50 polarizing microscope. The coverslip was then fixed to an AFM sample disc using epoxy and the disc was mounted in a small volume liquid cell in a Digital Instruments Multimode Nanoscope IIIa instrument. All contact mode imaging was conducted at room temperature.

2.4.3 Chemical Force Microscopy

Commercial V-shaped 100-200μm Si_3N_4 cantilevers (Digital Instruments, Santa Barbara) were coated by sputtering a 20 Å layer of chromium followed by 200 Å of gold. The gold coated cantilevers were then functionalized by immersion in 2-3 mM ethanolic solutions of various thiols for 22 hrs (Figure 2.5).[28] The cantilevers were subsequently rinsed with absolute ethanol and dried under nitrogen. The spring constant of individual tips was determined using the

reference cantilever method[45] against a CLFC-NOBO tipless rectangular cantilever (Veeco Metrology) of known spring constant. Chemically modified tips had an average spring constant of 0.25 ± 0.05 N/m.

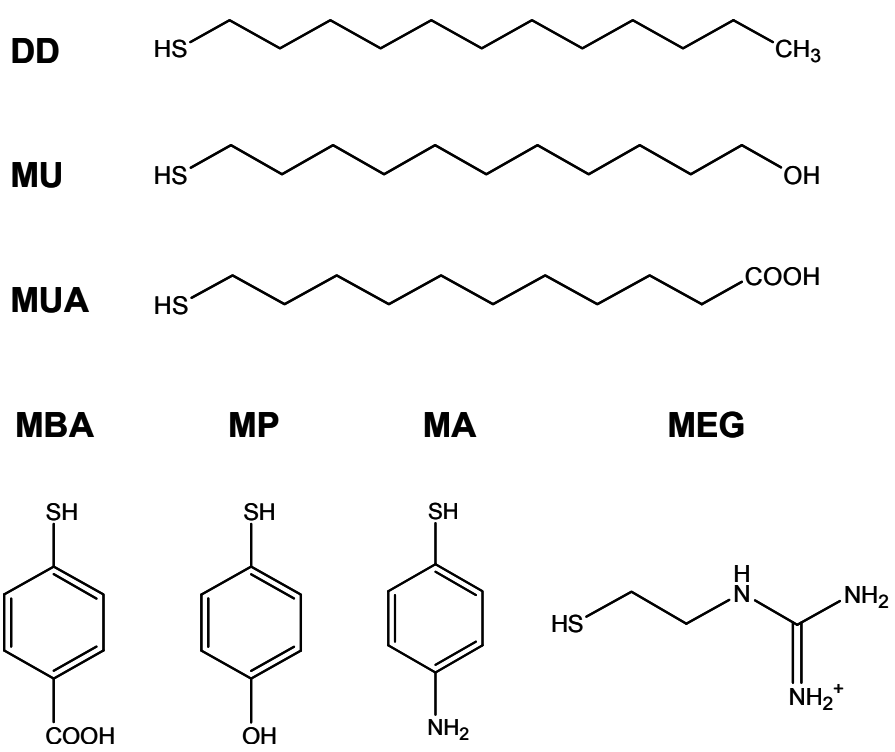

Figure 2.5. Chemical structures of thiols used in this study: 1-dodecanethiol (DD), 11-mercapto-1-undecanol (MU), 11-mercaptoundecanoic acid (MUA), 4-mercaptobenzoic acid (MBA), 4-mercaptophenol (MP), 4-mercaptoaniline (MA), mercaptoethylguanidine (MEG).

All experiments on single crystal UA were performed in either unbuffered distilled water, artificial urine[42] or McIlvaine buffer.[41] Topographical images of the UA (100) surface under fluid environments were obtained prior to force measurements. Individual force-distance curves were acquired at a rate of 2 Hz in relative trigger mode with a trigger threshold set to 20 nm.

Over 500 individual force-distance curve measurements were acquired for each type of modified tip on at least 10 different locations per crystal. Individual deflection versus Z-position curves were converted into force using Scanning Probe Image Processor (SPIP) software from Image Metrology (Lyngby, Denmark). Adhesion data were plotted in a histogram with the normal distribution curve defined by the average and standard deviation.

2.5 Adhesion Force Measurements

UA crystallizes in a layered structure (Figure 2.6). Each layer in the *bc* plane consists of parallel ribbons of uric acid molecules hydrogen-bonded head-to-head ($O_2\cdots H\text{-}N_1$: 1.826 Å, 175.0°) and tail-to-tail ($O_8\cdots H\text{-}N_7$: 1.734 Å, 155.8°) with the ribbon plane nearly perpendicular to the (100) surface. No hydrogen bonding exists between ribbons within a layer, though ribbons in adjacent layers are also hydrogen bonded to one another to create a 3D network. The (100) surface therefore presents a 2D array of edge-on uric acid molecules with both H-bond donor (N-H) and H-bond acceptor (C=O) groups projecting from the surface. Previous in situ AFM work[27] showed that (100) surface topography is fairly smooth with a high proportion of unit cell height steps (14 Å) and multiples thereof aligned parallel to the crystallographic *b* direction.

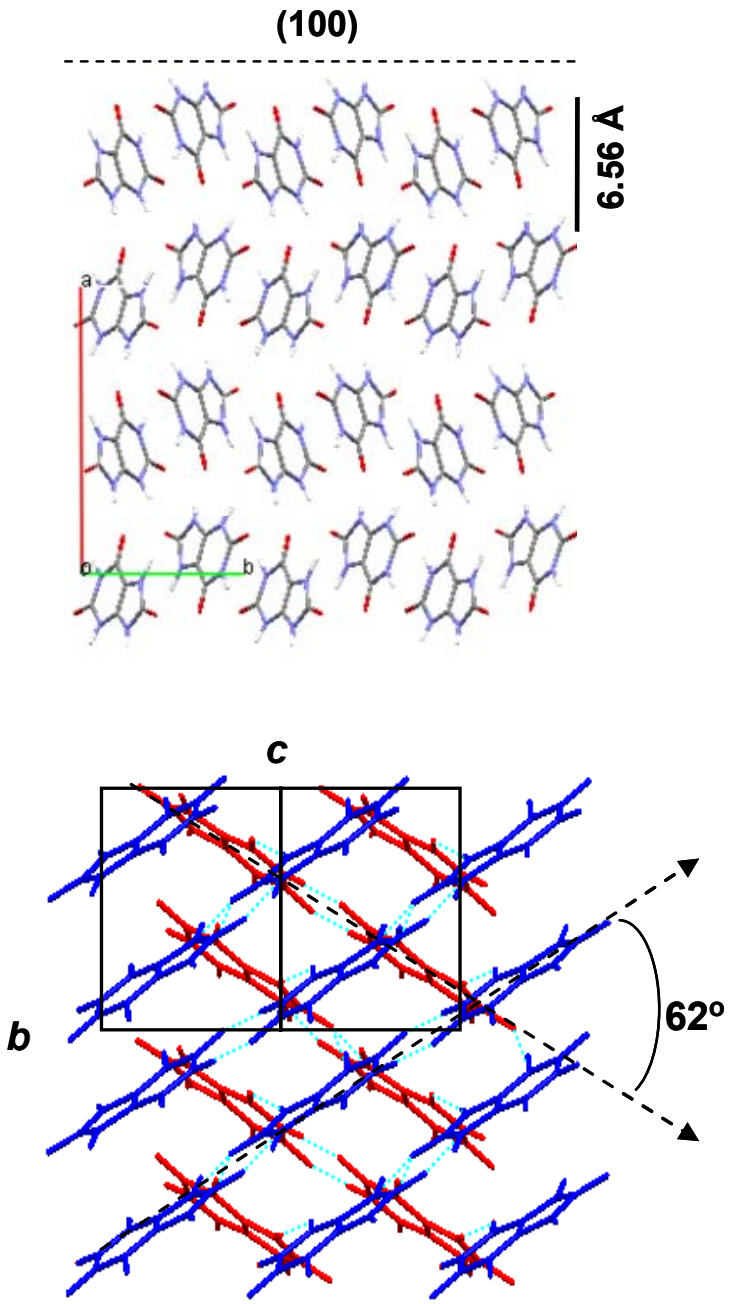

Figure 2.6. Crystal packing diagram for UA constructed from fractional coordinates reported by Ringertz.[15] Layers in the *bc* plane viewed normal to the (100) plane in which adjacent layers are colored blue and red to better show their relative orientation and near perpendicular orientation relative to the (100) surface.

Adhesion force measurements between single crystal UA (100) surfaces and seven different types of functionalized probe tips (Figure 2.5) were obtained under aqueous and model urine conditions. Accurate average forces can be derived from the statistical analysis of numerous force distance curve data obtained under identical conditions. Statistical treatment of the data minimizes variations in the individual forces measured for any given tip-surface combination due to minor variations in tip shape and radius[28, 46] as well as difficulties in quantifying the exact geometry between the tip and the sample.[47]

In our experiments, a minimum of 500 individual force curves were assessed for each tip-sample combination under a given set of solution conditions. At least three different UA crystals were used for each type of tip, and approximately 10 force curves were obtained at each point with a minimum of 10 points per UA sample. Most individual adhesion values fell within the normal distribution curve with only a few outliers with unusually high forces, which are presumably due to multiple contacts between tip and UA sample. The average adhesion forces and standard error of the mean reported herein were calculated from all measured values.

Tips terminated with hydrophobic (methyl), hydrophilic (hydroxyl, amino) and ionic (amidinium, carboxylate) groups cover a range of potential binding interactions that can occur *in vivo* between biomolecules and the UA surface. DD, MU, MEG, and MUA coated tips mimic alanine, serine, arginine and glutamic acid side chains, respectively. Interactions with arenethiol functionalities (i.e. MBA, MP, MA) were also examined to assess whether steric factors contribute to the adhesion forces measured.

2.5.1 Adhesion Forces in Distilled Water

Adhesion force measurements between UA (100) and the variously functionalized tips were first carried out in distilled water (pH = 6.5 ± 0.4). Representative histograms appear in Figure 2.7. A comparison of the adhesion forces in water also appears in Figure 2.8. Overall, the average adhesion force measured for the different tips varied by a factor of 3. The cationic tip MEG (2.22 nN) had an average adhesion force ~ 33% higher than any other type of tip. The three tips with ionizable groups MA, MBA and MUA, had the next highest forces in a similar range (1.62-1.70 nN). The two hydroxyl terminated tips MP and MU were similar (1.29-1.34 nN), and the lowest adhesion was obtained from methyl terminated tips DD (0.78 nN).

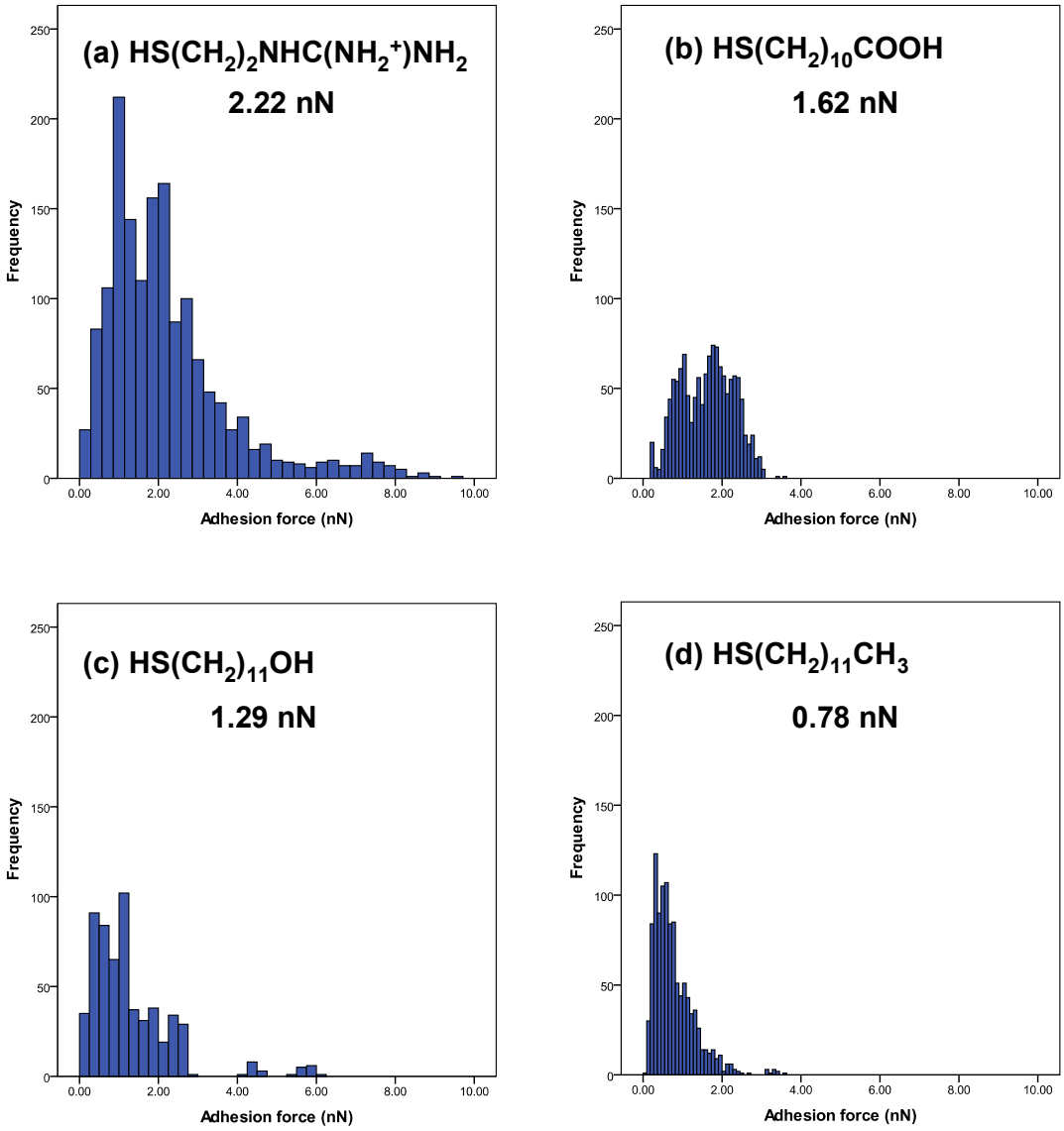

Figure 2.7. Frequency distribution of adhesion forces between UA (100) face and different thiol-coated tips performed in distilled water with pH~6.5. (a) MEG, 2.22 ± 0.04 nN, (b) MUA, 1.62 ± 0.02 nN, (c) MU, 1.29 ± 0.04 nN, (d) DD, 0.78 nN ± 0.02 nN.

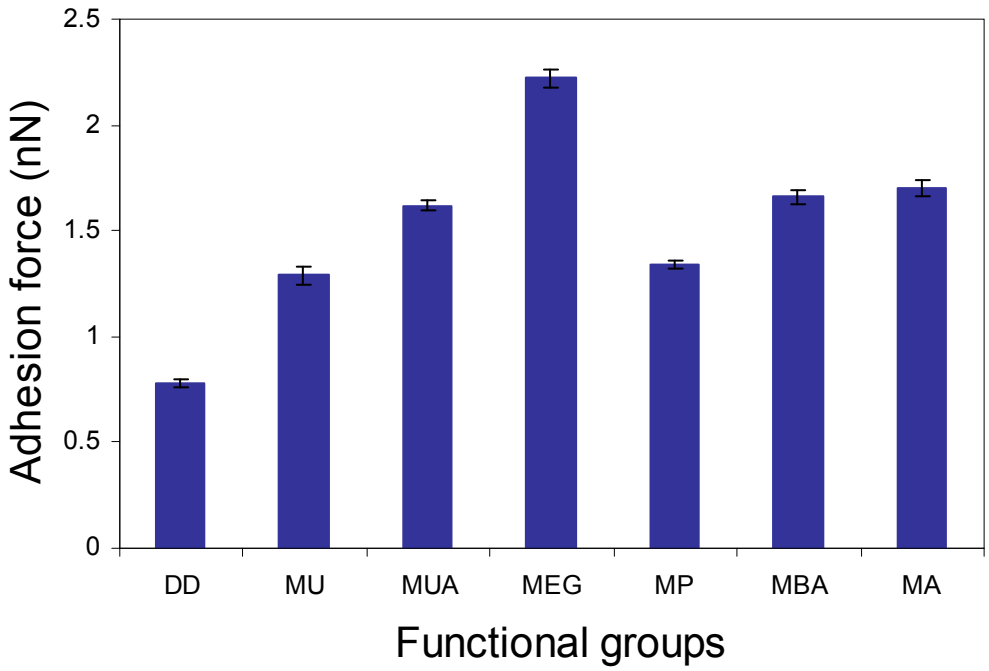

Figure 2.8. Adhesion forces measured between UA (100) and different functionalized tips measured in distilled water.

The significantly higher adhesion observed between cationic tips (MEG) and UA (100) we attribute to both charge-assisted hydrogen bonding and electrostatic interactions. The pK_a of uric acid is 5.5.[48] In solutions where the pH > pK_a, one expects the majority of uric acid molecules in solution to be ionized to urate by loss of a proton at the N3 position.[49] Molecules in the bulk of a UA crystal must still be protonated regardless of the solution conditions, however, given the near perpendicular orientation of uric acid molecules relative to the UA (100) plane, it should be feasible to deprotonate at least some of the surface molecules, thereby imparting a partial negative charge to the surface. Previous electrophoretic mobility studies on UA particles indicate that UA crystal surfaces under some conditions bear a small negative charge.[50] It

follows that cationic tips would therefore have the highest adhesion to these types of surfaces. The potential for a MEG tip to interact with surface uric acid molecules with varying protonation states on a given UA (100) surface may also help to explain the comparatively larger number of individual adhesion measurements that were 2+ standard deviations above the mean.

The ionization state of amino-terminated thiols is dependent on both the solution pH and whether they are free in solution or bound to a substrate. The pK_a of protonated MA in solution is 4.3, however, when bound to a surface the pK_a is estimated to shift to 6.9±0.5.[51] Under the CFM conditions used (pH = 6.5), the MA tip will more likely act as a hydrogen bond donor at the tip-crystal interface and not form complementary charged pairs with surface urates. Aliphatic carboxylic acids like MUA typically have a pK_a of ~ 4.8 in solution, but reportedly shift to higher values ~ 5.2 when bound to a surface.[52] The pK_a of aromatic carboxylic acids such as MBA is 5.5 in solution but shifts to 7.0 when bound to a surface.[53] In a pH 6.5 solution, one expects MBA coated tips to be protonated, but MUA coated tips to be partially or fully ionized to carboxylate. The different ionization states should affect the type of interactions at the tip-crystal interface, with only the former able to act as both a hydrogen bond acceptor and donor. However, the overall adhesion properties for these two tips were similar.

Tips with hydroxyl end groups (i.e. MP and MU) can hydrogen bond to surface uric acid molecules, though the strength of the alcohol hydrogen bonds tends to be weaker than the carboxyl hydrogen bonds. That there are only minor differences in adhesion between aliphatic and aromatic tips suggests that steric factors do not significantly affect the adhesion measurements. The lowest mean adhesion force of 0.78 nN observed with the DD methyl-

terminated tip was expected, given the polar nature of the UA surface and the non-polar nature of the tip.

2.5.2 Adhesion Forces in Model Urine Solution

In an effort to better assess the adhesion properties under physiologic conditions, adhesion was reexamined in model urine solution. Urine is a complex fluid whose composition and concentration varies greatly depending on a variety of factors including diet, exercise and degree of hydration. The model urine used in this study was derived from an established standard[42] consisting of Na_2SO_4 (14.9 mM), KCl (92.6 mM), NH_4Cl (65.1 mM), $MgSO_4 \cdot 7H_2O$ (6.7 mM), Na_2HPO_4 (1.8 mM), $Na_2HPO_4 \cdot H_2O$ (39.6 mM), NaCl (213.9 mM), $Na_3C_6H_5O_7 \cdot 2H_2O$ (2.7 mM), and urea (291.4 mM). The model urine solution had a pH of 5.0 – 5.10 and an ionic strength of ~0.5M.

Over 1200 individual force curves between each type of thiol and UA (100) surfaces were collected in artificial urine solution. At least six different crystal samples were used for each type of tip. Representative histograms for some tip-surface combination appear in Figure 2.9 and the values obtained are plotted in Figure 2.10 (red bars). Adhesion forces measured in artificial urine were all lower than the corresponding forces in aqueous solution (blue bars). In most cases, adhesion was reduced by 38-47% in model urine, the exception being the DD tips which decreased by only ~ 13%. Aqueous solution and model urine differ in two key respects – the latter has a lower pH (5 vs 6.5) but a much higher ionic strength. Notably, despite differences in the solutions, the trends in the relative forces were identical in water and model urine (e.g. MEG > MA, MBA, MUA > MP, MU > DD).

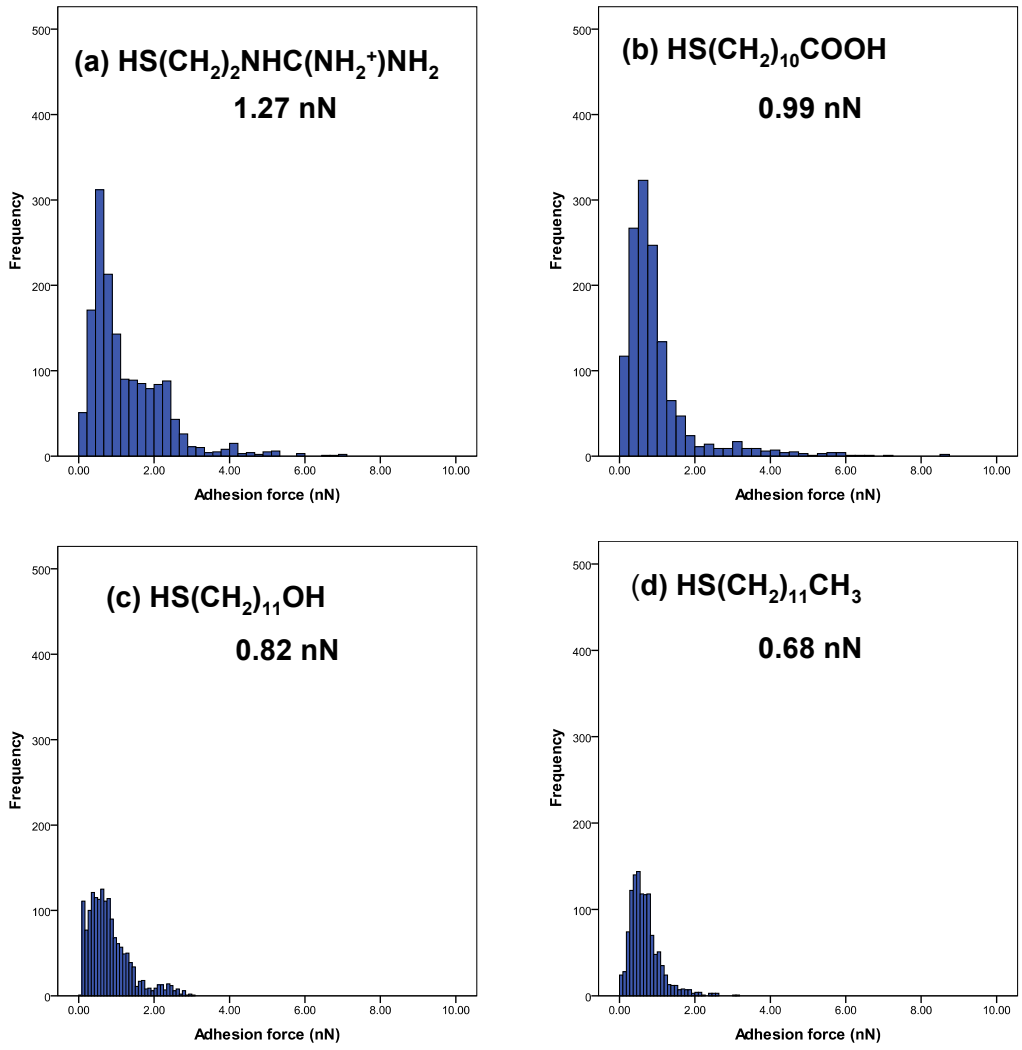

Figure 2.9. Frequency distribution of adhesion forces between UA (100) face and different thiol-coated tips performed in model urine solution with pH~5. (a) MEG, 1.27 ± 0.03 nN, (b) MUA, 0.99 ± 0.03 nN, (c) MU, 0.82 ± 0.01 nN, (d) DD, 0.68 nN ± 0.01 nN.

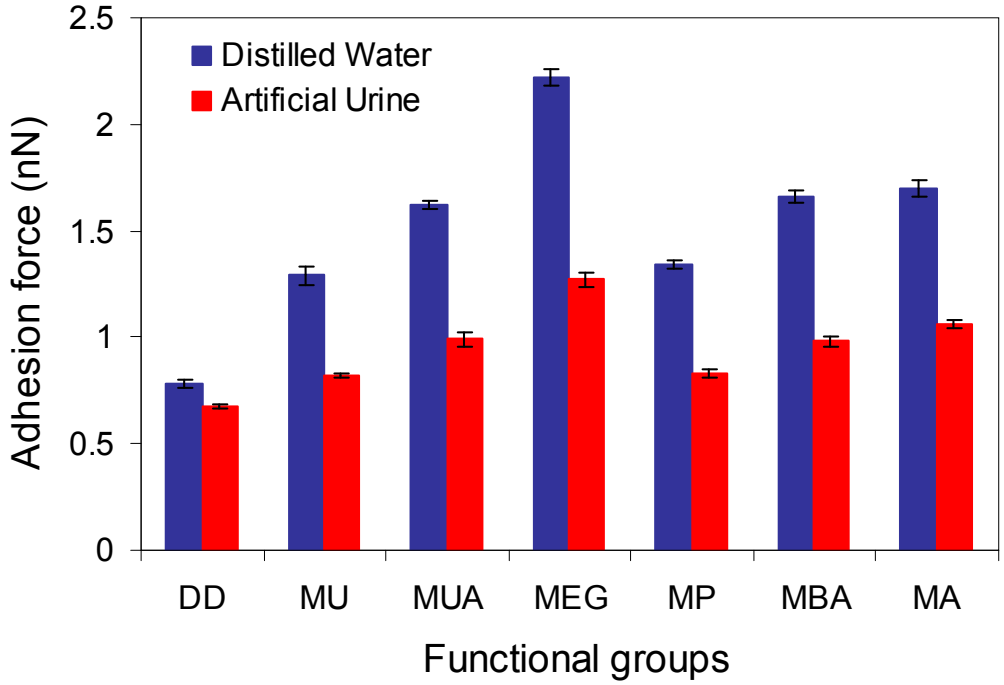

Figure 2.10. Adhesion forces measured between UA (100) and different functionalized tips measured in distilled water (blue bars) and model urine solution (red bars).

2.5.3 Effect of pH and Ionic Strength on Adhesion Forces

In order to assess the relative contribution of pH and ionic strength, we examined adhesion of MEG, MUA and DD tips in a series of McIlvaine buffers ($C_6H_8O_7 \cdot H_2O$, Na_2HPO_4) prepared at pH 5, 6 and 7. The advantage of using this buffer system is that KCl could be added to each solution to maintain a constant ionic strength (IS) of 0.5 M. The IS of human urine typically ranges from 0.3 - 0.6 M.[54]

Both DD and MEG tips showed little variation in the average adhesion over this pH range under fixed IS conditions. The ionization state of the tips does not change over this range – DD is always neutral and MEG is always cationic. Adhesion forces between MUA tips and UA

(100) decreased by 13% from pH 5 to 6. If one assumes the UA surface maintains the same negative surface charge over the pH range examined, the reduction in MUA adhesion at elevated pH can be explained by changes in the ionization of the tip. With increased pH, one expects a greater % of the COOH groups in MUA to be deprotonated to COO- and a consequent reduction in this tip's adhesion to a negatively charged UA surface. Other factors may also contribute to the reduction in adhesion at higher pH. Previous studies on UA particles showed that the surface electric potential increases over a pH range of 2.0 – 6.5, although the increase is fairly minor in the upper pH 5 - 6.5 range.[50] Also worth noting is that there was some difficulty in obtaining measurements at higher pH values since UA solubility increases exponentially when the pH > pK_a.[55] The changing uric acid solution concentration at higher pH may also influence the adhesion observed at a given pH. Adhesion measurements obtained in McIlvaine buffer were lower than the analogous measurements obtained in distilled water with equivalent pH but more comparable in magnitude to those obtained in model urine.

We attempted to assess the influence of ionic strength on adhesion by measuring the interactions between a non-ionizable MU tip at pH 5 in McIlvaine buffers with ionic strengths ranging from 0.3M – 0.7 M. Only a modest increase in adhesion forces was observed from 0.70 nN (0.3 M), 0.80 nN (0.5 M), and 1.03 nN (0.7 M). Again, the magnitude of the force in these various ionic strength solutions was more comparable to forces obtained in model urine. Both pH and ionic strength clearly influence the magnitude of adhesion with some types of functionalities. It is well known that the pH and ionic strength of actual urine can vary significantly with numerous factors ranging from time of day, diet and exercise. Presumably

adhesion to renal epithelial cells and/or aggregation of UA to other particulate matter occurs more/less readily under some local conditions than others.

2.6 Conclusions

Chemical force microscopy has been used to directly quantify the adhesion between UA (100) surfaces and various types of chemical functionalities. Measurements obtained in distilled water and model urine showed similar trends, with the highest adhesion found between UA (100) and cationic surfaces. The magnitude of any force was found to be very much dependent on the mediating solution. Ionic strength and pH are clearly influential solution parameters, though other factors may also affect the magnitude of the adhesion.

That UA crystal adhesion to cationic surfaces was higher than anionic surfaces highlights a major difference between molecular crystal surfaces (in this case of a weak acid) and most other inorganic biominerals. The latter typically are thought to interact through strong electrostatic interactions with other charged species, both anionic and cationic. For small molecule organic crystals, the types of intermolecular interactions are usually considered to be weaker, e.g. typically some combination of hydrogen bonding and/or van der Waals forces. A previous study by Koka *et al.* on the adhesion of UA crystals to renal epithelial cells[56] concluded that hydrogen bonding (rather than ionic bonding) plays the major role in UA crystal-cell interactions under conditions where UA is electrically neutral. What the present study reveals is that electrostatic interactions can also be significant, particularly when the solution conditions alter the ionization state of the crystal surface.

2.7 References

1. Stamatelou, K. K.; Francis, M. E.; Jones, C. A.; Nyberg, L. M. J.; Curhan, G., "Time trends in reported prevalence of kidney stones in the United States: 1976-1994." *Kidney Intl.* **2003,** 63, 1817-1823.

2. Ajayi, L.; Jaeger, P.; Robertson, W.; Unwin, R., "Renal stone disease." *Medicine* **2007,** 35, (8), 415-419.

3. Herring, L. C., *http://www.herringlab.com/a.html*.

4. Negri, A. L.; Spivacow, R.; Del Valle, E.; Pinduli, I.; Marino, A.; Fradinger, E.; Zanchetta, J. R., "Clinical and biochemical profile of patients with ‘‘pure’’ uric acid nephrolithiasis compared with ‘‘pure’’ calcium oxalate stone formers." *Urol. Res.* **2007,** 35, 247-251.

5. Feig, D. I.; Kang, D.-H.; Johnson, R. J., "Uric Acid and Cardiovascular Risk." *N Engl J Med* **2008,** 359, 1811-21.

6. Maalouf, N. M.; Cameron, M. A.; Moe, O. W.; Sakhaee, K., "Metabolic Basis for Low Urine pH in Type 2 Diabetes." *Clin. J. Am. Soc. Nephrol.* **2010,** 5, 1277–1281.

7. Maalouf, N. M., "Metabolic Syndrome and the Genesis of Uric Acid Stones." *J Renal Nutrition* **2011,** 21, (1), 128-131.

8. McCREA, L. E., "Formation of uric acid calculi during chemotherapy for leukemia." *J. Urol.* **1955,** 73, (1), 29-34.

9. Lonsdale, K.; Mason, P., "Uric Acid, Uric Acid Dihydrate, and Urates in Urinary Calculi, Ancient and Modern." *Science* **1966,** 152, 1511-1512.

10. Schubert, G.; Reck, G.; Jancke, H.; Kraus, W.; Patzelt, C., "Uric acid monohydrate - a new urinary calculus phase." *Urol. Res.* **2005,** 33, 231-238.

11. Herring, L. C., "Observation on the analysis of ten thousand urinary calculi." *J. Urol.* **1962,** 88, 545-565.

12. Mandel, N. S.; Mandel, G. S., "Urinary Tract Stone Disease in the United States Veteran Population. II. Geographical Analysis of Variations in Composition." *J. Urol.* **1989,** 142, 1516-1521.

13. Delatte, L. C.; Bellanato, J.; Santos, M.; Rodriguez-Miñon, J. L., "Monosodium urate in urinary calculi." *Eur. Urol.* **1978,** 4, (6), 441-447.

14. Pichette, V.; Bonnardeaux, A.; Cardinal, J.; Houde, M.; Nolin, L.; Boucher, A.; Ouimet, D., "Ammonium Acid Urate Crystal Formation in Adult North American Stone-Formers." *Am. J. Kidney Diseases* **1997,** 30, (2), 237-242.

15. Ringertz, H., "The Molecular and Crystal Structure of Uric Acid." *Acta Cryst.* **1966,** 20, 397-403.

16. Rinaudo, C.; Boistelle, R., "The occurrence of uric acids and the growth morphology of the anhydrous monoclinic modification: $C_5H_4N_4O_3$." *J. Cryst. Growth* **1980,** 49, 569-579.

17. Verkoelen, C. F., "Crystal Retention in Renal Stone Disease: A Crucial Role for the Glycosaminoglycan Hyaluronan?" *J. Am. Soc. Nephrol.* **2006,** 17, 1673-1687.

18. Binnig, G.; Quate, C. F.; Gerber, C., "Atomic Force Microscope." *Phys. Rev. Lett.* **1986,** 56, 930-933.

19. Keel, T. R.; Thompson, C.; Davies, M. C.; Tendler, S. J. B.; Roberts, C. J., "AFM studies of the crystallization and habit modification of an excipient material, adipic acid." *Int. J. Pharm.* **2004,** 280, 185-198.

20. Thompson, C.; Davies, M. C.; Roberts, C. J.; Tendler, S. J. B.; Wilkinson, M. J., "The effects of additives on the growth and morphology of paracetamol (acetaminophen) crystals." *Int. J. Pharm.* **2004,** 280, 137-150.

21. Abendan, R. S. Characterization and Dissolution Studies of Cholesterol Monohydrate Single Crystals. Georgetown University, Washington, DC, 2005.

22. Geng, Y. L.; Xu, D.; Sun, D. L.; Du, W.; Liu, H. Y.; Zhang, G. H.; Wang, X. Q., "Atomic force microscopy studies on growth mechanisms of LAP crystals grown in solution containing excessive amount of L-arginine." *Mater. Chem. Phys.* **2005,** 90, 53-56.

23. Taulelle, P.; Astier, J. P.; Hoff, C.; Pepe, G.; Veesler, S., "Pharmaceutical compound crystallization: growth and mechanism of needle-like crystals." *Chem. Engg. Techn.* **2006,** 29, 239-246.

24. Perrin, C. M.; Dobish, M. A.; Van Keuren, E.; Swift, J. A., "Monosodium urate monohydrate crystallization." *CrystEngComm* **2011,** 13, 1111-1117.

25. Perrin, C. M.; Swift, J. A., "Steps kinetics on monosodium urate monohydrate single crystal surfaces: an *in situ* AFM study." *CrystEngComm* **2012,** 14, 1709-1715.

26. Rimer, J. D.; An, Z.; Zhu, Z.; Lee, M. H.; Goldfarb, D. S.; Wesson, J. A.; Ward, M. D., "Crystal Growth Inhibitors for the Prevention of L-Cystine Kidney Stones Through Molecular Design." *Science* **2010,** 330, 337-341.

27. Sours, R. E.; Zellelow, A. Z.; Swift, J. A., "An in Situ Atomic Force Microscopy Study of Uric Acid Crystal Growth." *J. Phys. Chem. B* **2005,** 109, 9989-9995.

28. Noy, A.; Frisbie, C. D.; Rozsnyai, L. F.; Wrighton, M. S.; Lieber, C. M., "Chemical Force Microscopy: Exploiting Chemically-Modified Tips to Quantify Adhesion, Friction, and Functional Group Distributions in Molecular Assemblies." *J. Am. Chem. Soc.* **1995,** 117, 7943-7951.

29. Barattin, R.; Voyer, N., "Chemical modifications of AFM tips for the study of molecular recognition events." *Chem. Commun.* **2008**, 1513-1532.

30. Danesh, A.; Davies, M. C.; Hinder, S. J.; Roberts, C. J.; Tendler, S. J. B.; Williams, P. M.; Wilkins, M. J., "Surface Characterization of Aspirin Crystal Planes by Dynamic Chemical Force Microscopy." *Anal. Chem.* **2000,** 72, 3419-3422.

31. Abendan, R. S.; Swift, J. A., "Surface Characterization of Cholesterol Monohydrate Single Crystals by Chemical Force Microscopy." *Langmuir* **2002,** 18, (12), 4847-4853.

32. Sheng, X.; Ward, M.; Wesson, J. A., "Adhesion between Molecules and Calcium Oxalate Crystals: Critical Interactions in Kidney Stone Formation." *J. Am. Chem. Soc.* **2003,** 125, 2854-2855.

33. Sheng, X.; Jung, T.; Wesson, J. A.; Ward, M. D., "Adhesion at Calcium Oxalate Crystal Surfaces and the Effects of Urinary Constituents." *Proc. Natl. Acad. Sci. USA* **2005,** 102, (2), 267-272.

34. Sheng, X.; Ward, M. D.; Wesson, J. A., "Crystal Surface Adhesion Explains the Pathological Activity of Calcium Oxalate Hydrates in Kidney Stone Formation." *J. Am. Soc. Nephrol.* **2005,** 16, 1904-1908.

35. Christmas, K. G.; Gower, L. B.; Khan, S. R.; El-Shall, H. E., "Aggregation and Dispersion Characteristics of Calcium Oxalate Monohydrate: Effect of Urinary Species." *J. Colloid and Interface Sci.* **2002,** 256, 168-174.

36. Cao, X.; Sun, C.; Thamann, T. J., "A Study of Sulfamerazine Single Crystals Using Atomic Force Microscopy, Transmission Light Microscopy, and Raman Spectroscopy." *J. Pharm. Sci.* **2005,** 94, (9), 1881-1892.

37. Wesson, J. A.; Ward, M. D., "Pathological Biomineralization of Kidney Stones." *Elements* **2007,** 3, 415-421.

38. Muster, T. H.; Prestidge, C. A., "Face Specific Surface Properties of Pharmaceutical Crystals." *J. Pharm. Sci.* **2002,** 91, (6), 1432-1444.

39. Smith, D. A.; Conell, S. D.; Robinson, C.; Kirkham, J., "Chemical Force Microscopy: Applications in Surface Characterization of Natural Hydroxyapatite." *Anal. Chim. Acta.* **2003,** 479, 39-57.

40. Robinson, C.; Connell, S.; Kirkham, J.; Shore, R.; Smith, A., "Dental enamel—a biological ceramic: regular substructures in enamel hydroxyapatite crystals revealed by atomic force microscopy." *J. Mater. Chem.* **2004,** 14, 2242-2248.

41. Perrin, D. D.; Dempsey, B., *Buffers for pH and Metal Ion Control*. John Wiley & Sons: New York, 1974.

42. Isaacson, L. C., "Urinary composition in calcific nephrolithiasis." *Invest. Urol.* **1969,** 6, (4), 356-363.

43. Sours, R. E.; Fink, D. A.; Swift, J. A., "Dyeing Uric Acid Crystals with Methylene Blue." *J. Am. Chem. Soc.* **2002,** 124, 8630-8636.

44. Sours, R. E.; Swift, J. A., "Uric Acid Crystals and Their Relationship to Kidney Stone Disease." *Trans. ACA* **2004,** 39, (9), 1-7.

45. Tortonese, M.; Kirk, M., "Characterization of application specific probes for SPMs." *Proc. SPIE* **1997,** 3009, 53-60.

46. Sinniah, S. K.; Steel, A. B.; Miller, C. J.; Reutt-Robey, J. E., "Solvent Exclusion and Chemical Contrast in Scanning Force Microscopy." *J. Am. Chem. Soc.* **1996,** 118, 8925-8931.

47. Thio, B. J. R.; Meredith, J. C., "Measurement of polyamide and polystyrene with coated-tip atomic force microscopy." *J. Colloid Interface Sci.* **2007,** 314, 52-62.

48. Smith, R. C.; Gore, J. Z.; McKee, M.; Howard, H., "The First Dissociation Constant of Uric Acid." *Microchem. J.* **1988,** 38, 118-124.

49. Mandel, N. S.; Mandel, G. S., "Monosodium Urate Monohydrate, the Gout Culprit." *J. Am. Chem. Soc.* **1976,** 98, 2319-2323.

50. Adair, J. H.; Aylmore, L. A. G.; Brockis, J. G.; Bowyer, R. C., "An Electrophoretic Mobility Study of Uric Acid with Special Reference to Kidney Stone Formation." *J. Colloid and Interface Sci.* **1988,** 124, (1), 1-13.

51. Bryant, M. A.; Crooks, R. M., "Determination of Surface pK_a Values of Surface-Confined Molecules Derivatized with pH-Sensitive Pendant Groups." *Langmuir* **1993,** 9, 385-387.

52. van der Vegte, E. W.; Hadziioannou, G., "Acid-Base Properties and Chemical Imaging of Surface-Bound Functional Groups Studied with Scanning Force Microscopy." *J. Phys. Chem. B* **1997,** 101, 9563-9569.

53. Chechik, V.; Crooks, R. M.; Stirling, C. J. M., "Reactions and Reactivity in Self-Assembled Monolayers." *Adv. Mater.* **2000,** 12, (16), 1161-1171.

54. Ronteltap, M.; Maurer, M.; Gujer, W., "Struvite precipitation thermodynamics in source-separated urine." *Water Research* **2007,** 41, 977-984.

55. Wang, Z.; Seidel, J.; Wolf, G.; Königsberger, R., "Dissolution enthalpies of uric acid and uric acid dihydrate." *Thermochim. Acta* **2000,** 354, 7-13.

56. Koka, R. M.; Huang, E.; Lieske, J. C., "Adhesion of Uric Acid Crystals to the Surface of Renal Epithelial Cells." *Am. J. Physiol. Renal Physiol.* **2000**, F989-F998.

CHAPTER 3 URIC ACID DIHYDRATE CRYSTAL GROWTH AND CHARACTERIZATION

3.1 Introduction

Uric acid is the most abundant organic component in human kidney stones. It exists in numerous forms under physiological conditions: anhydrous uric acid (UA),[1] uric acid monohydrate (UAM),[2] uric acid dihydrate (UAD),[1] and various salts such as monosodium urate monohydrate (MSU)[3]. Compositional studies of numerous kidney stone samples revealed that when UAD is present, it is almost always associated with UA.[1] Chapter 3 describes the crystal growth of UAD (Figure 3.1) from different solutions and its characterization.

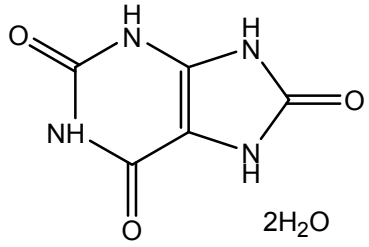

Figure 3.1. Molecular structure of uric acid dihydrate, $C_5H_4N_4O_3 \cdot 2H_2O$.

3.2 Experimental Methods and Materials

3.2.1 Materials

All chemical reagents were used as received and without further purification. Water was purified by passage through two Barnstead deionizing cartridges followed by distillation. Uric acid solutions of pH 4 were prepared from uric acid (>99%, Sigma), sodium acetate (99% EMD), and acetic acid (99.7%, EMD). Artificial urine[4] solution was prepared from Na_2SO_4 (99.9%, Sigma), KCl (99.0%, Sigma), NH_4Cl (99.8%, EM Science), $MgSO_4 \cdot 7H_2O$ (98-102%, EM Science), Na_2HPO_4 (99.5%, Fisher), $Na_2HPO_4 \cdot H_2O$ (99.1%,Fisher), NaCl (99%, EM Science), $Na_3C_6H_5O_7 \cdot 2H_2O$ (Certified, Fisher), and urea (Certified ACS, Fisher). For atomic absorption spectrophotometry (AAS) experiments, stock standard solutions of sodium, potassium, and magnesium were prepared from $NaNO_3$ (99.1%, Sigma-Aldrich), KNO_3 (99+%, Fisher), and $Mg(NO_3)_2 \cdot 6H_2O$ (100.1%, Fisher), respectively.

3.2.2 UAD Crystal Growth from Distilled Water

Crystals of uric acid dihydrate (UAD) were grown by dissolving 180-200 mg of uric acid (1-1.2 mM) in 1 L boiling distilled water as described in section 1.2.3.[5] The pH of the solution was buffered to 4.0 with sodium acetate and acetic acid and maintained at 25° C for 48 hours. UAD crystals were vacuum-filtered through Whatman #1 filter paper and air-dried.

3.2.3 UAD Crystal Growth from Various Salt Solutions

Supersaturated aqueous solutions were prepared by dissolving 18 mg of uric acid powder (1 mM) in 100 mL boiling water. Salt solutions of concentration ranging from 6-214 mM were

added to the uric acid solutions. The solutions were kept at 25° C and crystals were harvested after 48 hours. Similar growth of UAD in the presence of higher salt concentration (0.2-0.12 M) was described in previous work by Zellelow *et al*.[6] For clarity, we denote the crystals grown this way as **UAD-salt**.

3.2.4 UAD Crystal Growth from Artificial Urine Solutions

To mimic physiological conditions, UAD crystals were grown from artificial[4] urine solution (pH is 5.00-5.10). Artificial urine has previously been used as a growth medium for other crystalline materials found in kidney stones.[7-9] The concentration of model urine component is summarized in Table 3.1. Approximately 750 mg of uric acid powder (4.5 mM) was mixed in 1 L artificial urine solution. The solution was heated and stirred until the uric acid completely dissolved. The solution was then filtered and stored at two different temperatures: at room temperature (~25° C) for 4 days or in a 37° C water bath for 1 day. UAD crystals grew from both solutions, and were vacuum-filtered through Whatman #1 filter paper and air-dried.

In another crystal growth experiment, the same general procedure above was followed in which approximately 750 mg of uric acid powder (4.5 mM) was mixed in 1 L artificial urine solution. The solution was filtered, cooled, and pH was adjusted to 4.0 by adding acetic acid, and stored at room temperature (25° C) or in a 37° C water bath for 1 day. UAD crystals were vacuum-filtered through Whatman #1 filter paper and air-dried.

For crystals grown from artificial urine (**UAD-urine**), we use the nomenclature **UAD-urine**$^{\mathbf{T}}_{\mathbf{pH}}$ to denote the temperature and pH of the growth solutions. Table 3.2 lists all the UAD growth conditions and their respective nomenclature.

Table 3.1. Components of artificial urine solution.[4]

Species	Concentration (mM)
Na_2SO_4	14.9
KCl	92.6
NH_4Cl	65.1
$MgSO_4 \cdot 7\ H_2O$	6.7
Na_2HPO_4	1.8
$NaH_2PO_4 \cdot H_2O$	39.6
NaCl	213.9
$Na_3C_6H_5O_7 \cdot 2H_2O$	2.7
Urea	291.4

Table 3.2. UAD growth conditions and their respective nomenclature.

Growth condition	Nomenclature
Distilled water, 25°C, pH 4	$UAD^{25°C}_{pH4}$ or pure UAD
Artificial urine, 25°C, pH 4	$UAD\text{-}urine^{25°C}_{pH4}$
Artificial urine, 25°C, pH 5	$UAD\text{-}urine^{25°C}_{pH5}$
Artificial urine, 37°C, pH 4	$UAD\text{-}urine^{37°C}_{pH4}$
Artificial urine, 37°C, pH 5	$UAD\text{-}urine^{37°C}_{pH5}$

3.3 UAD Characterization

A wide variety of analytical techniques such as optical microscopy, hot stage microscopy, X-ray diffraction, thermal analysis, atomic absorption spectrophotometry and scanning electron microscopy attached to energy dispersive spectroscopy were employed to characterize UAD crystals.

3.3.1 Crystal Morphology

The morphology and size of UAD crystals varied depending on their growth conditions. Optical microscopy and X-ray diffraction techniques were used to characterize single crystal morphologies.

3.3.1.1 Optical Microscopy

All micrographs were taken using an Olympus BX-50 polarizing microscope fitted with a Nikon COOLPIX995 digital camera operated with krinnicam_v1-03 software (Nikon Corp). Figures 3.2, 3.3 and 3.4 show the morphology of UAD crystals grown from distilled water (**UAD$^{25°C}_{pH4}$**), various salt solutions (**UAD-salt**) and artificial urine solution (**UAD-urine**), respectively. **UAD$^{25°C}_{pH4}$** crystals and **UAD-salt** crystals are mostly ~100-200 μm rectangular plates while **UAD-urine** crystals have more variable sizes and morphologies ranging from elongated plates to needles. Distinct needle-like crystals were observed for **UAD-urine$^{25°C}_{pH4}$** (Figure 3.4a).

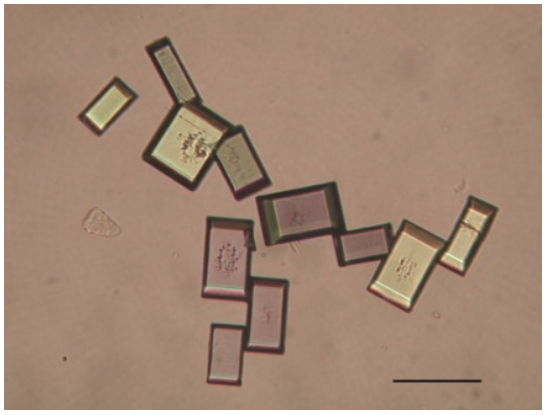

Figure 3.2. Photomicrograph of UAD crystals grown from distilled water. Scale bar = 100 μm.

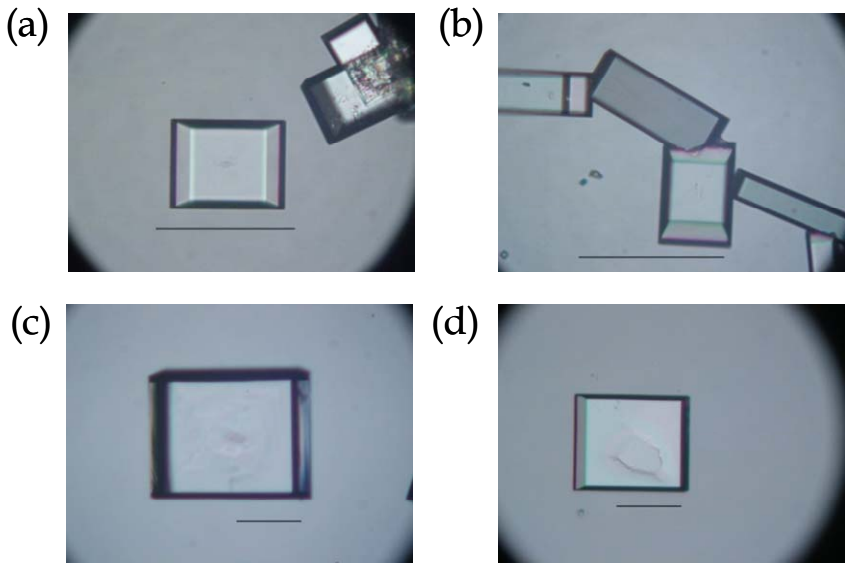

Figure 3.3. Photomicrographs of UAD grown from salt solutions. (a) With 92.6 mM KCl; (b) With 6.7 mM $MgSO_4 \cdot 7H_2O$; (c) With 213.9 mM NaCl; (d) With 65.1 mM NH_4Cl. Scale bar = 100 µm.

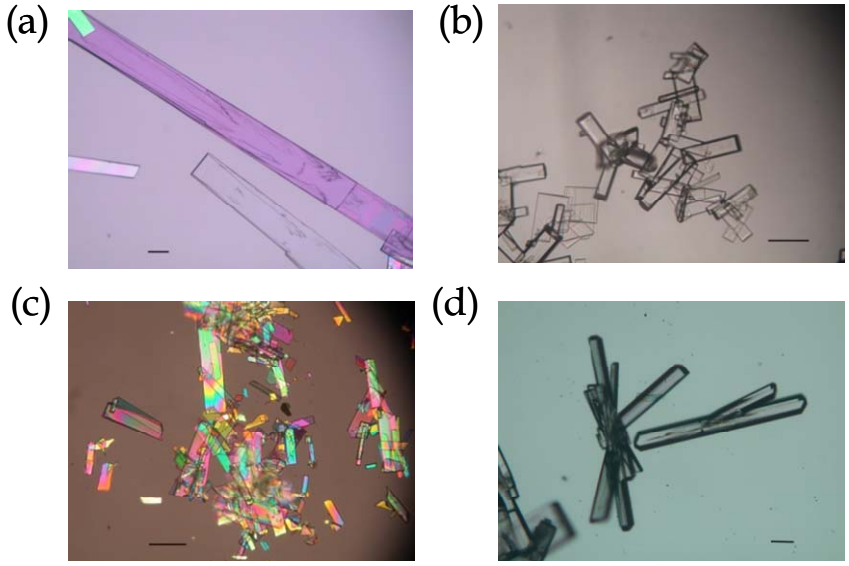

Figure 3.4. Photomicrograph of UAD crystals grown from artificial urine. (a) UAD-urine$^{25°C}{}_{pH4}$; (b) UAD-urine$^{37°C}{}_{pH4}$; (c) UAD-urine$^{25°C}{}_{pH5}$, (d) UAD-urine$^{37°C}{}_{pH5}$. Scale bar = 100 µm.

Aside from morphology changes, different uric acid phases crystallize at the same temperature in different solutions. UAD crystallizes in supersaturated aqueous uric acid solution (1.0 mM) stored at 25° C, while UA crystallizes at 37° C. In artificial urine solution, UAD crystallizes in both 25° C and 37° C when the supersaturation of uric acid in solution is high, such as the 4.5 mM that was used in this study. At low supersaturation (1.3 mM), UA can crystallize in pH 5.5 artificial urine solution at 37° C as reported by Grases *et al*.[9]

3.3.1.2 Single Crystal Face Indexing

Previous work[10] characterized the morphology of UAD grown from distilled water. UAD crystals grown from artificial urine were examined by single crystal X-ray diffraction (Bruker SMART or APEX Platform CCD diffractometer) to determine the crystal faces. APEX2 software was used for crystal face indexing. After unit cell determination, a video is collected as the crystal is spun 360 degrees around the instrument's Phi axis. When the video is fully collected, the face indexing initial view will appear. The user can then rotate the crystal within the software using a dial control at the bottom of the screen. The software notes when particular planes should be visible in these images based on the video camera's orientation relative to the determined unit cell. The user can then mark when these faces are clearly perpendicular to the viewer thus assigning Miller Indices to the faces. As more faces are defined, the software displays a graphical model superimposed over the video images (Figure 3.5). Crystallographic faces can be input into the software and thus placed onto the image to check if known faces are present or to determine if one of two similar faces is a better match. WinXMorph[11] (Figure 3.6) was then used to draw the morphology of the crystal that had been indexed with APEX2 software.

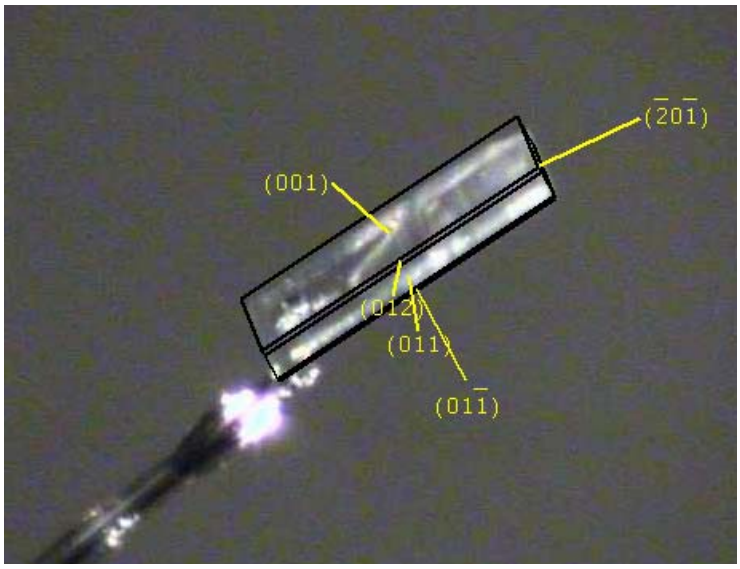

Figure 3.5. Screen capture from APEX2 showing representative indexing of a UAD-urine$^{25°C}{}_{pH4}$ crystal.

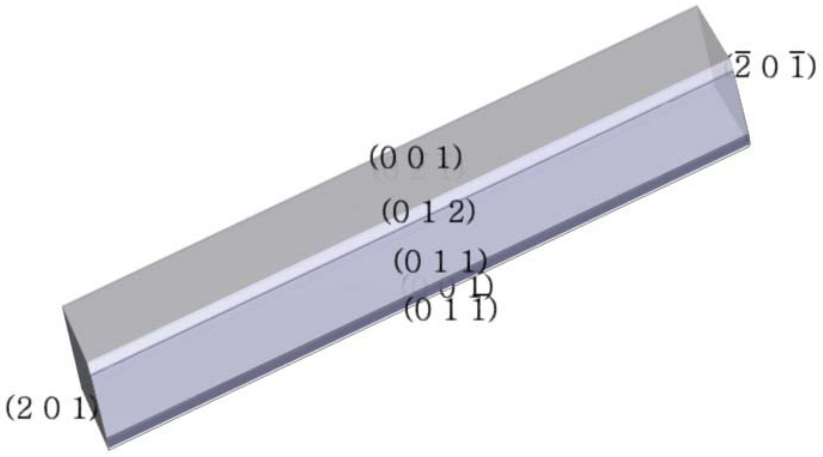

Figure 3.6. WinXMorph[11] generated schematic of the UAD crystal indexed in Figure 3.5.

Figure 3.7 shows the schematic of the UAD crystals grown from different solutions. **UAD-urine** crystals showed faces that are also found in **UAD$^{25°C}_{pH4}$**. Although new faces appear in **UAD-urine** crystals, the largest face for both elongated plate (Figure 3.7 b) and needle-like crystals (Figure 3.7 c) is (001) similar to what was observed in **UAD$^{25°C}_{pH4}$** (Figure 3.7a).

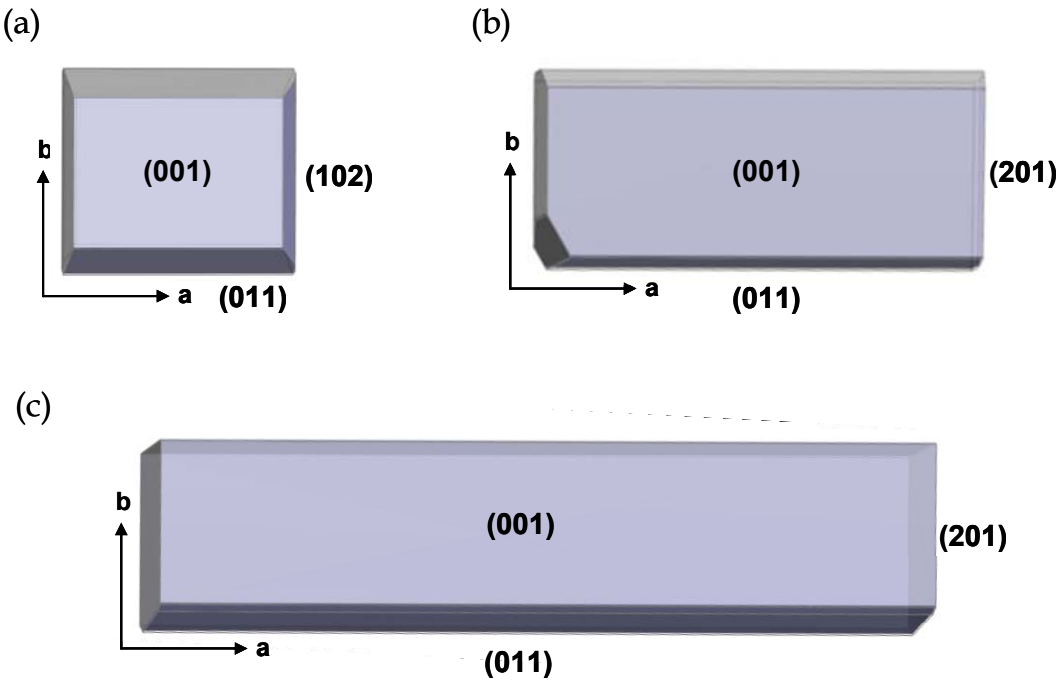

Figure 3.7. Schematic of the UAD crystals grown from different solutions. (a) UAD$^{25°C}_{pH4}$ (b) UAD-urine$^{37°C}_{pH4}$; (c) UAD-urine$^{25°C}_{pH4}$.

We also tried a full data collection at 100 K on single crystals of UAD grown from artificial urine which exhibited cell axes of a = 7.2135 (2) Å, b = 6.3788 (19) Å, c = 17.4563 (5) Å. Parkin and Hope reported a crystal structure collected at 120 K of UAD grown from distilled water with cell dimensions of a = 7.237 (3) Å, b = 6.363 (4) Å, c = 17.449 (11) Å.[12] The similar cell

parameters of both determinations unambiguously indicated that the crystals grown from artificial urine are UAD.

Other uric acid phases found in physiologic condition are also known to form as needle-like crystals. One such example is monosodium urate monohydrate (MSU).[3] However, the cell dimensions of a = 10.888 (5) Å, b = 9.534 (3) Å, c = 3.567 (1) Å for MSU are different from those obtained for crystals grown in artificial urine solution. Clearly, the crystals that deposit from artificial urine solutions are UAD based on the cell parameters obtained. Thermal analysis and powder diffraction data which are described in section 3.3.3 and 3.3.4, respectively, further supported this finding.

3.3.2 Hot Stage Microscopy

Previous work used hot stage microscopy to examine the isothermal dehydration of pure UAD crystals.[13] Dehydration experiments were performed on **UAD-urine** crystals using an HS1-STCC20A hot stage regulated by an STC200 standalone temperature controller (Instec, Inc.). UAD crystals were placed on 1 mm thick microscope glass slides before placement on the heating stage. The dehydration was monitored by heating the single crystals from room temperature to 200° C at 10° C/min while collecting sequential photomicrographs over regular time intervals. The heating stage was calibrated against known standards and has a standard deviation of 1° C over the temperature range used.

UAD-urine crystals are mostly plates and needles with elongated a-axes. In one 3700 μm crystal along a-axis (Figure 3.8), numerous cracks form parallel to the b-axis and the crystals turn opaque during the course of heating. This is due to dehydration and the conversion to

polycrystalline UA. This anisotropy in the crack direction is similar to what has been previously observed in rectangular UAD crystals grown in distilled water.[13] The needle-like **UAD-urine** crystals appears to bend at temperatures ranging from 84.5° to 200° C.

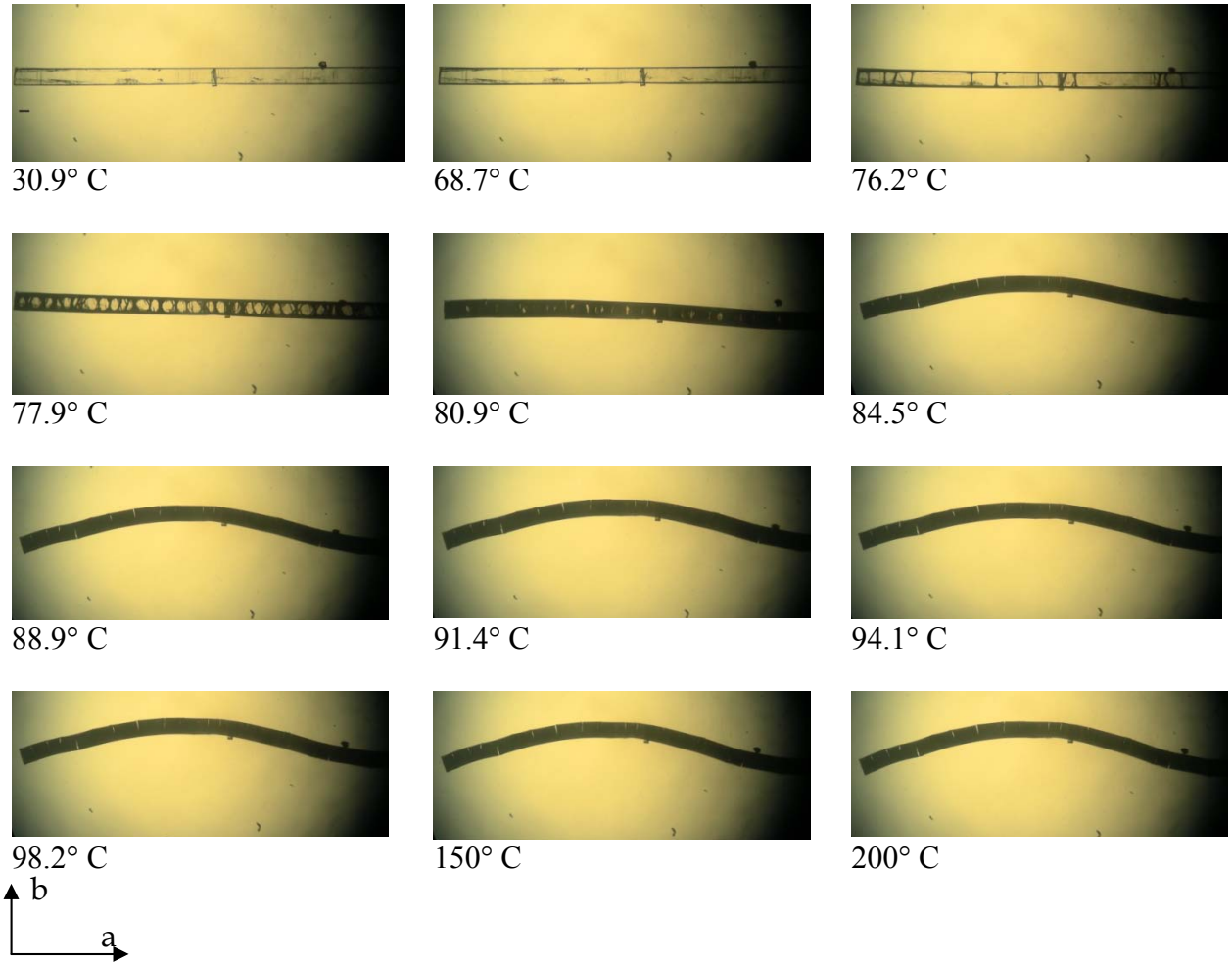

Figure 3.8. Hot stage microscopy images of UAD-urine$^{25°C}_{pH4}$ subjected to heating up to 200° C. The crystal is viewed through the (001) face with the ± *a* axis horizontal and ±*b* axis vertical. Scale bar = 100 µm.

3.3.3 Thermal Properties

3.3.3.1 Thermogravimetric Analysis

Thermogravimetric analyses were performed on a SDT Q600 TA instrument (New Castle, DE). Samples were analyzed in an alumina pan from room temperature to 150° C at 10° C/min under a stream of nitrogen gas. A nitrogen flow rate of 50 mL/min was used and each set of experiments was performed in triplicate. All the experiments were conducted using open 90 μL alumina pans (TA instruments). Samples were used without sieving or grinding. All experimental curves were analyzed with TA's Universal Analysis Software. Figure 3.9 shows a typical TGA scan of **UAD**$^{\mathbf{25°C}}_{\mathbf{pH4}}$ and **UAD-urine**$^{\mathbf{37°C}}_{\mathbf{pH5}}$. In the majority of the TGA scans, the onset temperature for UAD dehydration from distilled water occur several degrees earlier than in the UAD crystals grown from artificial urine solution. However, there is no significant difference in the initial weight loss for both UAD crystals. The amount of residual water removed at the tail end of the curve is also comparable at typically ~1% for both crystals.

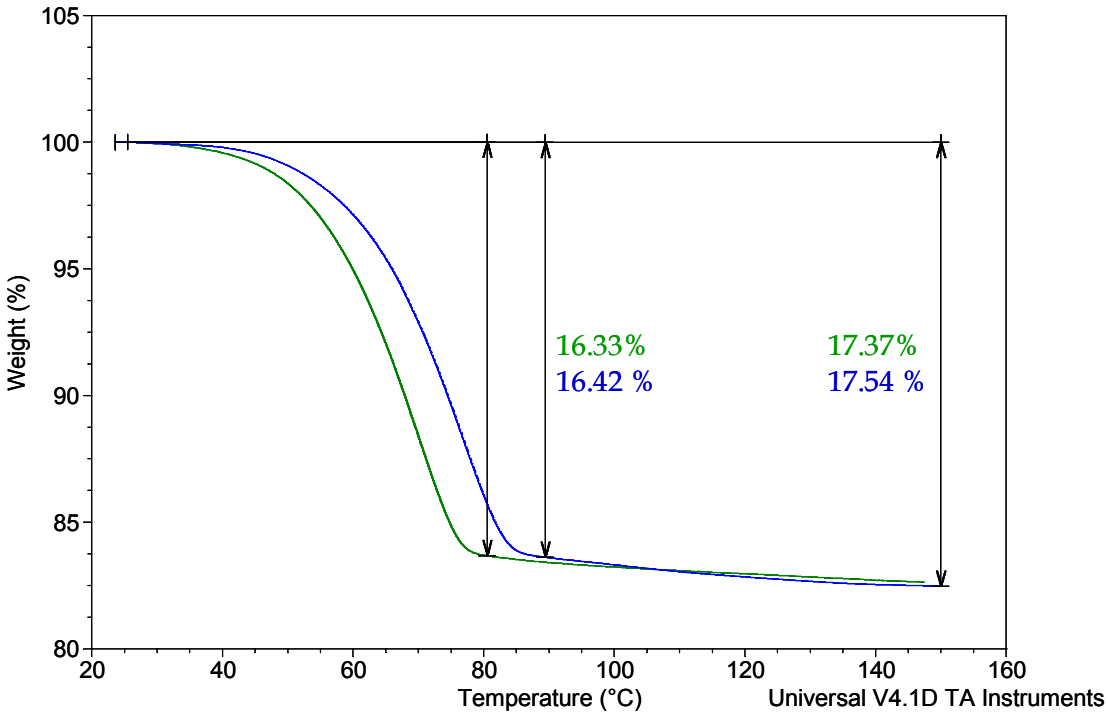

Figure 3.9. TGA curve of the dehydration of UAD$^{25°C}_{pH4}$ (green) and UAD-urine$^{37°C}_{pH5}$ (blue). The presence of two water molecules is shown by a weight loss of 17.37 and 17.54 % (theoretical weight loss is 17.65%).

3.3.3.2 Differential Scanning Calorimetry

The dehydration process can in principle be affected by factors such as crystal morphology and size. Experiments aimed at assessing dehydration as a function of crystal size were performed on a TA Instruments 2900 DSC equipped with a RCS cooler (New Castle, DE). **UAD-urine$^{25°C}_{pH4}$** crystals were vacuum filtered, quickly air-dried, and then separated using a mini-sieve (Fisher Scientific, USA) into groups with eight different size ranges: 25 mesh = 710-500 μm; 35 mesh = 500-355 μm; 45 mesh = 355-250 μm; 60 mesh = 250-180 μm; 80 mesh = 180-125 μm; 120 mesh = 125-90 μm; 170 mesh = 90-62 μm, and ≤ 62 μm. Samples (2-3 mg) were placed in hermetic

aluminum pans and loosely sealed with a manual press. To prevent crushing the crystals, the pans were capped with the lid forming a "top-hat"-like shape leaving some space between the lid and the crystals. A similarly sealed empty hermetic pan was used as a reference. All experiments were run in triplicate with a temperature ramping mode of 10.0° C/min from room temperature to 150° C. The DSC cell was continuously purged with nitrogen gas at 50 mL/min. The instrument temperature was calibrated against indium, zinc, and tin standard metals. All temperatures cited refer to peak temperatures, not onset temperatures. All experimental curves were analyzed with TA's Universal Analysis Software.

The DSC of **UAD-urine$^{25°C}_{pH4}$** crystals resulted in a single endothermic peak with T_m at 100.84° C (±1.12), 100.63° C (±1.85), 101.09° C (±0.47), 98.64° C (±1.20), 98.76° C (±1.36), 89.96° C (±0.54), 90.78° C (±0.55), and 90.34° C (±0.15) for each of the eight groups in decreasing size, respectively (Table 3.3). The observed dehydration temperatures suggest that the contribution of any particle size effects to the overall dehydration temperature for crystals >125 μm is relatively small. Similarly, crystals <125 μm had a similar dehydration temperature, though it was ~10^o lower for the smaller crystals. The significant difference in the dehydration may be due to several factors. Small crystals might nucleate later than large ones giving them either a different impurity content or degree of perfection (from slower growth). Alternatively, decrease in dehydration may be due to the fractured nature of the crystals which pass through many sieves. Small crystals tend to have significantly more cracks/less perfect edges after sieving. In previous work by Zellelow *et al.,* DSC of unsieved UAD crystals grown from distilled water showed a single endothermic peak at an average temperature of 87.39° C (± 0.20).[13]

Table 3.3. Uric acid dihydrate dehydration temperatures.

Size of crystal, μm	Dehydration temperature, T_m (°C) grown from artificial urine	Dehydration temperature, T_m (°C) grown from distilled water[13]
710-500	100.84 ± 1.12	
500-355	100.63 ± 1.85	
355-250	101.09 ± 0.47	
250-180	98.64 ± 1.20	
180-125	98.76 ± 1.36	90.97 ± 1.63
125-90	89.96 ± 0.54	89.90 ± 0.11
90-62	90.78 ± 0.55	89.55 ± 0.52
≤ 62	90.34 ± 0.15	
Unsieved		87.39 ± 0.20

The dehydration changes of UAD crystals grown from distilled water was also examined as a function of particle size.[13] UAD crystals with size ranges of 180-125 μm, 125-90 μm, and 90-62 μm showed dehydration of 90.97° C (± 1.63), 89.90° C (± 0.11), and 89.55° C (± 0.52), respectively (Table 3.3). The ~1° C difference in the dehydration temperature at these size ranges suggested that the contribution of particle size effect is relatively small. Interestingly, the dehydration temperatures observed for UAD crystals grown from artificial urine solution are higher than those grown from distilled water at all sizes. This suggests something fundamentally different about the materials. Matrix inclusion of ionic species present in artificial urine was hypothesized to be the source of the temperature differences in urine and aqueous grown UAD crystals.

3.3.4 Powder X-ray Diffraction

Powder X-ray diffraction analyses were performed on different UAD samples at room temperature on a Rigaku R-AXIS RAPID-S X-ray diffractometer using Cu Kα radiation with

40kV tube voltage and 30 mA tube current. The samples were prepared by packing them in 0.5 mm glass capillaries (Charles Super Company). Each capillary was mounted onto a goniometer head that is motorized to permit spinning of the capillary during data acquisition. Using a 0.3 mm collimator, the data was collected for 1 hour with a Phi spin rate of 1° per second. The diffraction pattern was integrated over a 2θ range from 4° to 50° with a step size of 0.01 degrees. Data analysis was performed using Rigaku RAPID/XRD Version 2.3.3, AreaMax software and Jade v5.035 software (Material Data Inc.). Since sample grinding may contribute to the premature dehydration of UAD, all PXRD analyses were performed on unground samples.

The powder X-ray diffraction patterns for UAD grown from distilled water and artificial urine along with UAD calculated pattern are shown in Figure 3.10. Characteristic diffraction lines of (002), (011), (102), (112), (210), and (21-1) are observed in all powder data.

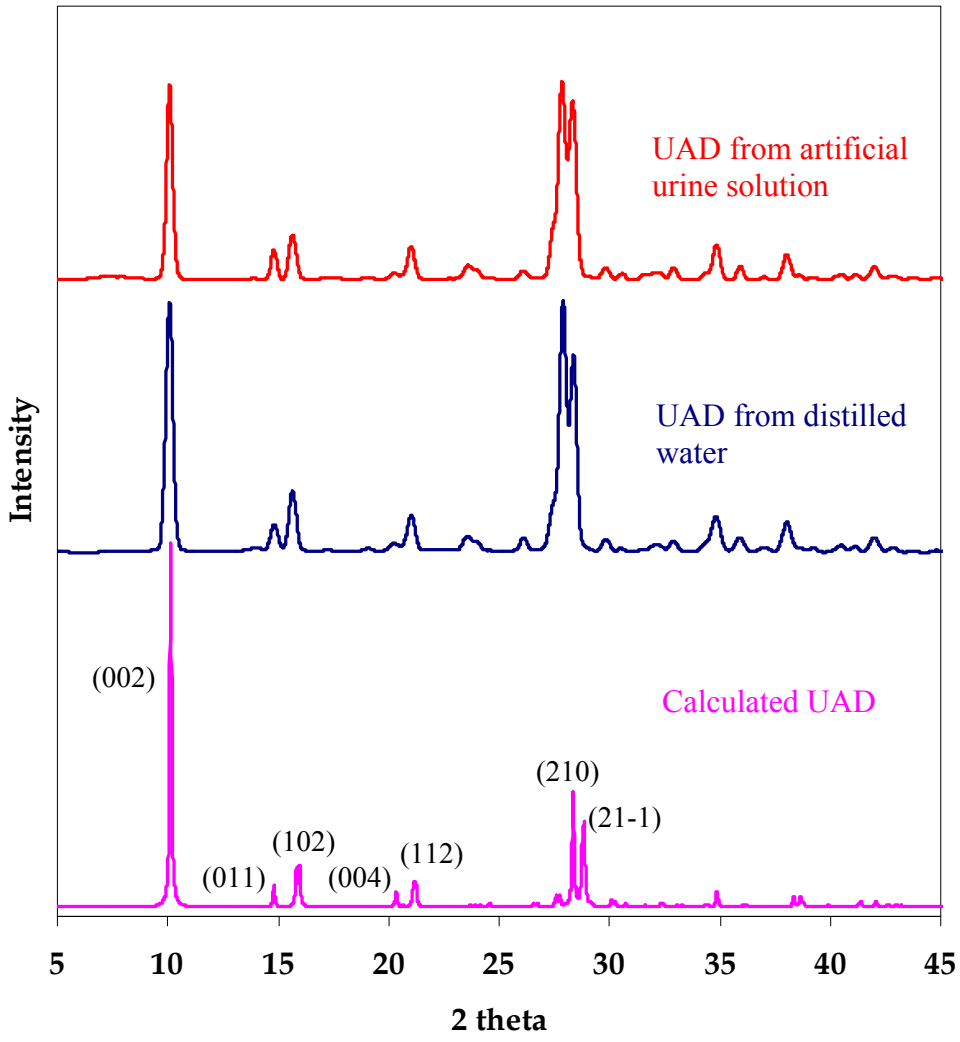

Figure 3.10. UAD calculated pattern (bottom), UAD grown from distilled water (middle), UAD grown from artificial urine (top).

PXRD data were also collected for **UAD-urine**$^{25°C}{}_{pH4}$ crystals that were sieved into different mesh sizes. PXRD were performed at room temperature on a Rigaku Ultima IV Xray Diffractometer using Cu Kα radiation with 40 kV tube voltage and 44 mA tube current. PXRD data was analyzed using Jade v9 software. PXRD was performed on both unground and ground samples. The diffraction data on unground samples for all UAD size ranges are the same, but

they all showed preferred orientation. To clearly assess the diffraction patterns of the different UAD crystal sizes, PXRD was performed on ground samples. Their diffraction patterns along with the UAD grown from distilled water, and calculated UAD and UA patterns are depicted in Figure 3.11. Characteristic diffraction lines of UAD (002), (011), (102), (112), (210), and (21-1) are observed in the **UAD-urine**$^{25°C}_{pH4}$ crystals at all sizes. The appearance of a diffraction line that seemed to coincide with UA (11-1) we attribute to premature dehydration of UAD on ground samples.

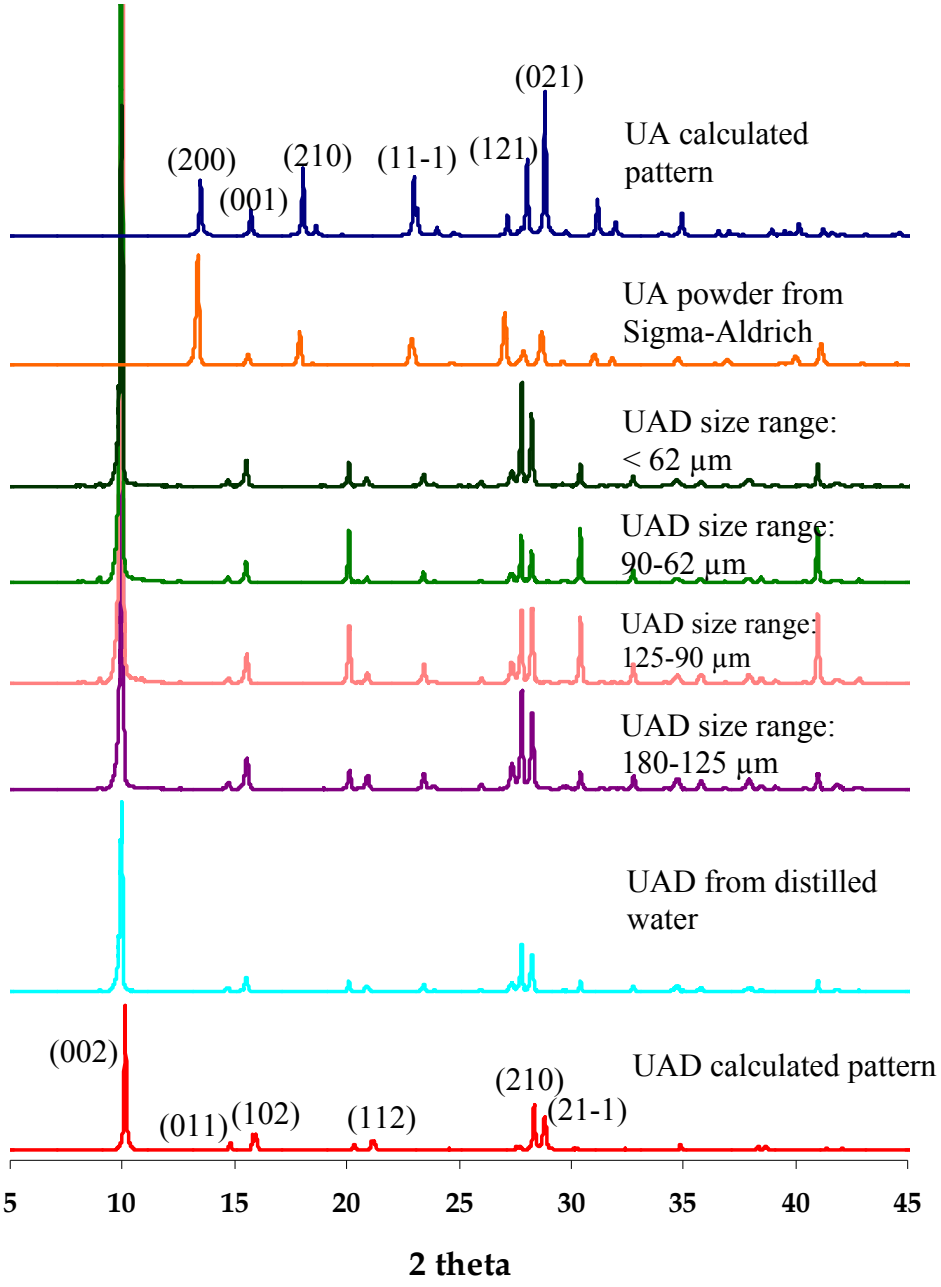

Figure 3.11. PXRD patterns of the different size ranges of **UAD-urine$^{25°C}_{pH4}$** crystals. Diffraction patterns of these crystals are compared to UAD from distilled water, calculated UAD (bottom), and calculated UA (top).

3.3.5 Atomic Absorption/Emission Spectrophotometry

Atomic absorption/emission spectrophotometry (AAS/AES) is an analytical technique that is highly specific for the analysis of metals in various matrices. The method is based on the selective absorption/emission of line radiation by atomic species in the vapor phase. Samples were analyzed for their Na, K, and Mg content.

3.3.5.1 Standard Preparation

A 1000 ppm sodium stock solution was prepared by dissolving 0.9243 g of $NaNO_3$ in 250 mL of 0.3 M HNO_3. A 1000 ppm potassium stock solution was made by dissolving 0.6465 g of KNO_3 in 250 mL of 0.3 M HNO_3. A 1000 ppm magnesium stock solution was prepared by dissolving 2.6380 g $Mg(NO_3)_2 \cdot 6H_2O$ in 250 mL of 0.3 M HNO_3. All stock standard solutions were stored in polyethylene bottles. Intermediate standard solutions of 100 ppm and 10 ppm were prepared from the stock standard solutions. Individual solutions over the range 0.0 to 2.0 ppm of each element in 0.3 M HNO_3 were prepared from 10 ppm intermediate standard solutions.

3.3.5.2 Sample Preparation

UAD-urine crystals (49.9 - 50.9 mg) were dissolved in 1 mL concentrated HNO_3 and diluted to 50 mL in a volumetric flask. Samples were prepared in triplicate.

3.3.5.3 Analysis

All experiments were carried out with a Buck Scientific 200A spectrophotometer. The analytical wavelength was set to the manufacturer's recommended conditions for sodium,

potassium, and magnesium at 579 nm, 766.5 nm, and 285 nm, respectively. At the optimized operating conditions, the atomic absorption spectrophotometer was zeroed against a 0.3 M HNO_3 solution. Calibration curves for each metal were prepared by aspirating the standard solutions into an air-acetylene flame and recording the absorbance or emission of all solutions. The absorbance or emission of the sample solutions were then measured using the same conditions that were used for the preparation of the calibration curves. Potassium and magnesium were determined in absorption mode, while sodium was determined in emission mode because a hollow cathode lamp for the analysis of sodium was not available.

Table 3.4 shows the cation content in **UAD-urine** crystals. The reported values are averages and standard deviations of three samples per growth condition. All growth conditions resulted in inclusion of Na^+, K^+, and Mg^{2+}, though the concentrations varied. For all the cations studied, greater ionic inclusion was observed at higher pH. For every 10^7 UAD molecules, 17-117 Na^+, 7-67 K^+ and 3-7 Mg^{2+} were present. Urate ions are presumably also included for charge balance. The higher ion load seen at higher solution pH may be related to the highest urate concentration at these pH values.

Table 3.4. Cation content in UAD grown from artificial urine solution of varying pH and temperature.

Crystal	mg Na^+/ kg UAD	mg K^+/ kg UAD	mg Mg^{2+}/ kg UAD	Total ion inclusion (mg/kg)
UAD-urine$^{25°C}_{pH4}$ (n=3)	0.078 ± 0.008	0.354 ± 0.117	0.049 ± 0.016	0.481
UAD-urine$^{25°C}_{pH5}$ (n=3)	1.323 ± 0.022	1.279 ± 0.046	0.062 ± 0.003	2.664
UAD-urine$^{37°C}_{pH4}$ (n=3)	0.136 ± 0.199	0.134 ± 0.051	0.032 ± 0.004	0.302
UAD-urine$^{37°C}_{pH5}$ (n=3)	0.415 ± 0.081	1.174 ± 0.311	0.079 ± 0.005	1.668

It is worthwhile to compare the ionic inclusions in UAD crystals grown in artificial urine solutions to those grown in salt solutions of varying concentration. Zellelow *et al.*[6] doped UAD crystals with Na^+, K^+, Ca^{2+}, and Mg^{2+} using salt concentration ranging from 0.02 to 0.12 M. The morphologies of these doped crystals (**UAD-salt**) are similar to those grown from pure aqueous solutions. The concentrations of Na^+, K^+, and Mg^{2+} dopant included in the matrix were found to be 14-33 Na^+, 5-10 K^+, and 13-19 Mg^{2+} for every 10^4 uric acid molecules. In these systems, the amount of dopant included generally increased with solution concentration. Direct comparison of dopant levels in **UAD-urine** and **UAD-salt** solutions have some caveats. Ionic inclusions in **UAD-salt** crystals are ~3 orders of magnitude higher than the **UAD-urine** crystals. However, the **UAD-salt** growth solutions contained much higher initial salt concentrations than those in the

UAD-urine experiments. **UAD-urine** crystals also include multiple types of cations simultaneously.

In addition to differences in ionic inclusion behavior, a comparison can also be made between the dehydration temperatures observed in **UAD-urine** crystals and previous work[14] on **UAD-salt** crystals doped with Na^+, K^+, and Mg^{2+} ions. **UAD-salt** crystals were obtained from growth in aqueous solutions with 0.02-0.12 M single salt concentrations. The majority of the **UAD-salt** samples showed little change in the dehydration temperature compared to pure UAD, although a modest increase in the dehydration temperature (90-91^o C) was exhibited in some samples grown from KCl, $MgCl_2$ and $MgSO_4$ solutions.[14] Interestingly, dehydration of the largest size range **UAD-urine** crystals showed a dehydration temperature of ~10° higher than that for pure UAD or **UAD-salt**. We hypothesize that this is likely due to either particle size effects and/or the cooperative inclusion of multiple types of cations in the UAD crystal matrix.

3.3.6 Scanning Emission Microscopy-Energy Dispersive Spectroscopy

Uric acid dihydrate was mounted onto a 12 mm double stick carbon circles (M.E. Taylor Engineering, Inc.) attached to an aluminum SEM mounting stub (M.E. Taylor Engineering, Inc.). An Oxford Instruments energy dispersive X-ray spectrometer attached to a Zeiss Supra™ 55VP Scan Electron Microscope operated at 20 kV was used to analyze metal ion content in uric acid dihydrate.

SEM photographs in Figure 3.12 revealed that UAD undergo partial dehydration to UA under the application of heat and vacuum, and hence the observed cracking of UAD crystal in Figure 3.12c. No Mg^{2+} was evident on any of the crystals examined, though atomic percent of up to

0.06 % Na and 0.04% K were detected. The absence of Mg^{2+} is likely due to the detection limits of the instrument. This is consistent with the noticeably lower Mg^{2+} concentrations observed (relative to K^{+} and Na^{+}) in the AAS experiments as well.

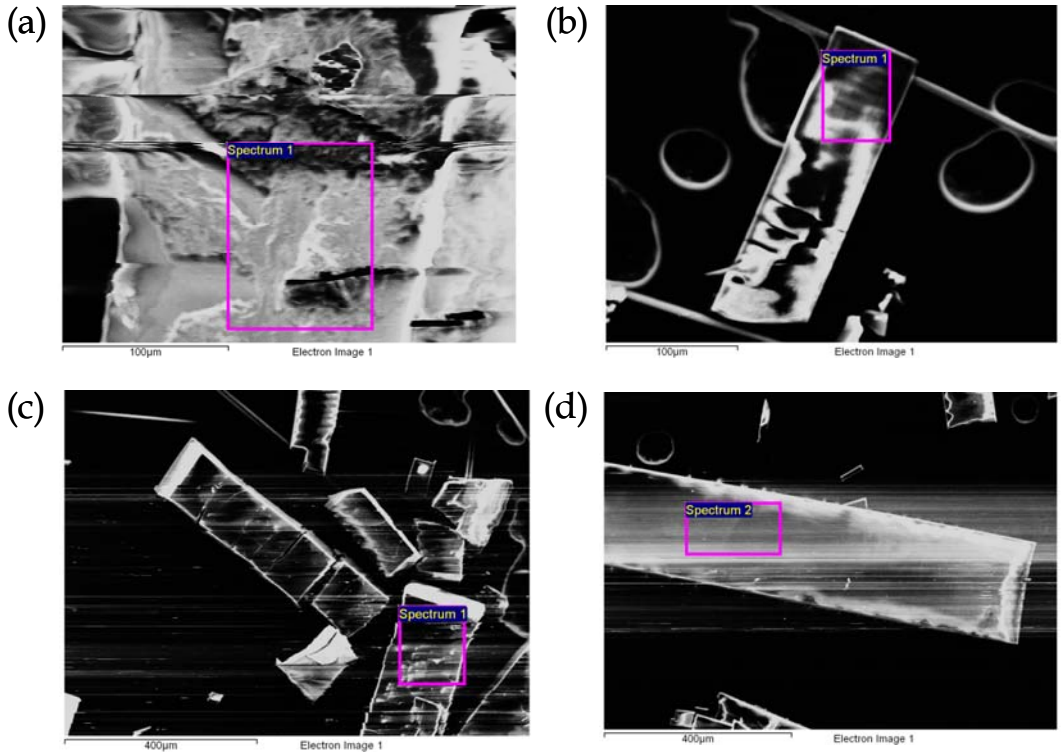

Figure 3.12. SEM micrograph of UAD crystals grown from artificial urine. (a) UAD-urine$^{25°C}{}_{pH4}$; (b) UAD-urine$^{25°C}{}_{pH5}$; (c) UAD-urine$^{37°C}{}_{pH4}$; (d) UAD-urine$^{37°C}{}_{pH5}$. Scale bar for *a* and *b* = 100 µm, for *c* and *d* = 400 µm.

3.4 Conclusions

UAD crystals were grown in solutions of different composition. The morphology, size, impurity and thermal stability of UAD crystals grown from various solutions show some similarities and differences. In general, UAD deposit as clear, colorless, rectangular plates from all solutions. Crystals from distilled water are typically 100-300 μm with a slight elongation along the *a* axis. UAD grown from artificial urine solution are elongated along the *a* axis resulting in a needle-like morphology with an aspect ratio sometimes as high as 40:1 (a:b). The large faces of these crystals are not new but their relative sizes vary.

Inorganic impurities in the growth solution such as Na^+, K^+, and Mg^{2+} are included into UAD crystals. Artificial urine-grown UAD crystals seem to include more monovalent cations than divalent cations, and greater amounts of cation inclusion are found in higher pH solutions. Inclusion of these dopants alters the dehydration temperature of the crystals. The inclusion of Na^+, K^+ and Mg^{2+} ions along with urate seem to impart additional thermal stability to the UAD crystals, presumably because it replaces H-bonding interactions with stronger electrostatic interactions which must be overcome to effect dehydration.

Crystal growth in artificial urine has been adapted in various studies of crystallization of materials responsible for kidney stone formation. Urine is a complex mixture composed of a wide variety of ionic salts, organic compounds, and macromolecules. We used model urine solution composed mostly of inorganic salts that closely mimic human urine. Understandably, the physio-chemical characteristics of urine may be quite different from the synthetic inorganic

solutions. Uric acid precipitated *in vivo* contain many other types of impurities[15, 16] which may also serve to alter their physical properties relative to laboratory grown samples.

3.5 References

1. Lonsdale, K.; Mason, P., "Uric Acid, Uric Acid Dihydrate, and Urates in Urinary Calculi, Ancient and Modern." *Science* **1966,** 152, 1511-1512.

2. Schubert, G.; Reck, G.; Jancke, H.; Kraus, W.; Patzelt, C., "Uric acid monohydrate - a new urinary calculus phase." *Urol. Res.* **2005,** 33, 231-238.

3. Mandel, N. S.; Mandel, G. S., "Monosodium Urate Monohydrate, the Gout Culprit." *J. Am. Chem. Soc.* **1976,** 98, 2319-2323.

4. Isaacson, L. C., "Urinary composition in calcific nephrolithiasis." *Invest. Urol.* **1969,** 6, (4), 356-363.

5. Sours, R. E.; Fink, D. A.; Swift, J. A., "Dyeing Uric Acid Crystals with Methylene Blue." *J. Am. Chem. Soc.* **2002,** 124, 8630-8636.

6. Zellelow, A. Z.; Abiye, M.; Fink, D. A.; Ford, C. E.; Kim, K.-H.; Sours, R. E.; Yannette, C. M.; Swift, J. A., "Doping Uric Acid Crystals. 1. Uric Acid Dihydrate." *Cryst. Growth. Des.* **2010,** 10, 3340-3347.

7. Opalko, F. J.; Adair, J. H.; Khan, S. R., "Heterogeneous nucleation of calcium oxalate trihydrate in artificial urine by constant composition." *J. Crystal Growth* **1997,** 181, 410-417.

8. Lee, T.; Lin, Y. C., "Mimicking the Initial Development of Calcium Urolithiasis by Screening Calcium Oxalate and Calcium Phosphate Phases in Various Urinelike Solutions, Time Points, and pH Values at 37^{o}C." *Cryst. Growth. Des.* **2011,** 11, 2973-2992.

9. Grases, F.; Villacampa, A. I.; Costa-Bauzá, A.; Söhnel, O., "Uric acid calculi: types, etiology and mechanisms of formation." *Clin. Chim. Acta.* **2000,** 302, 89-104.

10. Boistelle, R.; Rinaudo, C., "Phase transition and epitaxies between hydrated orthorhombic and anhydrous monoclinic uric acid crystals." *J. Cryst. Growth* **1981,** 53, 1-9.

11. Kaminsky, W., "WinXMorph: a computer program to draw crystal morphology, growth sectors and cross-sections with export files in VRML V2.0 utf8-virtual reality format." *J. Appl. Crystallogr.* **2005,** 38, 566-567.

12. Parkin, S.; Hope, H., "Uric Acid Dihydrate Revisited." *Acta Cryst.* **1998,** B54, 339-344.

13. Zellelow, A. Z.; Kim, K.-H.; Sours, R. E.; Swift, J. A., "Solid-State Dehydration of Uric Acid Dihydrate." *Cryst. Growth. Des.* **2010,** 10, 418-425.

14. Zellelow, A. Z. Crystallization and Phase Transformation of Uric Acids. Georgetown University, Washington, DC, 2010.

15. Coe, F. L.; Evan, A.; Worcester, E., "Kidney stone disease." *J. Clin. Invest.* **2005,** 115, 2598-2608.

16. Pinto, B.; Rocha, E.; Ruiz-Marcellan, F. J., "Isolation and characterization of uricine from uric acid stones." *Kid. Interl.* **1976,** 10, 437-443.

CHAPTER 4 SOLUTION-MEDIATED PHASE TRANSFORMATIONS OF URIC ACID DIHYDRATE

4.1 Introduction

Uric acid, a product of protein metabolism, is the most abundant organic component in human kidney stones. Different forms of uric acid occur under physiological conditions, including anhydrous uric acid (UA)[1], uric acid monohydrate (UAM)[2], uric acid dihydrate (UAD)[1], and various salts such as monosodium urate monohydrate (MSU)[3]. Previous work by Zellelow *et al.*[4] have shown that UAD (Figure 4.1) is metastable and readily dehydrates to UA in air. Compositional analysis of kidney stones revealed that when UAD is present, it is generally found associated with the anhydrous phase.[1] This suggests that phase transformation may also occur under physiologic deposition conditions. The purpose of this work is to assess the kinetics of this transformation under model solution conditions. In Chapter 5, the effect of impurities on the phase transformation is investigated.

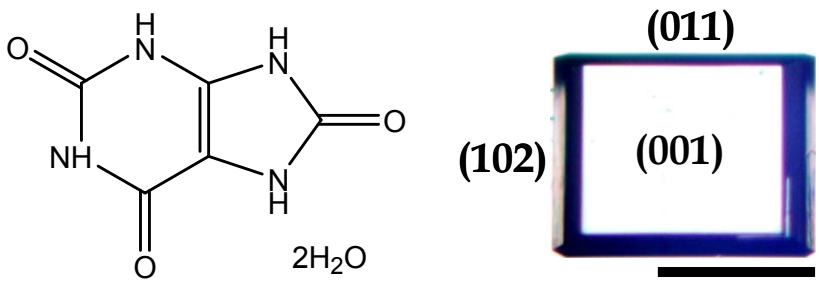

Figure 4.1. Molecular structure and typical plate-like morphology of uric acid dihydrate grown from distilled water. Scale bar = 100 μm.

Several structural determinations of UAD have been reported in the past. The first complete crystal structure of UAD, determined from a human urinary sediment sample by Artioli *et al.*[5] assigned it to an orthorhombic space group *Pnab* (a = 7.409 (1), b = 17.549 (3), c = 6.332 (1) Å). The structure of a laboratory grown UAD crystal was later reported by Parkin and Hope as having a disordered monoclinic unit cell, with a $P2_1/c$ space group and a = 7.237 (3) Å, b = 6.363 (4) Å, c = 17.449 (11), Å, and β=90.51 (1)°.[6] Both structures are nearly identical topologically, though we refer to the latter cell parameters in our discussion. In this structure, hydrogen-bonded uric acid molecules form parallel ribbons in the *ab* plane and are separated by layers of water (Figure 4.2). Water molecules are hydrogen-bonded to both N2 and N4, and all 3 oxygen atoms of the uric acid molecules. O1 and O3 form a single hydrogen bond (to either water depending on the disorder component), whereas O2 coordinates to both.

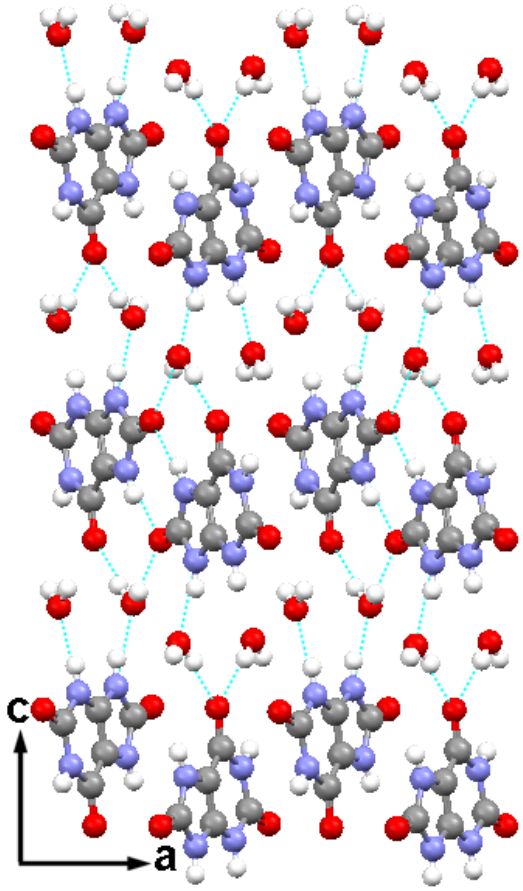

Figure 4.2. Crystal packing diagram of UAD as viewed along *b* constructed from fractional coordinates (refcode:ZZZPPI02).[6]

The crystal structure of anhydrous uric acid (UA) is monoclinic with a $P2_1/a$ space group and four molecules per unit cell. The unit cell dimensions are a = 14.464(3), b = 7.403(2), c = 6.208(1) Å, and β = 65.10(5)°.[7] Each layer in the *bc* plane consists of parallel ribbons of uric acid molecules hydrogen-bonded head-to-head (O_2···H-N_1: 1.826 Å, 175.0°) and tail-to-tail (O_8···H-N_7: 1.734 Å, 155.8°), with the ribbon plane perpendicular to the (100) surface and no hydrogen bonding between ribbons within a layer (Figure 4.3). The layers in UA are spaced 6.56 Å apart with adjacent layers.

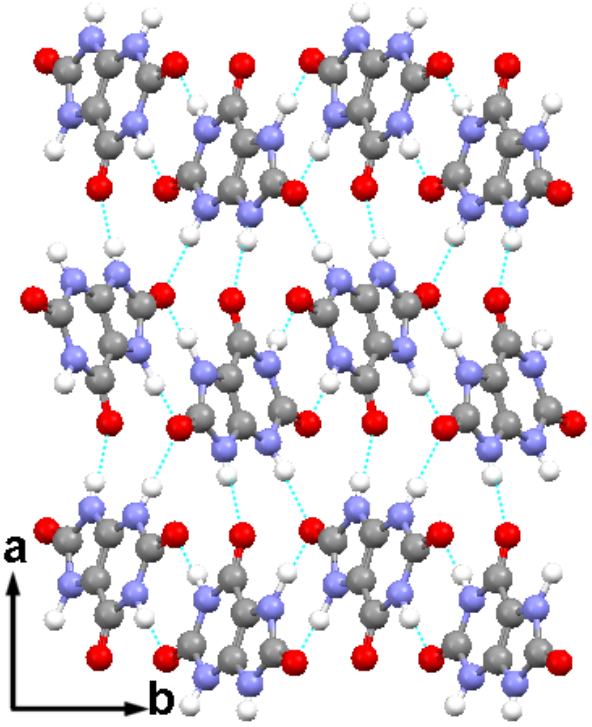

Figure 4.3. Crystal packing diagram of UA as viewed along c constructed from fractional coordinates (refcode: URICAC).[7]

Previously, Zellelow *et al.*[4] reported a detailed mechanistic and kinetic study of the UAD to UA phase transformation in air. This current work investigates the phase transformation in solution. Though both pathways lead to the same end product, the mechanisms are fundamentally different. In the former, UAD dehydration occurs by the escape of water molecules and the subsequent rearrangement of uric acid molecules to form polycrystalline UA and a new hydrogen bonding network. In the latter, UAD transformation is solution-mediated where the metastable UAD undergoes dissolution, and subsequent growth yields the stable UA. The specific objective of the present study was to investigate the transformation of UAD to UA as a function of pH, particle size and time, in both aqueous and model urine solutions.

The solution-mediated transformation of UAD to UA is potentially important because many uric acid phases appear in kidney stones, with UA typically in the highest abundance. At issue is whether UA directly precipitates from solution, or if it can result from the transformation of metastable crystalline intermediates on a timescale appropriate for kidney stone formation. This study seeks to explore the feasibility of the two-step dissolution-recrystallization model by looking at the transformation process in both model aqueous solutions with known ionic strengths and pH as well as model urine solutions. Phase transformation from dihydrate to anhydrous uric acid was carried out in different solutions monitored with offline analysis techniques including optical microscopy, powder X-ray diffraction (PXRD), and thermogravimetry (TGA).

4.1.1 Solution-Mediated Transformation Theory

The mechanism for a solution-mediated transformation of a metastable form to a stable form involves three processes: (a) dissolution of the metastable form, (b) nucleation of the stable form, and (c) crystal growth.[8-10] This transformation is driven by the solubility difference between the metastable form and stable form. The overall kinetics depend on the rate-limiting steps, which can be either dissolution or growth.[8]

A solvent-mediated transformation can be described by considering a phase diagram of temperature against concentration for a monotropic system as shown in Figure 4.4.[8, 10] The blue curve is the stable phase and the red curve is the metastable phase. The metastable phase has a higher solubility than the stable phase. A solution with concentration x_i at a certain temperature is supersaturated with respect to both forms. According to Ostwald's Rule of Stages,[11] the metastable phase precipitates first which results in a drop of solution composition to the

solubility of the metastable phase, x_I. At this point, while the metastable phase is the major solid appearing, some nuclei of the stable phase may also be present. As the stable crystals grow, the solution composition falls towards the solubility of the stable phase, x_{II}, and becomes undersaturated with respect to the metastable phase. Metastable crystals dissolve affording a supply of solute molecules for the continuous growth of stable crystals. This dissolution-crystallization process continues until all of metastable crystals have disappeared and the transformation is complete.

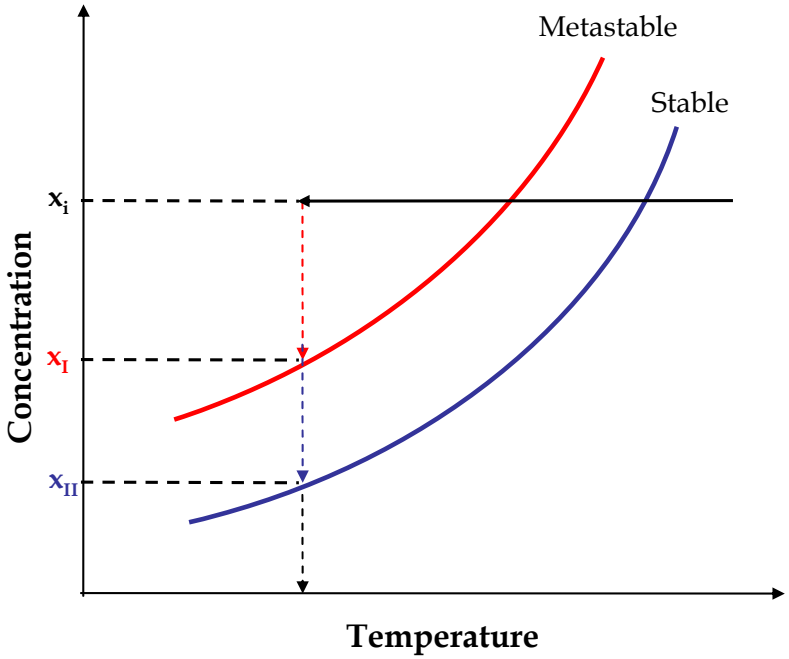

Figure 4.4. Typical solubility curves for two monotropic polymorphs as a function of temperature. The red curve is the metastable phase and the blue curve is the stable phase. Adapted from Cardew and Davey.[8]

The general features of time dependence of supersaturation during a solvent-mediated transformation are illustrated in Figure 4.5.[8, 10] The overall transformation process depends on the dissolution rates of the metastable phase and on the nucleation and growth rates of the stable phase. In a solvent-mediated transformation, the driving force for the growth of the stable phase is the supersaturation, which at the start is equivalent to S_{12}. In a simplistic view of the kinetics, at some point in the transformation, the growth and dissolution rates of the two phases must be balanced.[10] So as the transformation progresses, a supersaturation plateau, S_p, is reached in which the amount of material dissolving balances the amount of material needed for growth. *Sp* remains constant until all the metastable phase has dissolved and the supersaturation becomes zero due to growth of stable phase from solution.

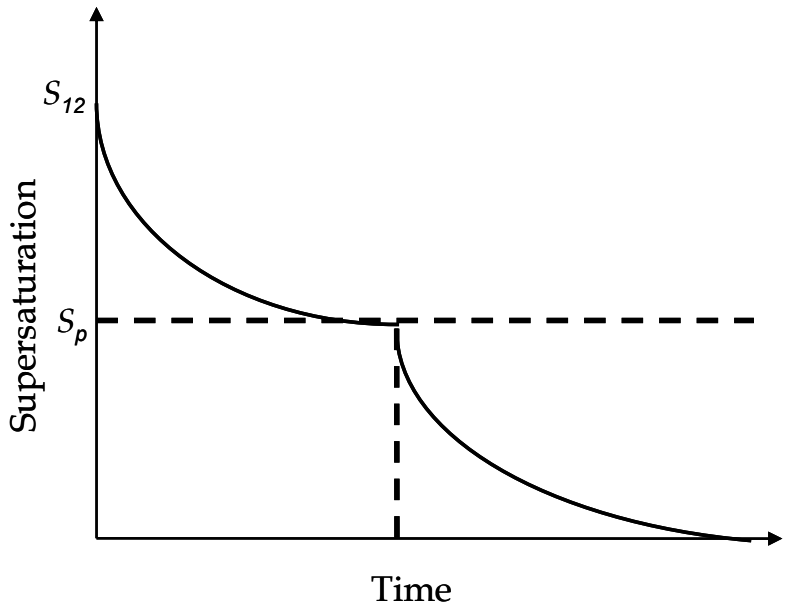

Figure 4.5. General features of time dependence of supersaturation during a solvent-mediated transformation. S_p is the supersaturation ratio at the plateau. Adapted from Davey and Cardew.[10]

At issue is the behavior of UAD and UA in solution. As described in section 1.2.2, the solubility curves of temperature against solubility of UAD and UA show that UAD is more soluble than UA. For example at 37° C, the solubility of metastable UAD in aqueous solutions (0.63 mM) is about twice that of UA (0.31 mM), respectively (Figure 4.6).

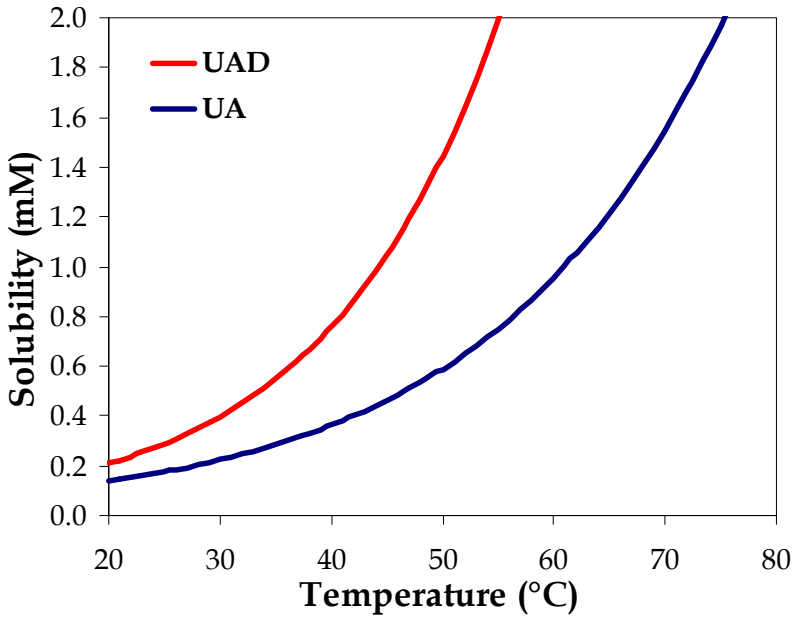

Figure 4.6. Solubility of UAD (red curve) and UA (blue curve) as a function of temperature. Data based on Königsberger and Königsberger.[12]

The aqueous solubilities of UAD and UA are independent of pH when pH ≤ 3. In solutions with an ionic strength range of 0.15 - 0.30 M, the solubility of uric acid is constant regardless of the nature and concentration of any inorganic components of urine, and/or the presence of organic substances like urea and creatine.[13] The same solubility was cited in standard reference artificial urine.[13] At higher solution pH, uric acid dissociates to an ionized urate form. To account

for the contribution of the urate form, the solubility of both UA and UAD are calculated using the following modified equation:

$$[U]_{tot} = K_s \left(1 + \frac{K'_1}{H^+}\right) \tag{4.1}$$

where $[U]_{tot}$ is the sum of the concentration of uric acid and urate in solution. The contribution of diurate is negligible in the pH range studied. The solubility of UAD and UA at 37° C as a function of pH is shown in Figure 4.7.

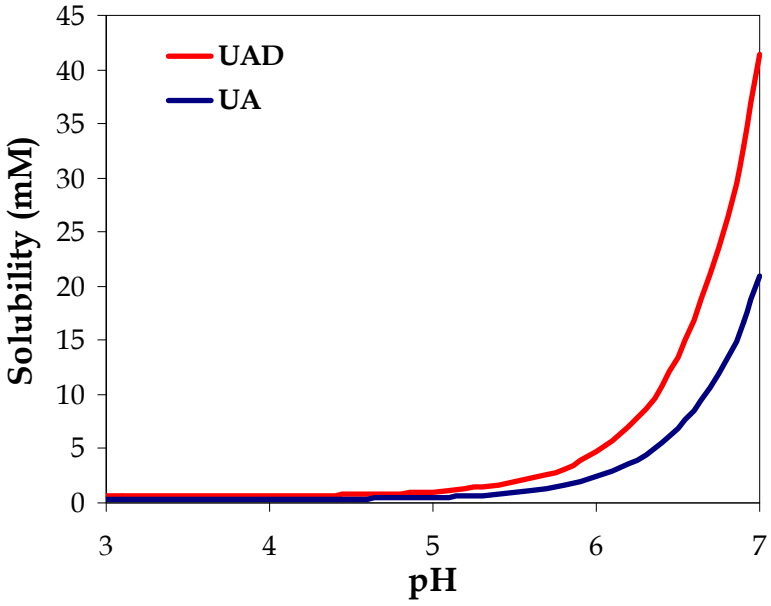

Figure 4.7. Solubility of UAD (red curve) and UA (blue curve) at 37°C as a function of pH. Data based on Königsberger and Königsberger.[12]

4.1.2 Previous Solution-Mediated Transformation Studies

Phase transformations of hydrates and polymorphs have been studied in great detail.[14-23] In pharmaceutical systems, understanding the phase transformation of active pharmaceutical ingredients (APIs) is very important because different polymorphs can differ in their solubility, dissolution rate, chemical/physical stability, and bioavailability.[14, 21, 23] Factors such as temperature,[17, 24] crystal size,[9] solvent,[9, 17, 25] seed crystals,[26, 27], additives,[22, 28, 29] and agitation[9] have been reported to influence the kinetics of phase transformation.

Solvent-mediated phase transformation is a complex process. It involves mechanisms such as dissolution of metastable form, heterogeneous and secondary nucleation of the stable form, and growth of the stable form. Any of these mechanisms can be rate-limiting. Crystallization of the stable form as the rate-controlling step has been illustrated in systems such as the transformation of anhydrous carbamazepine to its stable hydrate[17] and the polymorphic phase transition of 2,6-dihydroxybenzoic acid.[30] On the other hand, the polymorphic transformation of metastable β-glycine to its stable α form is an example in which the dissolution rate of the metastable form is rate-limiting step.[15] In another example, anhydrous theophylline crystals can act as heterogenous substrates for the epitaxial growth of the more stable monohydrate phase.[21]

Phase transformation studies have also been performed on other compounds that are found in kidney stones such as calcium oxalate[31] and uric acid.[32, 33] Calcium oxalate forms three hydrates, the thermodynamically stable monohydrate, and the metastable dihydrate and trihydrate. The transformation kinetics of these hydrates was studied in batch precipitation experiments.[31] The distribution of hydrates in the initial stages of precipitation was found to be dependent on the

mixing process. Calcium oxalate dihydrate transformation into thermodynamically stable monohydrate appears to be a solution-mediated process.

The phase transition of uric acid dihydrate was previously studied by Boistelle[32] and Grases *et al*.[33] Their qualitative investigation of the transformation of uric acid dihydrate to anhydrous uric acid in aqueous solutions was shown to be dependent on temperature and solution pH. During the transformation process, UAD crystals grow opaque and UA crystals were observed to grow epitaxially into the hydrate.[32] *In vitro* studies by Grases *et al*.[33] have shown that UAD precipitated from artificial urine at pH 5.5 transformed into anhydrous uric acid in two days, however, they did not quantify the composition of the suspensions that were sampled at select time intervals.

To better understand the transformation of UAD in solution, we performed experiments in model aqueous solutions with controlled pH and ionic strengths as well as model urine solutions. The effect of seeding on the transformation kinetics was also investigated. The effect of impurities on the transformation process is described in Chapter 5.

4.2 Experimental Methods and Materials

4.2.1 Materials

All chemical reagents were used as received and without further purification. Water was purified by passage through two Barnstead deionizing cartridges followed by distillation. Uric acid solutions of pH 4 were prepared from uric acid (>99%, Sigma), sodium acetate (99% EMD), and acetic acid (99.7%, EMD). McIlvaine buffers[34] with controlled pH and ionic strength were prepared from $C_6H_8O_7 \cdot H_2O$ (99.0%, EMD), Na_2HPO_4 (99.5%, Fisher), and KCl (99.0%, Sigma).

Artificial urine[35] solution was prepared from Na_2SO_4 (99.9%, Sigma), KCl (99.0%, Sigma), NH_4Cl (99.8%, EM Science), $MgSO_4 \cdot 7H_2O$ (98-102%, EM Science), Na_2HPO_4 (99.5%, Fisher), $Na_2HPO_4 \cdot H_2O$ (99.1%, Fisher), NaCl (99%, EM Science), $Na_3C_6H_5O_7 \cdot 2H_2O$ (Certified, Fisher), and urea (Certified ACS, Fisher).

4.2.2 Crystal Growth

Crystals of UAD were grown by dissolving 180-200 mg of uric acid in 1 L boiling distilled water as described in section 1.2.3. The pH of the solution was buffered to 4.0 with sodium acetate and acetic acid and kept at 25° C for 48 hours. UAD crystals were vacuum-filtered through Whatman #1 filter paper and air-dried. Most crystals were ~100 μm rectangular plates with large (001) faces and smaller (102) and (011) side faces.

4.2.3 Transformation Experiments

UAD were used as grown without sieving or grinding. Approximately 20 mg of UAD was added to 24 glass bottles containing 50 mL of pH 4 McIlvaine buffer solutions (Ionic Strength, IS = 0.5 M). These suspensions were then placed in a 37° C water bath on the same day with a staggered start time. Every 6 hours, 3 bottles were removed from the water bath, the solid phase was vacuum-filtered through Whatman # 1 filter paper, washed with distilled water, air-dried and immediately subjected to TGA and PXRD analysis. The transformation of UAD was monitored for a period of 48 hours. Following the same procedure, the transformation of UAD was also performed in pH 5, 6, 6.2, 6.4, 6.6, 6.8, and 7 McIlvaine buffer solutions (IS = 0.5 M), as well as artificial urine solution. Artificial urine solution was prepared according to Isaacson (see section 3.2.4).[35] The effect of seeding on the transformation of UAD to UA in artificial urine solution

was also evaluated by adding 10% (w/w) anhydrous uric acid to the starting material. In another experiment, 20 mg UAD was added to 50 mL artificial urine solution saturated with uric acid and the UAD transformation was monitored for 48 hours.

For comparison, the transformation of UAD to UA was monitored at room temperature (~25° C) for up to two weeks. The effect of stirring on the transformation was also studied.

4.2.4 Optical Microscopy

After a defined time interval, samples were removed from the 37° C water bath and the suspended solids were transferred to a glass microscope slide with a disposable Pasteur pipette. The morphology and size of the crystals were examined with an Olympus BX-50 polarized optical microscope fitted with a Nikon COOLPIX995 digital camera operated with krinnicam_v1-03 software (Nikon Corp.).

4.2.5 Thermal Analysis

Thermogravimetric analyses (TGA) were performed on a SDT Q600 TA instrument (New Castle, DE) as described in section 3.3.3.1. Samples removed from the water bath at defined time intervals were filtered and the solid was immediately subjected to TGA analysis. All experiments were conducted in triplicate using open 90 μL alumina pans (TA instruments) and heated from room temperature to 150° C at 10°C/min under a stream of nitrogen gas. A nitrogen flow rate of 50 mL/min was used. All experimental curves were analyzed with TA's Universal Analysis Software. The calculated weight loss of pure UAD dehydration is 17.65 %. The extent to which UAD was converted to UA was determined by the difference method. All measurements,

performed at least in triplicate, showed relatively low standard deviation. Figure 4.8 shows a typical TGA scan of UAD that was filtered from pH 6 McIlvaine buffer.

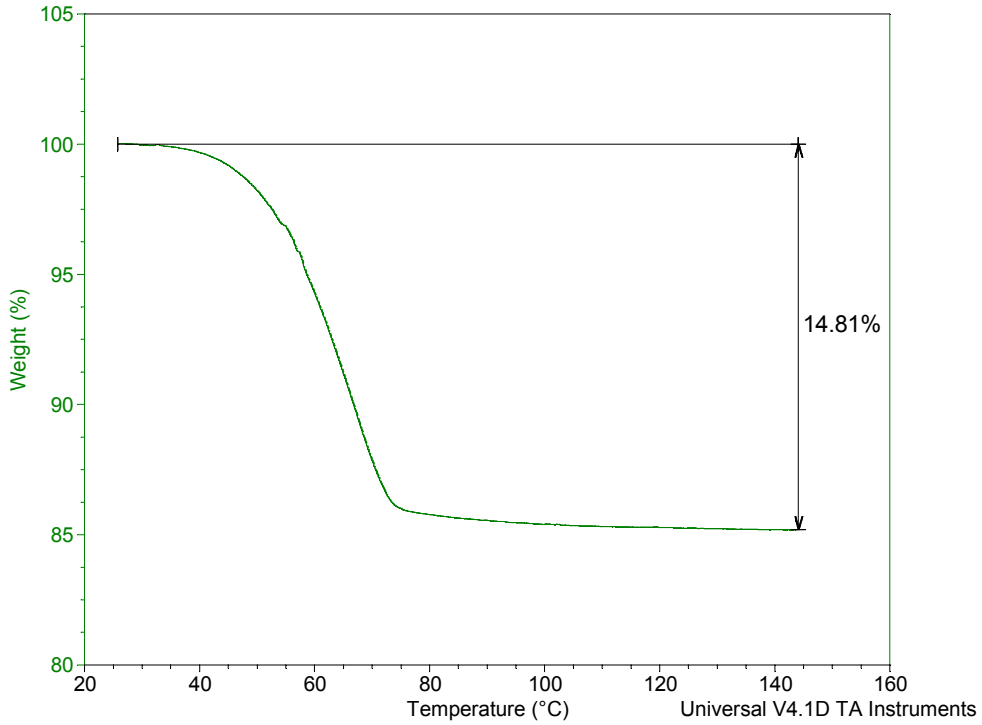

Figure 4.8. Sample TGA curve of the dehydration of UAD in pH 6 McIlvaine buffer at 18 hours in a 37 °C water bath.

4.2.6 Powder X-ray Diffraction

Powder X-ray diffraction was performed using a Rigaku R-AXIS RAPID-S X-ray diffractometer under the following conditions: tube voltage of 40kV, tube current of 30 mA, and Cu Kα radiation. The samples were scanned in steps of 0.01° over a 2θ range of 4° to 50° at a speed of 0.1°/sec with a total scan time of 60 min. Data analysis was performed using Jade v5.035 software (Material Data Inc.). As grinding of samples may contribute to the premature

dehydration of UAD, PXRD analyses were performed on unground samples. The transformation of UAD to UA was tracked by the appearance and disappearance of several characteristic diffraction lines in specific 2θ regions where there is little or no overlap between UAD and UA reflections. The calculated PXRD patterns of UAD and UA appears in Figure 4.9. Intense diffraction lines for UAD are (002), (011), (102), (004), (112), (210), and (21-1) while that for UA are (200), (001), (210), (11-1), (121), and (021). The 2θ values for all reflections in UAD and UA are listed in Table 4.1.

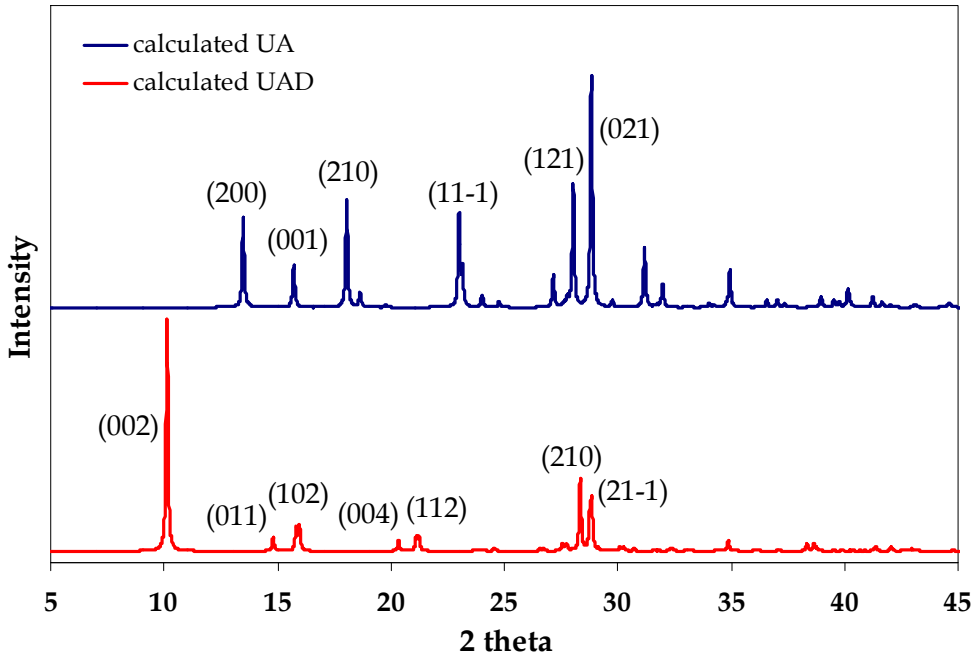

Figure 4.9. Calculated PXRD patterns for UAD (red) and UA (blue). UAD based on coordinates from Reference 6 (refcode: ZZZPPI02), and UA from Reference 7 (refcode: URICAC).

Table 4.1. UAD and UA 2θ values and their corresponding reflections.

UAD		UA	
2θ	Reflections	2 θ	Reflections
10.045	(002)	13.374	(200)
14.787	(011)	15.695	(001)
15.998	(102)	17.915	(210)
20.336	(004)	22.859	(11-1)
21.345	(112)	27.096	(400)
28.408	(210)	28.004	(121)
28.711	(21-1)	28.812	(021)
34.865	(024)	31.132	(12-1)
		32.040	(312)
		35.067	(421)

4.3 Transformation of Uric Acid Dihydrate Crystals

The solution-mediated transformation of UAD to UA was studied in both model aqueous solutions and model urine solution. The effect of pH on the rate of transformation of the metastable UAD to the stable UA was measured at 37° and 25° C in McIlvaine buffer solutions of IS = 0.5 M. To mimic physiological condition, the transformation of UAD to UA was also performed in artificial urine solution. Solid samples of the metastable form were added to various solutions and analyzed every 6 hours at 37° C or every 48 hours at 25° C.

4.3.1 Transformation in Buffered Solutions at 37° C

Figures 4.10 shows microscopic images of the transformation of UAD at 37° C in pH 4 McIlvaine buffer (IS = 0.5 M). Complete transformation at this pH could be monitored in 6 hour intervals over a period of 48 hours. Crystals transformed to anhydrous uric acid over time. Mostly UAD was present 6 hours into the transformation, though the edges of the crystals appear

rougher than at T = 0. The micrographs at 12-36 hours showed a mixture of clear and opaque UAD crystals as well as the newly formed small UA. Closer examination of the micrograph at 18 hours revealed epitaxial nucleation of UA (red circle) on the surface of metastable UAD. This heterogeneous nucleation was in accordance with previous reports.[32, 36] As the growth of the anhydrous phase continued, UAD was consumed as shown by the smooth UA crystals observed at 42 to 48 hours. Similar trends were observed at pH 5 as shown by the photomicrographs in Figure 4.11. The color, size, and shape of the starting material and the end product may look similar, but in principle they can be differentiated by their distinct conoscopic interference patterns as described in section 1.2.6.

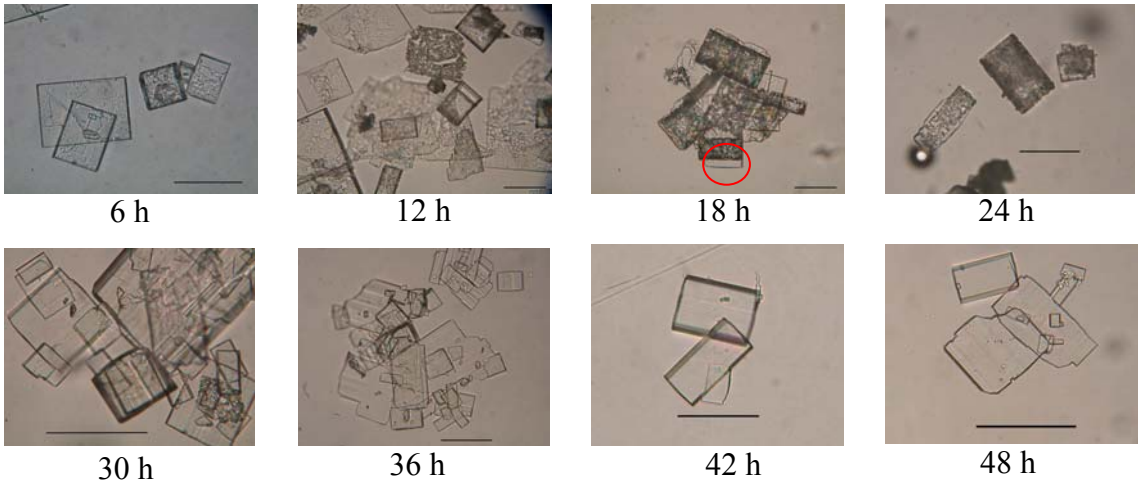

Figure 4.10. Photomicrographs taken at different times during the phase transformation of UAD to UA in pH 4 McIlvaine buffer at 37° C. Scale bar = 100 µm. Red circle at 18 h indicates the newly nucleated UA crystal.

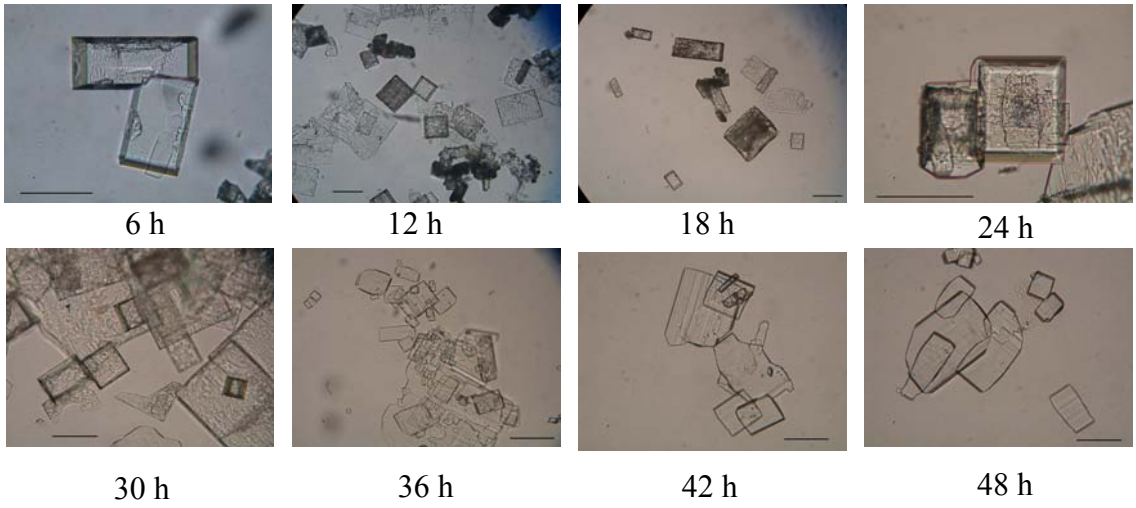

Figure 4.11. Photomicrographs taken at different times during the phase transformation of UAD to UA in pH 5 McIlvaine buffer at 37° C. Scale bar = 100 µm.

The phase composition of the samples was examined by PXRD. Since grinding UAD samples can contribute to their premature dehydration, PXRD analyses were performed on unground samples. This leads to some preferred orientations, but does not impact our qualitative analysis.

PXRD patterns collected on crystals suspended in pH 4, 5, 6 McIlvaine solutions showed relatively similar behavior. In general, complete transformation of UAD to UA was observed in 48 hours. No intense peaks other than those ascribable to UA or UAD phases were observed which suggests that the UAD to UA transformation involves no intermediate crystalline phases. These results were consistent with previous work by Ringertz,[37] who asserted that UAD dehydration leads directly to polycrystalline UA.

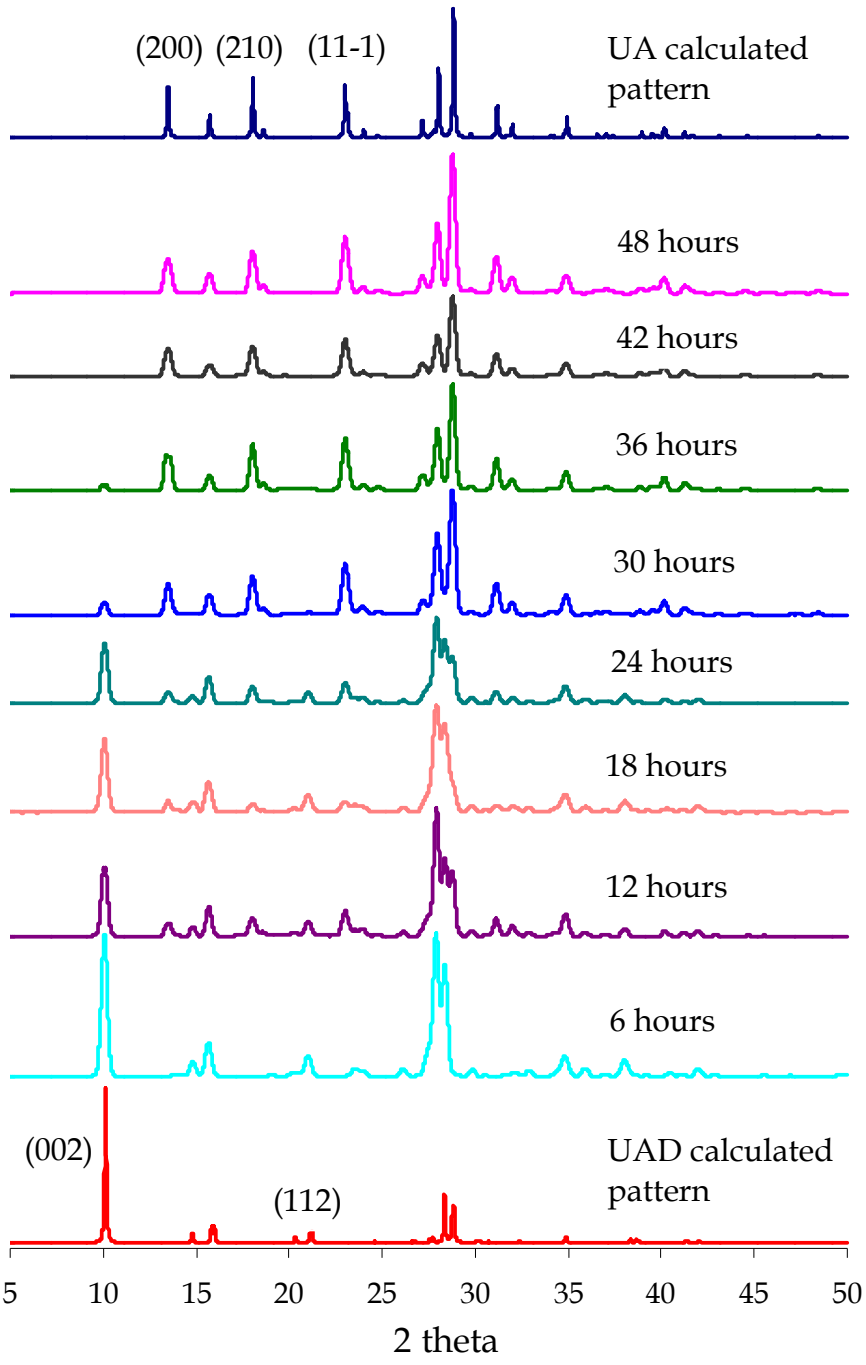

Figure 4.12. PXRD patterns of the transformation of UAD to UA in pH 4 McIlvaine buffer at 37° C.

Figure 4.12 illustrates how diffraction data change with the sample composition over time when suspended in pH 4 McIlvaine buffer. The transformation of UAD was marked by the appearance and disappearance of several characteristic diffraction lines. The diffraction pattern at 6 hours showed reflections corresponding mostly to UAD. Starting at 12 hours, distinct (200), (210), (11-1) UA reflections have emerged. The diffraction lines observed from 12-36 hours indicated the presence of both UAD and UA in the mixture. The decreased intensity and subsequent disappearance of UAD (002), (004), and (112) diffraction lines coincided with the appearance of strong UA (200), (210), and (11-1) reflections. By 42-48 hours, the only visible diffraction lines corresponded solely to UA indicating that the transformation was complete.

Quantifying the extent of UAD transformation was accomplished by thermogravimetric analysis (TGA) of the solid phase after removal of the suspensions at determined time intervals. All measurements were performed at least in triplicate. The extent of conversion of UAD to UA in pH 4-6 McIlvaine solutions is summarized in Figure 4.13 with the standard deviation shown for each time point. It can be seen from the graph that, although the transformation times are slightly different, the shapes of the transformation profiles at the three pH investigated are quite similar.

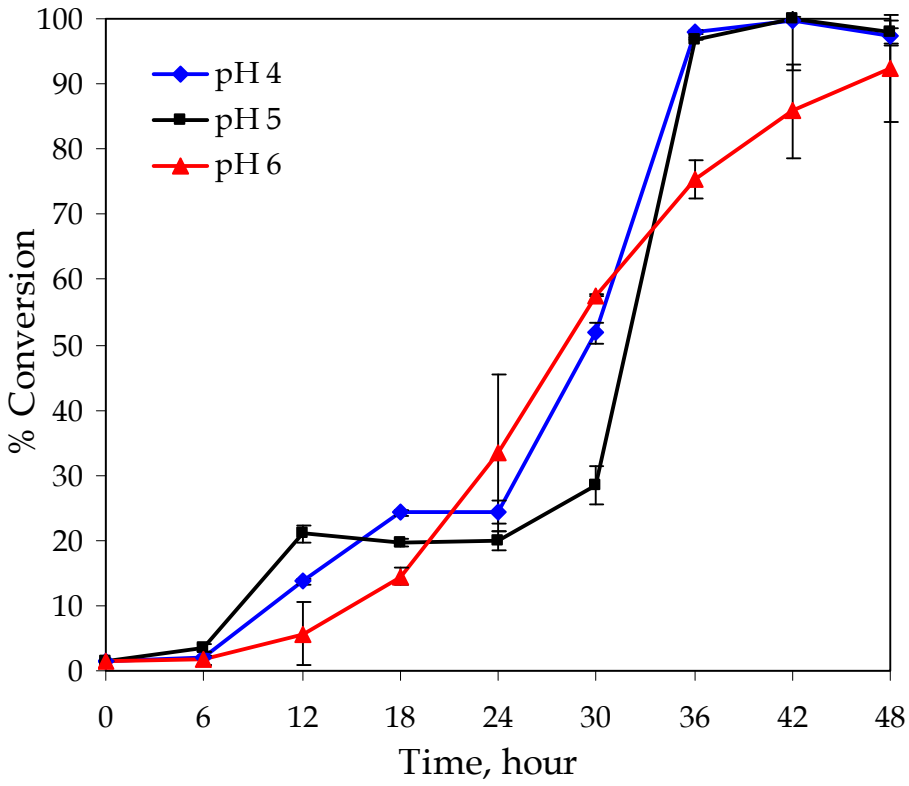

Figure 4.13. Summary of the % conversion of UAD to UA as a function of time in McIlvaine buffer solutions; Blue curve = pH 4, Black curve = pH 5, Red curve = pH 6.

As mentioned earlier, the solution-mediated phase transformation of UAD involves the dissolution of UAD followed by nucleation and growth of UA. UAD solubility increases with pH, so one might assume that the transformation of UAD should be faster as the solution pH is increased. Similar transformation rates are observed up to 24 hours at pH 4, 5, and 6. At pH 4 and 5, a fast acceleration and leveling off are observed showing a ~97 % conversion of UAD to UA at 36 hours. At pH 6, the transformation rate is continuous and exhibited a 75 % conversion at 36 hours.

Recall that the pK_a of uric acid is 5.5. At pH = 6, a majority of uric acid molecules in solution are ionized to urate, as indicated in the uric acid-urate equilibrium discussed in section 1.2.1. Sodium urate salts can in principle form in the transformation medium which is composed of citric acid monohydrate and sodium biphosphate. However, there was no evidence for them in PXRD at pH 6. Monosodium urate monohydrate (MSU), in particular, is a stable monohydrate, though we also do not see this in the TGA (dehydration temperature =224^o C).

As we increased the solution pH to 6.8, a new concomitant phase was observed at 42-48 hours transformation time. Micrographs of the sample taken after 42 hours show a mixture of plate-like and needle-like crystals (Figure 4.14). The TGA curve for this mixture shows two dehydration steps. The first weight loss from 0-150° C corresponds to the expected transformation of UAD to UA. The second weight loss observed from 150° C to 300° C is characteristic of the dehydration of MSU.

Figure 4.14. Photomicrograph of the transformation of UAD in pH 6.8 McIlvaine buffer at 37° C, taken after 42 hours. Scale bar = 100 μm.

A slight increase to pH 7 revealed a different behavior as shown in Figure 4.15. At 6-12 hours, the solid phase consists of UAD and UA. At 18 hours, only needle-like crystals are observed. These needle-like crystals are similar in appearance to those observed during the UAD transformation at pH 6.8 after 42 hours.

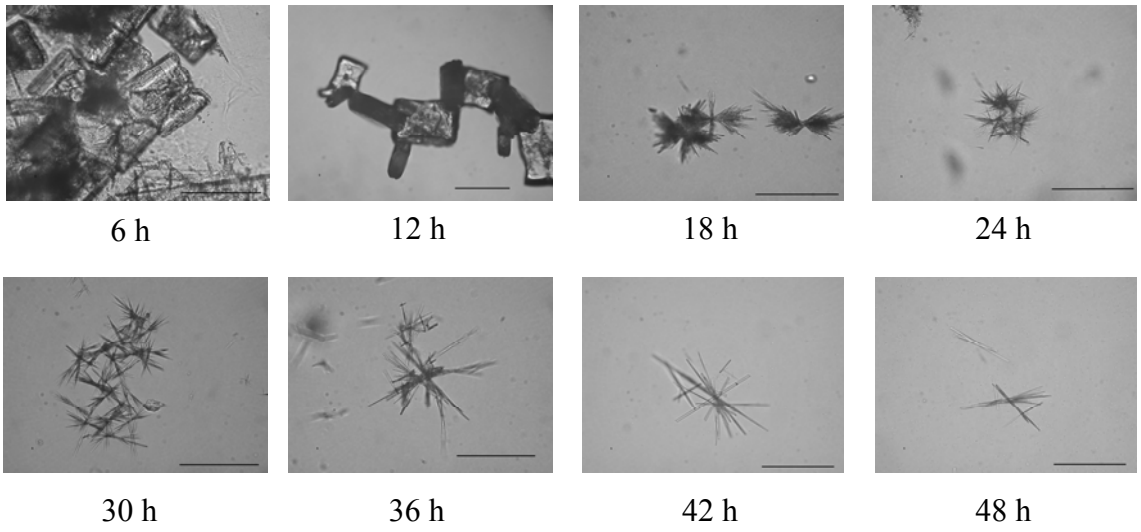

Figure 4.15. Photomicrographs taken at different times during the phase transformation of UAD in pH 7 McIlvaine buffer at 37° C. Scale bar = 100 μm.

Powder diffraction data for the transformation in pH 7 McIlvaine buffer was collected for samples in 6 hour intervals for up to 48 hours (Figure 4.16). The diffraction lines shown at 6-12 hours correspond mostly to UAD. Starting at 18 hours, a new diffraction pattern corresponding to MSU appeared. The identity of MSU was also confirmed by thermal analysis of the sample. A weight loss of 9.33% corresponds to the dehydration of MSU (theoretical % dehydration = 9.47%). The needle-like crystals produced in the transformation process are identical to the MSU crystals grown in uric acid solution with pH > 7.

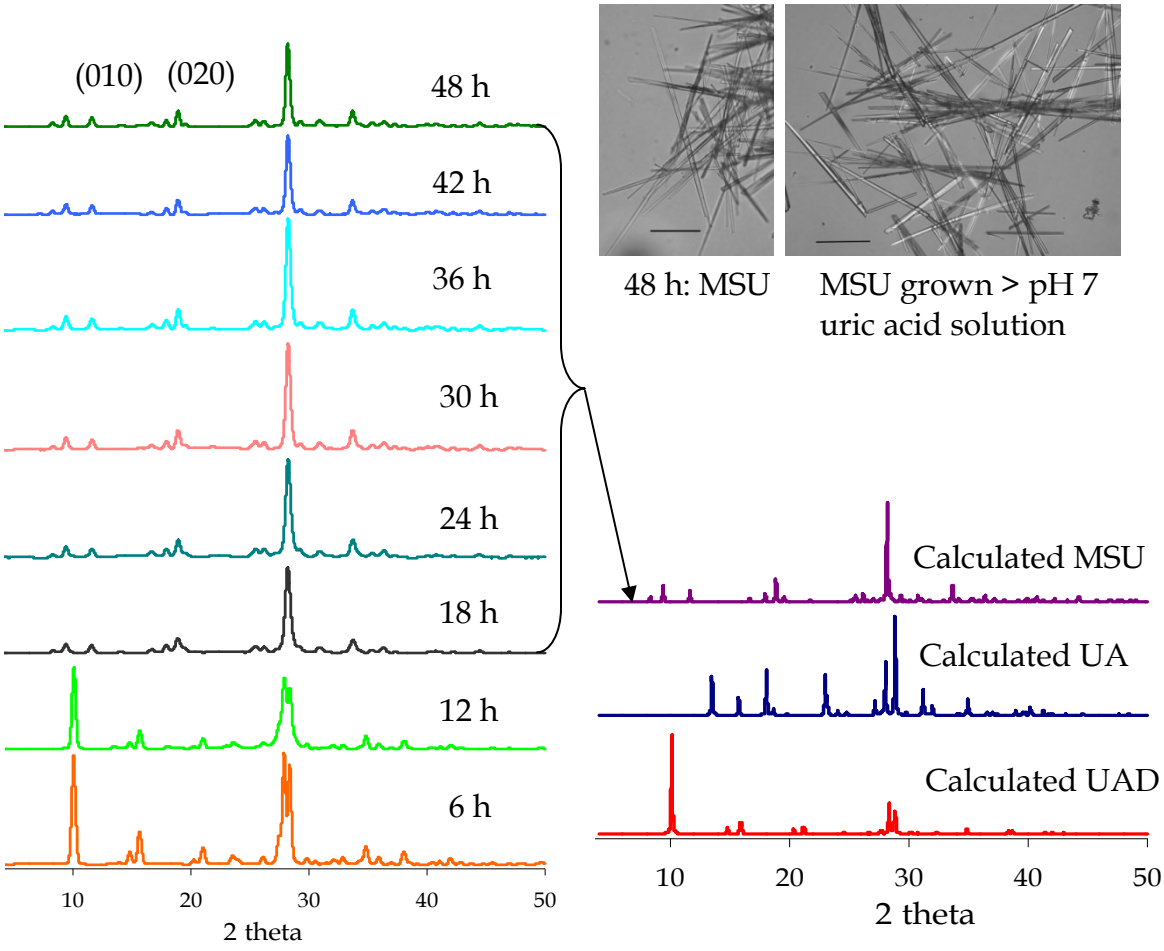

Figure 4.16. PXRD patterns of the transformation of UAD in pH 7 McIlvaine buffer at 37° C. Scale bar on the micrographs is 100 µm.

4.3.2 Transformation in Buffered Solutions at Room Temperature (~ 25° C)

UAD transformation in room temperature buffer solutions was conducted to determine the transformation rates at low temperature. A suspension of 20 mg UAD was placed into 100 mL of

the buffer solution and the solid composition was monitored every 2 days for up to 12 days. The transformation of UAD at room temperature is significantly slower than at 37^{o} C (Figure 4.17). For example, we observed only about 11.63 % and 18.93 % conversion of UAD to UA at pH 4 and 5, respectively, after 8 days. In a stirred solution, the transformation rate occurred twice as fast. This transformation rate is faster than the UAD to UA dehydration in air studied at 33%-75% relative humidity.

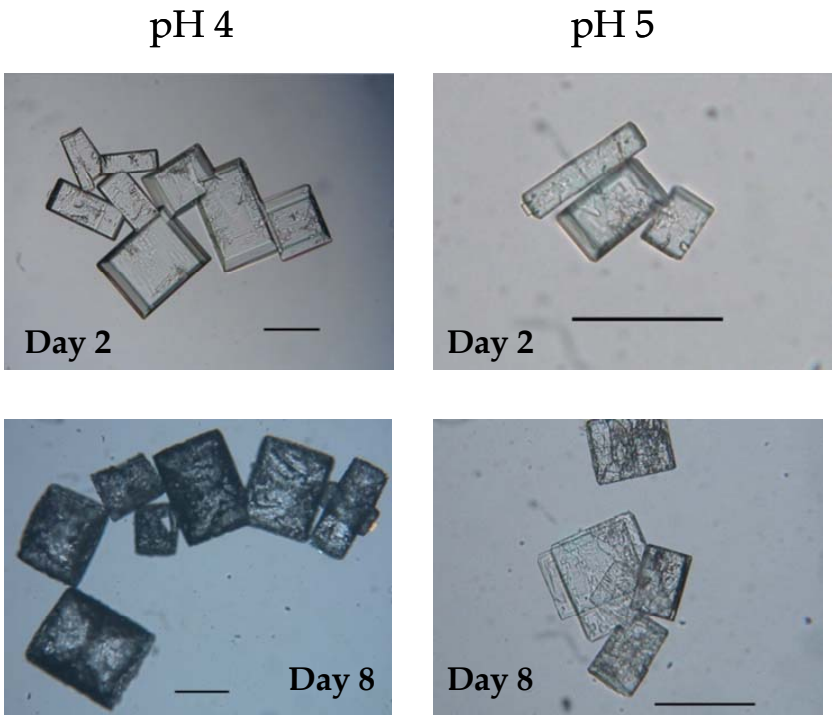

Figure 4.17. Photomicrographs of the transformation of UAD in pH 4 and 5 McIlvaine buffer at 25° C. Scale bar = 100 μm.

4.3.3 Transformation in Artificial Urine Solution at 37° C

To more closely mimic UAD under physiological conditions, the transformation of UAD was studied in artificial urine solution at pH ~5. Grases *et al*.[33] studied the transformation of UAD to UA, however, they did not quantify the composition of the suspensions that were sampled at select time intervals.

The optical micrographs in Figure 4.18 followed the transformation of UAD in artificial urine every 6 hours. Smooth and tiny crystalline materials are apparent in solution for 30 hours. Unlike the crystals grown in low pH McIlvaine solutions, these crystals in artificial urine have less well defined faces.

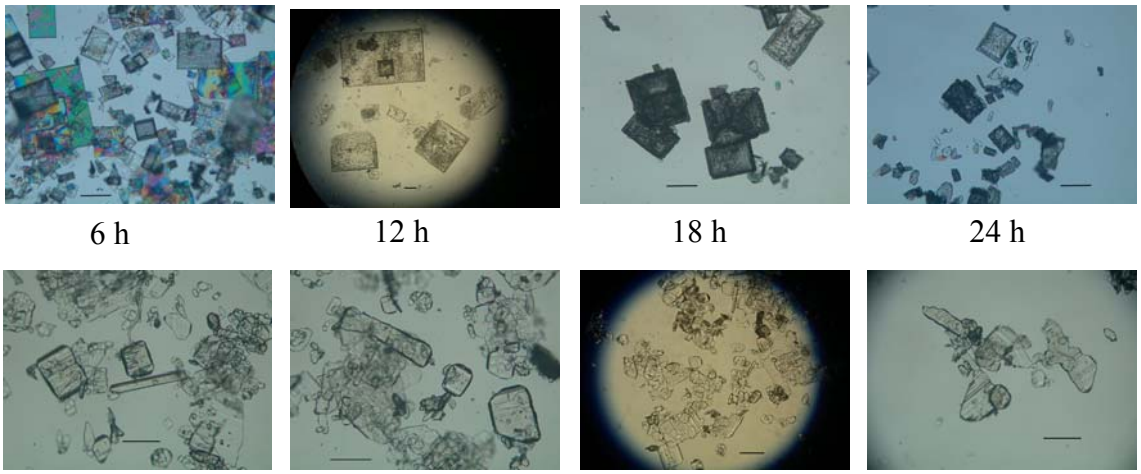

Figure 4.18. Photomicrographs taken at different times during the phase transformation of UAD to UA in artificial urine at 37° C. Scale bar = 100 μm.

PXRD data collected every 6 hours in artificial urine are shown in Figure 4.19. All diffraction patterns at 6-24 hours show the presence of both UAD and UA. The transformation process was followed until complete dissolution of UAD was observed, that is, until the complete disappearance of reflections related to UAD. Complete transformation of UAD to UA occurred at 30 hours. There are no reflections that would otherwise indicate intermediate crystalline phases. This observation was similar to the direct transformation of UAD to UA in McIlvaine buffer at low pH as described in section 4.3.1.

The distinctly different PXRD patterns of UAD and UA can in principle be used to quantitatively determine the phase transformation rate of UAD to UA. We attempted to quantify the UA:UAD ratios at each time interval using select PXRD reflections in the data shown in Figure 4.19 and the following equation:

(4.2) $$X_{UA} = \frac{A_{UA}}{A_{UA} + A_{UAD}}$$

where X_{UA} is the mass fraction of UA, A_{UA} is the total area of the peaks at $2\theta = 13.4^{o}$ and 17.9^{o}, and A_{UAD} is the total area of the peaks at $2\theta = 10.04^{o}$ and 21.3^{o}. A plot of the mass fraction changes of UAD and UA with time during the transformation of UAD in artificial urine solution at 37^{o} C appears in Figure 4.20.

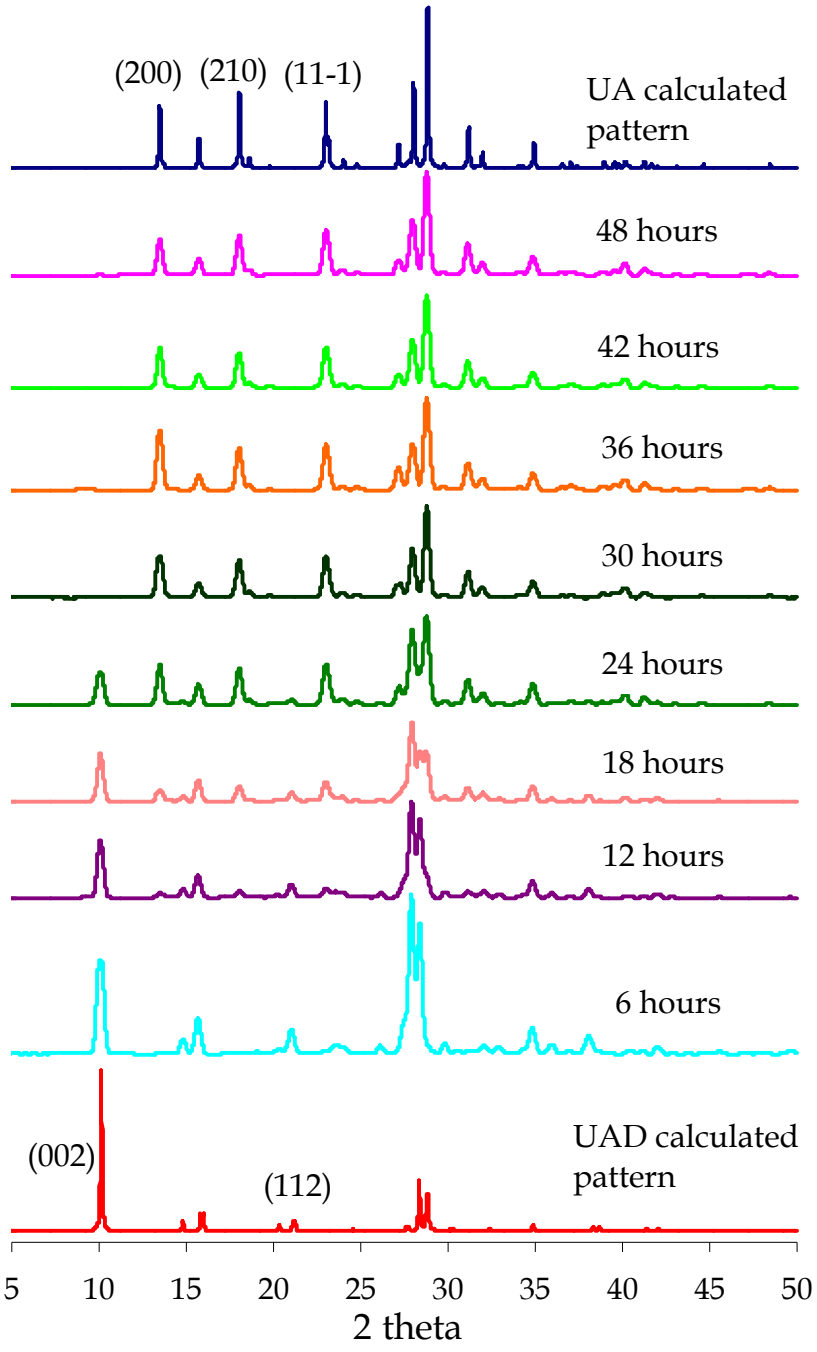

Figure 4.19. PXRD patterns of the transformation of UAD to UA in artificial urine solution at 37° C, pH ~5.

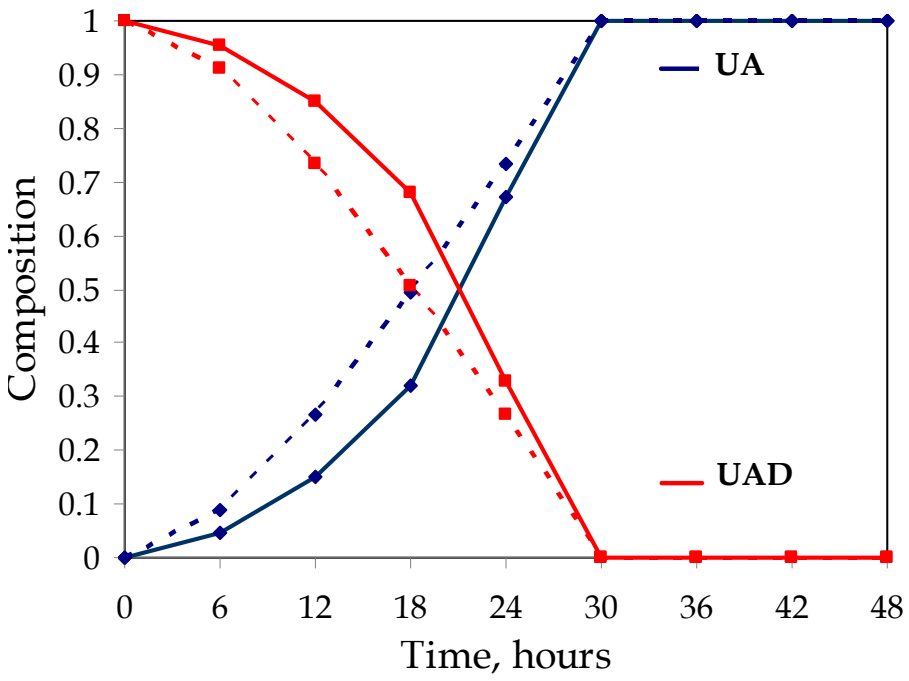

Figure 4.20 Mass fraction changes of UAD (red) and UA (blue) with time during the transformation of UAD in artificial urine solution at 37° C determined from PXRD data (solid lines) and TGA data (dashed lines).

As previously mentioned, PXRD data was collected on unground samples as grinding can contribute to the premature dehydration of UAD. Both UAD and UA exhibit plate-like morphology and the presence of some preferred orientations can affect the accuracy of the quantitative analysis. Nevertheless, we attempted to quantify the UA/UAD composition from integrating the area under select reflections, following a method described previously.[38] In Figure 4.20, the mass percent of UA (blue solid line) at 6, 12, 18, and 24 hours correspond to 4.5%, 15 %, 32 %, and 67%, respectively.

As discussed in section 4.3.1, TGA was the preferred method to more accurately quantify the extent of the transformation of UAD. Since only UAD and UA are present, we quantify each

component by the difference method. The % composition obtained by TGA appears as dashed lines in Figure 4.20. A consistently lower % UA in the PXRD data than was observed at 6-24 hours may be attributed to diminished /suppressed intensities of some diffraction peaks due to the issue of preferred orientations exhibited by the unground plate-like samples.

The effect of seeding on the transformation of UAD to UA in artificial urine solution was also studied by adding 10% (w/w) of anhydrous uric acid to the starting material. In a different set of experiment, artificial urine solution saturated with uric acid was prepared to which UAD crystals were suspended and the transformation was monitored for 48 hours. Optical micrographs for both of these sets of experiments are similar to the photomicrographs shown in Figure 4.18.

A plot of time versus the conversion of UAD to UA in artificial urine solution both with and without seeding at 37° C appears in Figure 4.21. The transformation of UAD suspended in artificial urine solution (black curve) starts slow with a ~9% conversion at 6 hours, then a rapid increase to ~50% at 18 hours and complete transformation at 30 hours. The complete transformation at 30 hours was also supported by the PXRD data shown in Figure 4.19. In experiments where 10% (w/w) uric acid was added as seed material (blue curve), a two-fold increase of the transformation was observed at 6 hours. The presence of UA seed crystals eliminates the need to nucleate UA. It has been reported in the past that seeds in polymorphic transformation acts as catalyst during the nucleation process.[22] While an increase in % conversion is observed at the beginning of the transformation process, complete transformation of the UAD in the seeded experiment occurred at 30 hours, similar to the results observed in unseeded experiments. The third set of data in Figure 4.21 refers to the transformation of UAD crystals suspended in artificial urine solution saturated with uric acid (red curve). Since the

solution is already saturated with uric acid, UAD does not dissolve as readily compared to other experiments. However, as stable UA nucleate and grow, solute is consumed and the dissolution of UAD crystals proceeds until a steady state is reached and only UA is observed. In artificial urine saturated with uric acid, the complete transformation required 48 hours.

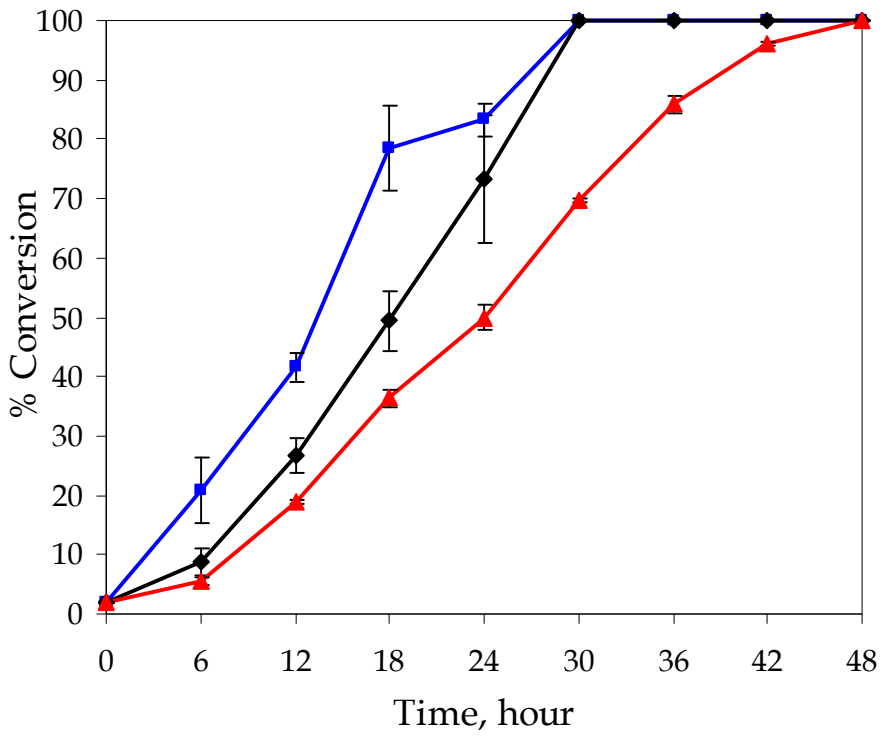

Figure 4.21 Transformation of UAD in artificial urine solution at 37° C. (Blue) UAD seeded with 10% (w/w) UA in artificial urine solution; (Black) UAD in artificial urine solution; (Red) UAD in artificial urine solution saturated with uric acid.

4.4 Conclusions

The solution-mediated transformation of metastable UAD into thermodynamically stable UA has been studied in the systems in which the transformation was initiated by suspending UAD crystals into model aqueous solutions and model urine solution. UAD dissolution creates

supersaturation for the crystallization of the stable UA. On formation of the nuclei of UA, the UAD transform into UA via dissolution and crystal growth process. The combined dissolution and growth processes continue until all the metastable UAD has dissolved and the system reaches its thermodynamically stable state, when the stable UA is the only phase present in the final suspension.

Monitoring and quantifying the transformation of metastable UAD to stable UA is a complex process since during the course of the transformation, the solution composition continually changes. Added to the complexity is the ability of UA to dissociate into urate at higher pH. The transformation of UAD to UA depends on the rate of dissolution of the metastable form, and the rates of nucleation and growth of the stable phase, all of which are sensitive to solution conditions such as pH, solution composition, presence of seed crystals, and temperature. UAD transforms faster in artificial urine solution than in McIlvaine solutions of low pH. UAD transforms directly to UA at low pH, suggesting that the transformation involves no intermediate crystalline phases. At high solution pH (≥ pH 6.8) where uric acid can ionize to urate, the process may involve transformation from UAD to UA then to MSU or it can be UAD to MSU directly.

4.5 References

1. Lonsdale, K.; Mason, P., "Uric Acid, Uric Acid Dihydrate, and Urates in Urinary Calculi, Ancient and Modern." *Science* **1966,** 152, 1511-1512.

2. Schubert, G.; Reck, G.; Jancke, H.; Kraus, W.; Patzelt, C., "Uric acid monohydrate - a new urinary calculus phase." *Urol. Res.* **2005,** 33, 231-238.

3. Mandel, N. S.; Mandel, G. S., "Monosodium Urate Monohydrate, the Gout Culprit." *J. Am. Chem. Soc.* **1976,** 98, 2319-2323.

4. Zellelow, A. Z.; Kim, K.-H.; Sours, R. E.; Swift, J. A., "Solid-State Dehydration of Uric Acid Dihydrate." *Cryst. Growth. Des.* **2010,** 10, 418-425.

5. Artioli, G.; Masciocchi, N.; Galli, E., "The Elusive Crystal Structure of Uric Acid Dihydrate: Implication for Epitaxial Growth During Biomineralization." *Acta Cryst.* **1997,** B53, 498-503.

6. Parkin, S.; Hope, H., "Uric Acid Dihydrate Revisited." *Acta Cryst.* **1998,** B54, 339-344.

7. Ringertz, H., "The Molecular and Crystal Structure of Uric Acid." *Acta Cryst.* **1966,** 20, 397-403.

8. Cardew, P. T.; Davey, R. J., "The kinetics of solvent-mediated phase transformation." *Proc. R. Soc. Lond.* **1985,** 398, 415-428.

9. Liu, W.; Wei, H.; Black, S., "An Investigation of the Transformation of Carbamazepine from Anhydrate to Hydrate Using in Situ FBRM and PVM." *Or. Process Res. Dev.* **2009,** 13, 494-500.

10. Davey, R. J.; Cardew, P. T., "Rate Controlling Processes in Solvent-Mediated Phase Transformations." *J. Crystal Growth* **1986,** 79, 648-653.

11. Ostwald, W., "Ostwald, Studien ü ber die bildung und umwandlung fester körper." *Z. Phys. Chem.* **1897**, 289-330.

12. Königsberger, E.; Königsberger, L.-C., "Thermodynamic Modeling of Crystal Deposition in Humans." *Pure Appl. Chem.* **2001,** 73, (5), 785-797.

13. Königsberger, E.; Wang, Z., "Solubility of Uric Acid in Salt Solutions." *Monatsh. Chem.* **1999,** 130, 1067-1073.

14. Murphy, D.; Rodriguez-Cintron, F.; Langevin, B.; Kelly, R. C.; Rodríguez-Hornedo, N., "Solution-mediated phase transformation of anhydrous to dihydrate carbamazepine and the effects of lattice disorder." *Int. J. Pharma.* **2002,** 246, 121-134.

15. Ferrari, E. S.; Davey, R. J.; Cross, W. I.; Gillon, A. L.; Towler, C. S., "Crystallization in Polymorphic Systems: The Solution-Mediated Transformation of β to α Glycine." *Cryst. Growth. Des.* **2003,** 3, (1), 53-60.

16. Ferrari, E. S.; Davey, R. J., "Solution-Mediated Transformation of α to β L-Glutamic Acid: Rate Enchancement Due to Secondary Nucleation." *Cryst. Growth. Des.* **2004,** 4, (5), 1061-1068.

17. Qu, H.; Louhi-Kultanen, M.; Rantanen, J.; Kallas, J., "Solvent-Mediated Phase Transformation Kinetics of an Anhydrate/Hydrate System." *Cryst. Growth. Des.* **2006,** 6, (9), 2053-2060.

18. Dharmayat, S.; Hammond, R. B.; Lai, X.; Ma, C.; Purba, E.; Roberts, K. J.; Chen, Z.-P.; Martin, E.; Morris, J.; Bytheway, R., "An Examination of the Kinetics of the Solution-Mediated Polymorphic Phase Transformation between α- and β-Forms of L-Glutamic Acid as Determined Using Online Powder X-ray Diffraction." *Cryst. Growth. Des.* **2008,** 8, (7), 2205-2216.

19. Nguyen, T. N. P.; Kim, K.-J., "Transformation of Monohydrate into Anhydrous Form of Risedronate Monosodium in Methanol-Water Mixture." *Ind. Eng. Chem. Res.* **2010,** 49, 4842-4849.

20. Nguyen, T. N. P.; Kim, K.-J., "Transformation of Hemipentahydrate to Monohydrate of Risedronate Monosodium by Seed Crystallization in Solution." *AIChE J.* **2011,** 00, (0), 1-9.

21. Rodríguez-Hornedo, N.; Lechuga-Ballesteros, D.; Wu, H.-J., "Phase transition and heterogeneous/epitaxial nucleation of hydrated and anhydrous theophylline crystals." *Int. J. Pharma.* **1992,** 85, 149-162.

22. Mukuta, T.; Lee, A. Y.; Kawakami, T.; Myerson, A. S., "Influence of Impurities on the Solution-Mediated Phase Transformation of an Active Pharmaceutical Ingredient." *Cryst. Growth. Des.* **2005,** 5, (4), 1429-1436.

23. Lee, S.; Choi, A.; Kim, W.-K.; Myerson, A. S., "Phase Transformation of Sulfamerazine Using a Taylor Vortex." *Cryst. Growth. Des.* **2011,** 11, (11), 5019-5029.

24. Ono, T.; Ter Horst, J. H.; Jansens, P. J., "Quantitative Measurement of the Polymorphic Transformation of L-Glutamic Acid Using In-Situ Raman Spectroscopy." *Cryst. Growth. Des.* **2004,** 4, (3), 465-469.

25. Kelly, R. C.; Rodríguez-Hornedo, N., "Solvent Effects on the Crystallization and Preferential Nuceation of Carbamazepine Anhydrous Polymorphs: A Molecular Recognition Perspective." *Or. Process Res. Dev.* **2009,** 13, 1291-1300.

26. Wikstrom, H.; Rantanen, J.; Gift, A. D.; Taylor, L. S., "Toward an Understanding of the Factors Influencing Anhydrate-to-Hydrate Kinetics in Aqueous Environments." *Cryst. Growth. Des.* **2008,** 8, (8), 2684-2693.

27. Schöll, J.; Bonalumi, D.; Vicum, L.; Mazzotti, M.; Müller, M., "In Situ Monitoring and Modeling of the Solvent-Mediated Polymorphic Transformation of L-Glutamic Acid." *Cryst. Growth. Des.* **2006,** 6, (4), 881-891.

28. Mohan, R.; Koo, K.-K.; Strege, C.; Myerson, A. S., "Effect of Additives on the Transformation Behaviour of L-Phenylalanine in Aqueous Solution." *Ing. Eng. Chem. Res.* **2001,** 40, 6111-6117.

29. Qu, H.; Louhi-Kultanen, M.; Kallas, J., "Additive Effects on the Solvent-Mediated Anhydrate/Hydrate Phase Transformation in a Mixed Solvent." *Cryst. Growth. Des.* **2007,** 7, (4), 724-729.

30. Davey, R. J.; Blagden, N.; Righini, S.; Alison, H.; Ferrari, E. S., "Nucleation Control in Solution Mediated Polymoprhic Phase Transformations: The Case of 2,6-Dihydroxybenzoic Acid." *J. Phys. Chem. B* **2002,** 106, 1954-1959.

31. Brečević, L.; Skrtic, D.; Garside, J., "Transformation of Calcium Oxalate Hydrates." *J. Crystal Growth* **1986,** 74, 399-408.

32. Boistelle, R.; Rinaudo, C., "Phase transition and epitaxies between hydrated orthorhombic and anhydrous monoclinic uric acid crystals." *J. Cryst. Growth* **1981,** 53, 1-9.

33. Grases, F.; Villacampa, A. I.; Costa-Bauzá, A.; Söhnel, O., "Uric acid calculi: types, etiology and mechanisms of formation." *Clin. Chim. Acta.* **2000,** 302, 89-104.

34. Perrin, D. D.; Dempsey, B., *Buffers for pH and Metal Ion Control*. John Wiley & Sons: New York, 1974.

35. Isaacson, L. C., "Urinary composition in calcific nephrolithiasis." *Invest. Urol.* **1969,** 6, (4), 356-363.

36. Sours, R. E.; Swift, J. A., "Uric Acid Crystals and Their Relationship to Kidney Stone Disease." *Trans. ACA* **2004,** 39, (9), 1-7.

37. Ringertz, H., "Optical and crystallographic data of uric acid and its dihydrate." *Acta Cryst.* **1965,** 19, 286-287.

38. Gu, C-H.; Young, V. J.; Grant, D. J. W., "Polymorphic Screening: Influence of Solvents on the Rate of Solvent-Mediated Polymorphic Transformation." *J. Pharm. Sci.* **2001,** 90, (11), 1878-1890.

CHAPTER 5 EFFECTS OF ADDITIVES ON SOLUTION-MEDIATED PHASE TRANSFORMATION OF URIC ACID DIHYDRATE

5.1 Introduction

The transformation of synthetic UAD in model aqueous solutions with known ionic strengths and pH, as well as in model urine solution was described in Chapter 4. UAD transforms to UA via a 2-step process - metastable UAD dissolution followed by nucleation and growth of the stable UA. The transformation of UAD in solution at 37^{o} C occurs within 48 hours and is faster than at 25^{o} C. UAD to UA transformation in solution (either 37^{o} C or 25^{o} C) is faster than the UAD dehydration in air at 25^{o} C studied at 33%-75% relative humidity.[1]

Synthetic UAD crystals are clear, colorless rectangular plates. Natural crystals are typically colored due to trapped pigments of biological origin and can have more unusual shapes.[2, 3] There are also several casual references in the literature to differences in the stability of natural and synthetic UAD, with the former being more resistant to spontaneous dehydration in air. This prompted us to grow UAD in the presence of molecular dyes and physiologically relevant ions.

A number of papers have reported on the inclusion behavior in uric acid crystals.[4-8] Herein we investigate how impurity inclusion affects the transformation of UAD.

The use of natural and synthetic dyes in the study of uric acid crystal growth *in vitro* was reported by Gaubert[9] in the 1930s and Kleeberg[10-13] in the 1970s. These early studies showed that dye molecules can be trapped in uric acid host crystals, though the effect of concentration and specificity of inclusion was not examined. In more recent work, the growth of UA and UAD phases in the presence of select dye probes was examined in detail.[4-8] Cationic and neutral dye additives were incorporated within the UAD and UA matrixes, though no detectable inclusion of anionic dyes were observed. Cationic Chrysoidin G (CG) and Bismarck Brown Y (BBY) were among the dye probes that can be included in both UA and UAD crystals (Figure 5.1). Physiologically relevant inorganic ions can also be included in the UA and UAD matrixes.[7, 8, 14] Herein we investigate the effect of these impurities on the transformation kinetics of metastable UAD to the thermodynamically stable UA in model aqueous solutions and model urine solution.

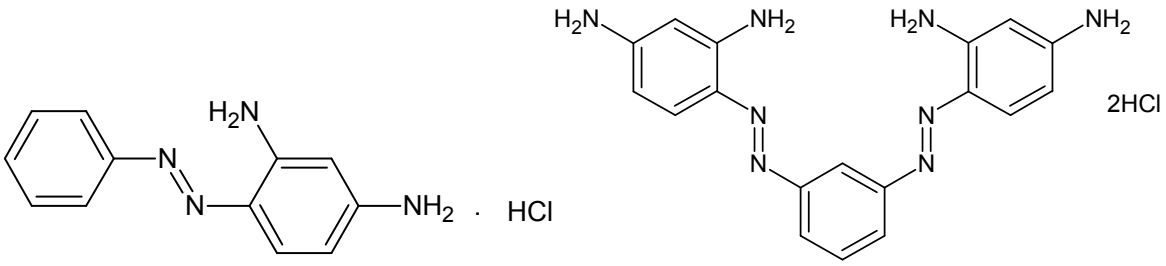

CG **BBY**

Figure 5.1. Molecular structures of Chrysoidin G (CG) and Bismarck Brown Y (BBY).

Impurities or additives are known to influence the phase transformation of many organic crystals[15-21] and inorganic crystals.[22, 23] Mohan *et al*.[16] described the effect of additives such as ammonium sulfate on the phase transformation of anhydrous L-phenylalanine into its monohydrate form. Ammonium sulfate lowers the solubility of anhydrous L-phenylalanine which inhibits its transformation to the more stable monohydrate. Yang *et al*.[17] reported the nucleation and polymorphic transformation of α-glycine to γ-glycine was promoted by the presence of NaCl. Further, the transformation rate was significantly accelerated with increasing ionic strength. In a different study, the solvent-mediated phase transformation of anhydrous to hydrated carbamazepine was inhibited by hydroxymethylcellulose[19] and accelerated by sodium lauryl sulfate.[24]

The effect of additives on phase transformation studies have also been performed on calcium oxalate dihydrate (COD), a known component of kidney stones.[22, 23] Amino acids such as histidine, serine, and tryptophan were reported to affect the transformation kinetics of COD to calcium oxalate monohydrate.[22] The slight inhibitory effect of histidine was thought to be due to the possible incorporation of histidine into COD crystals, which in turn, retards the dissolution process of COD. In another study, surfactants such as anionic sodium dodecyl sulfate and cationic dodecylammonium chloride both inhibited the phase transformation of COD.[23] In this chapter, the effects of additives on the solution-mediated phase transformation of UAD are described.

5.2 Experimental Methods and Materials

5.2.1 Materials

Water was purified by passage through two Barnstead deionizing cartridges (Barnstead International, USA) followed by distillation. Uric acid (>99%, Sigma) was used without further purification. Dyes were purchased from Aldrich [CAS #] and of the highest purity available: Bismarck Brown Y (BBY) [10114-58-6] 53% and Chrysoidin G (CG) [532-82-1] 90%. Compounds used to prepare artificial urine[25] solution were purchased from several vendors and used as received. From Aldrich: Na_2SO_4 (99.9%), KCl (99.0%); EM Science: NH_4Cl (99.8%), NaCl (99%), $MgSO_4 \cdot 7H_2O$ (98-102%); Fisher Scientific: Na_2HPO_4 (99.5%), $Na_2HPO_4 \cdot H_2O$ (99.1%), $Na_3C_6H_5O_7 \cdot 2H_2O$ (Certified), and Urea (Certified). McIlvaine buffers[26] with controlled pH and ionic strength were prepared from $C_6H_8O_7 \cdot H_2O$ (99.0%, EMD), Na_2HPO_4 (99.5%, Fisher), and KCl (99.0%, Sigma).

5.2.2 Crystal Growth

Pure UAD crystals (**UAD$^{25°C}_{pH4}$**) were prepared as described in section 1.2.3. UAD crystals were also grown from artificial urine (**UAD-urine**) at different temperatures and pH as described in section 3.2.4. At high supersaturation (4.5 mM), UAD could be directly precipitated from artificial urine solution at either room temperature (~25° C) or physiologic temperature (37° C). Determination of the level of inorganic impurities included in UAD crystals grown this way was described in section 3.3.5. For clarity, we use the nomenclature **UAD-urine$^{T}_{pH}$** to denote the temperature and pH of the growth solutions.

UAD with dye inclusions (**UAD-dye**) were prepared from supersaturated uric acid solutions (1.0 mM) which were cooled to near room temperature, after which dye powder was added to the growth solution to give a final $[dye]_{sol'n}$ = 0.5-200 μM.[7] The pH of the growth solutions were 4.45-4.56. After thorough mixing, the **UAD-dye** crystals were allowed to crystallize at room temperature (~25° C) in aluminum foil covered dishes by slow evaporation. All crystals were harvested for analysis after 2 days. For **UAD-dye** crystals, we use the nomenclature $\mathbf{UAD\text{-}dye^{T}_{c}}$ where *T* refers to the temperature of the growth solution and *c* is the $[dye]_{sol'n}$ and not the amount of dye included in the UAD crystal matrix. Table 5.1 lists all the UAD growth conditions and their respective nomenclature.

Table 5.1. Different UAD growth conditions and their respective nomenclature.

Growth condition	**Nomenclature**
Distilled water, 25°C, pH 4	$UAD^{25°C}_{pH4}$ or pure UAD
Artificial urine, 25°C, pH 4	$UAD\text{-}urine^{25°C}_{pH4}$
Artificial urine, 25°C, pH 5	$UAD\text{-}urine^{25°C}_{pH5}$
Artificial urine, 37°C, pH 4	$UAD\text{-}urine^{37°C}_{pH4}$
Artificial urine, 37°C, pH 5	$UAD\text{-}urine^{37°C}_{pH5}$
Distilled water with [BBY] =5μM	$UAD\text{-}BBY^{25°C}_{(5\mu M)}$
Distilled water with [BBY] =25μM	$UAD\text{-}BBY^{25°C}_{(25\mu M)}$
Distilled water with [CG] =200μM	$UAD\text{-}CG^{25°C}_{(200\mu M)}$

5.2.3 Optical Microscopy

As described in section 4.2.4, all micrographs were taken using an Olympus BX-50 polarizing microscope fitted with a Nikon COOLPIX995 digital camera operated with krinnicam_v1-03 software (Nikon Corp.).

5.2.4 Transformation Experiments

All samples were used as grown without sieving or grinding. Approximately 20 mg of **UAD-urine$^{25°C}_{pH4}$** was added to each of 24 glass bottles containing 50 mL of pH 5 McIlvaine buffer solution (IS = 0.5 M). These suspensions were then placed in a 37° C water bath on the same day with a staggered start time. Every 6 hours, 3 bottles were removed from the water bath, the solid phase was vacuum-filtered through Whatman # 1 filter paper, washed with distilled water, air-dried and immediately subjected to TGA and PXRD analysis. The transformation of **UAD-urine$^{25°C}_{pH4}$** was monitored for a period of 48 hours. The transformation of **UAD-urine$^{25°C}_{pH5}$**, **UAD-urine$^{37°C}_{pH4}$**, and **UAD-urine$^{37°C}_{pH5}$** were also monitored following the same procedure. In a parallel experiment, the transformation of the different **UAD-urine** crystals was performed in artificial urine solution (IS = ~0.5 M) at 37^{o} C.

Following the same procedure above, the transformation of **UAD-CG$^{25°C}_{(200\ \mu M)}$**, **UAD-BBY$^{25°C}_{(5\mu M)}$,** and **UAD-BBY$^{25°C}_{(25\mu M)}$** were performed in artificial urine solution (IS = ~0.5M) at 37^{o} C. For comparison, the transformation of **UAD$^{25°C}_{pH4}$** in artificial urine (described in Chapter 4) and artificial urine solutions containing $[dye]_{sol'n}$ = 0.5-200 μM were also monitored. All transformation experiments are tabulated in Table 5.2.

Table 5.2. UAD transformation experiments in different solutions.

Crystal	pH 5 McIlvaine buffer	pH ~5 Artificial urine	pH~5 Artificial urine + 200µM CG	pH ~5 Artificial urine + 5µM BBY	pH ~5 Artificial urine + 25µM BBY
$UAD^{25°C}_{pH4}$	✓	✓	✓	✓	✓
$UAD\text{-}urine^{25°C}_{pH4}$	✓	✓			
$UAD\text{-}urine^{25°C}_{pH5}$	✓	✓			
$UAD\text{-}urine^{37°C}_{pH4}$	✓	✓			
$UAD\text{-}urine^{37°C}_{pH5}$	✓	✓			
$UAD\text{-}CG^{25°C}_{(200\ \mu M)}$		✓			
$UAD\text{-}BBY^{25°C}_{(5\ \mu M)}$		✓			
$UAD\text{-}\ BBY^{25°C}_{(25\mu M)}$		✓			

5.2.5 Thermal Analysis

Thermogravimetric analyses (TGA) were performed on a SDT Q600 TA instrument (New Castle, DE) as described in 4.2.5. All experimental curves were analyzed with TA's Universal Analysis Software. The theoretical weight loss of UAD is 17.65%. The extent to which doped-UAD was converted to UA was determined by the difference method. All measurements were performed at least in triplicate and showed relatively low standard deviation.

5.2.6 Powder X-ray Diffraction

The transformation of doped UAD was qualitatively monitored by powder X-ray diffraction using a Rigaku R-AXIS RAPID-S X-ray diffractometer as described in section 4.2.6. As grinding of samples may contribute to the premature dehydration of doped-UAD, PXRD analyses were performed on unground the samples. The transformation was marked by the appearance and disappearance of several characteristic diffraction lines corresponding to UAD and UA.

5.3 Crystal Growth of Doped-Uric Acid Dihydrate Crystals

The morphology and size of UAD crystals was dependent on the growth condition. Crystals grown from artificial urine solution were mostly needle-like, elongated plates and agglomerates of plate-like crystals as shown in Figure 5.2. The altered habits are a consequence of electrostatic interactions between components in the solution and the various growing crystal faces. It is well established that additives influence the growth shape of crystals.[27-29]

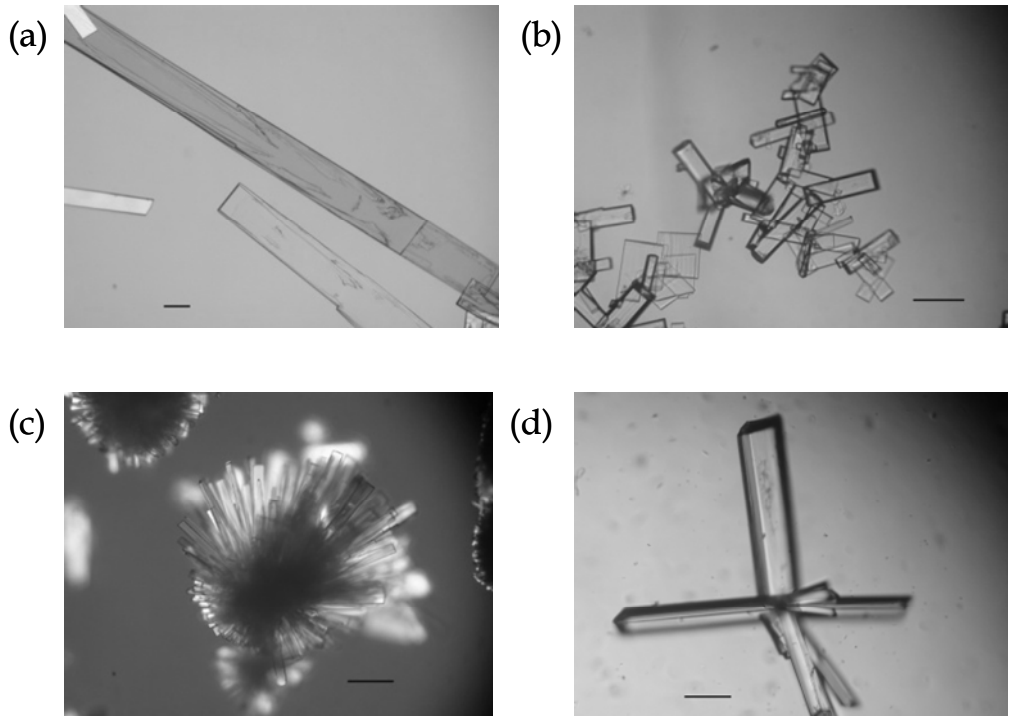

Figure 5.2. Photomicrographs of UAD grown from artificial urine solution. (a) UAD-urine$^{25°C}{}_{pH4}$, (b) UAD-urine$^{37°C}{}_{pH4}$, (c) UAD-urine$^{25°C}{}_{pH5}$, (d) UAD-urine$^{37°C}{}_{pH5}$. Scale bar = 100 μm.

In comparison, photomicrographs of pure UAD (**UAD$^{25°C}{}_{pH4}$**) and UAD grown in the presence of dyes (**UAD-CG$^{25°C}{}_{(200μM)}$, UAD-BBY$^{25°C}{}_{(5μM)}$, UAD-BBY$^{25°C}{}_{(25μM)}$**) appear in Figure 5.3. Both CG and BBY are cationic dyes. UAD crystals were grown from aqueous solutions containing 200 μM CG and 5 μM or 25 μM BBY. The amount of dye included in the crystal is a small fraction of the total dye concentration in solution. From UV-Vis experiments, an average of 1-2 CG molecules were included per 10^4 UA molecules, while 2-42 BBY molecules were included per 10^4 UA molecules.[7] CG and BBY were chosen as additives because their inclusion typically affected different growth sectors. An hour-glass inclusion was observed in UAD grown in the presence of CG. BBY was included in all sectors of the crystal and also changed the

morphology; the extent of change depends on the $[dye]_{sol'n}$. As the concentration is increased, the entire crystal became darkly colored and the morphology approached a diamond shape.

The morphology of **UAD-dye** crystals showed some similarities and differences to the crystals grown in pure distilled water. Compared to pure UAD (Figure 5.3a), **UAD-CG$^{25°C}_{(200\mu M)}$** (Figure 5.3.b) crystals are slightly longer along *a* than in *b*. In **UAD-BBY$^{25°C}_{(5\ \mu M)}$** and **UAD-BBY$^{25°C}_{(25\ \mu M)}$** (Figure 5.3.c-d), the *b* dimension is longer than *a,* and the {210} faces are more pronounced. An increase in $[BBY]_{sol'n}$ is accompanied by a relative increase in the size of the {210} faces.

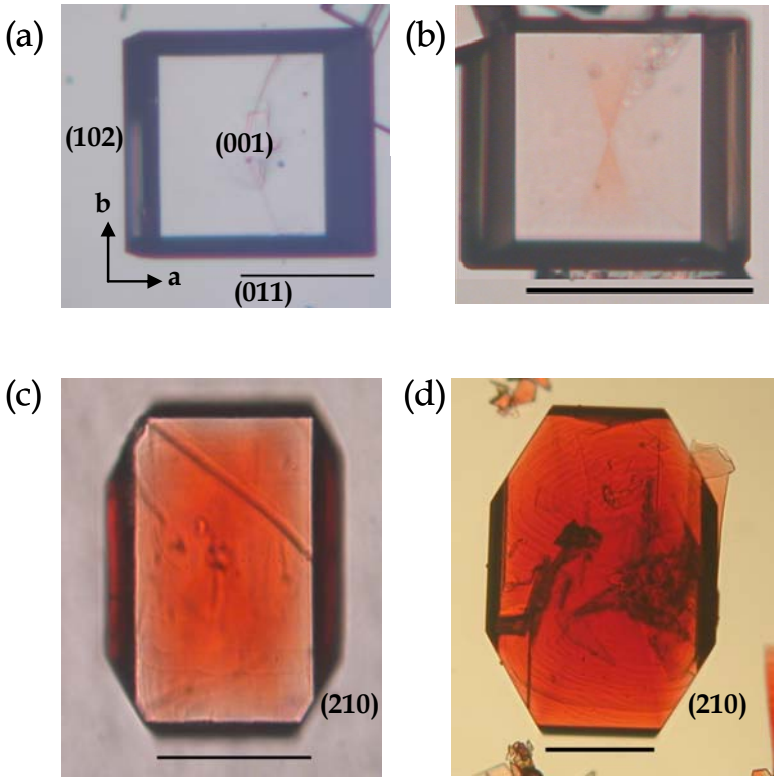

Figure 5.3. (a) UAD grown from distilled water and (b-d) UAD-dye crystals grown from various dye solutions. The $[dye]_{soln}$ were (b) 200 µM CG, (c) 5 µM BBY, and (d) 25 µM BBY. Scale bar=100 µm.

The orientation of CG and BBY additives inside UAD matrixes was difficult to establish. CG is conformationally flexible with two amino groups that can hydrogen bond with UA molecules. BBY is larger and is also conformationally flexible with rotational freedom about four single bonds (Figure 5.4). Low energy conformations can be calculated in the gas phase, but conformations can change to facilitate their incorporation into the crystals. Previous work suggested that included BBY spans two layers of a UAD crystal such that a single BBY molecule likely replaces at least 3 uric acid molecules and some water molecules.[30]

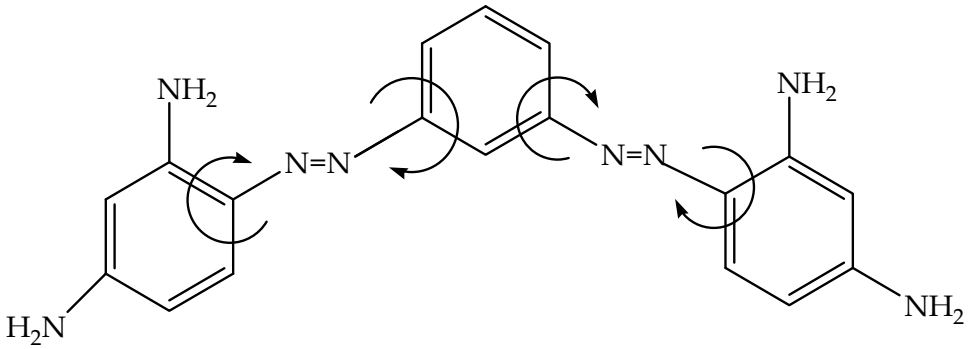

Figure 5. 4. Molecular structure of Bismarck Brown Y (BBY) indicating conformational freedom.

5.4 Transformation of Ion-doped Uric Acid Dihydrate Crystals

The solution-mediated transformation of **UAD-urine** crystals were studied in both pH 5 McIlvaine buffer solution and model urine solution. Solid samples immersed in various solutions at 37° C were analyzed every 6 hours for a total of 48 hours. Four types of artificial urine-grown UAD crystals were analyzed. The transformations of these ion-doped UAD are discussed separately.

5.4.1 Transformation in pH 5 McIlvaine Buffer Solution at 37° C

Figure 5.5 shows representative microscopic images of the transformation of different **UAD-urine** crystals in pH 5 McIlvaine buffer at 37° C for 48 hours. The morphology of the crystals remained the same during the course of the transformation. The use of optical microscopy and conoscopy to differentiate between UAD and UA crystals proved to be challenging as conoscopy only works well with smooth and thick crystals. The smooth albeit small crystals indicated by the red circles are the newly nucleated UA crystals.

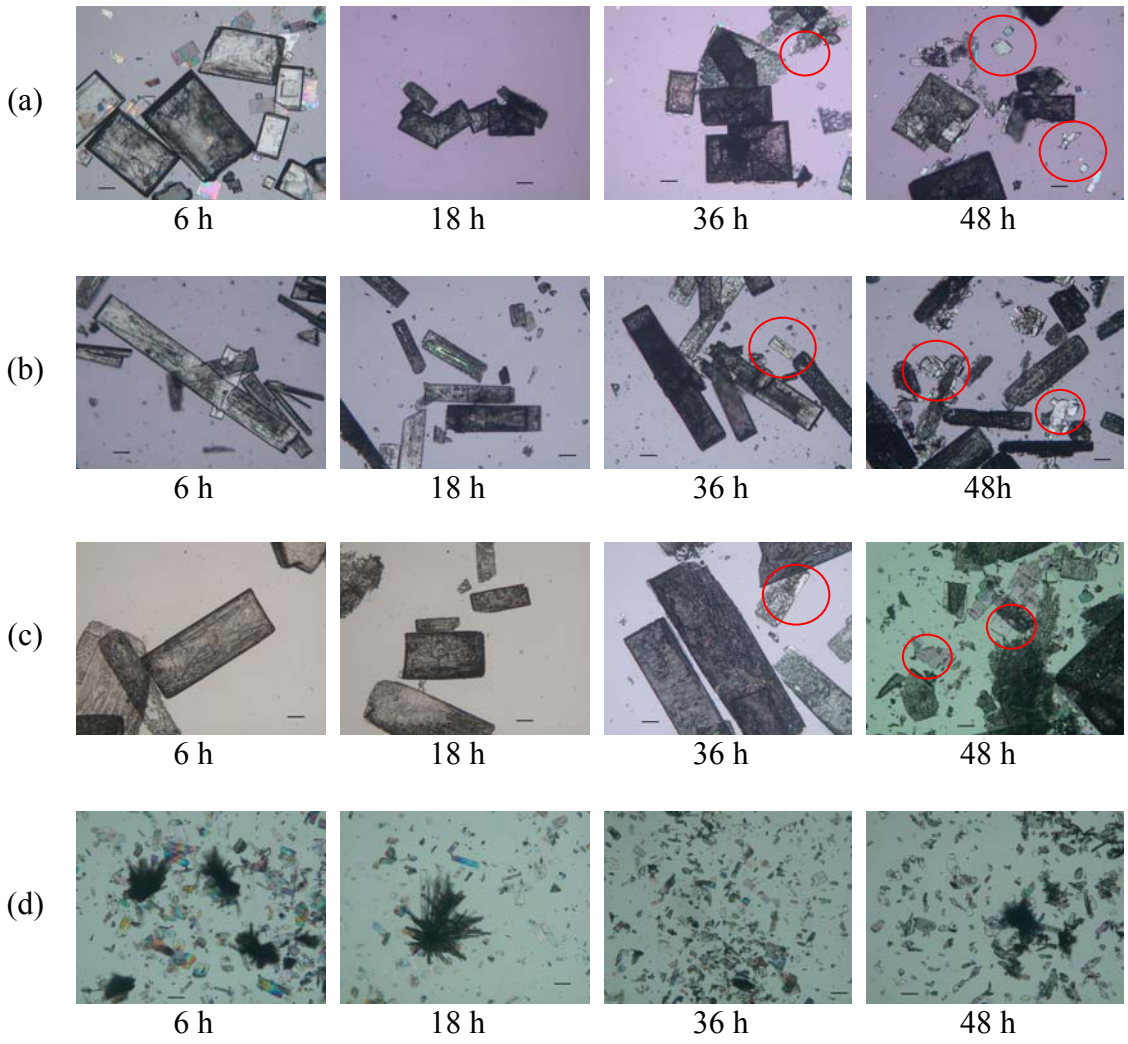

Figure 5.5. Photomicrographs of the transformation of **UAD-urine** in pH 5 McIlvaine buffer solution at 37° C. (a) UAD-urine$^{37°C}_{pH4,}$ (b) UAD-urine$^{37°C}_{pH5}$, (c) UAD-urine$^{25°C}_{pH4}$, and (d) UAD-urine$^{25°C}_{pH5}$. Scale bar = 100 µm. Red circles indicate the newly nucleated UA crystals.

The phase composition of the samples that were removed from suspensions at defined time intervals was qualitatively examined by PXRD. Diffraction data of the transformation of **UAD-urine$^{25°C}_{pH5}$** in pH 5 McIlvaine buffer at 37° C appear in Figure 5.6. These crystals are the smallest among the ion-doped UAD crystals and are the only ones that show complete

transformation within 48 hours in this solution. The diffraction patterns obtained at 6-24 hours show reflections attributed mostly to UAD. At 30-42 hours, distinct reflections of (200), (210), (11-1) corresponding to UA have emerged. The transformation appears to be complete by 48 hours.

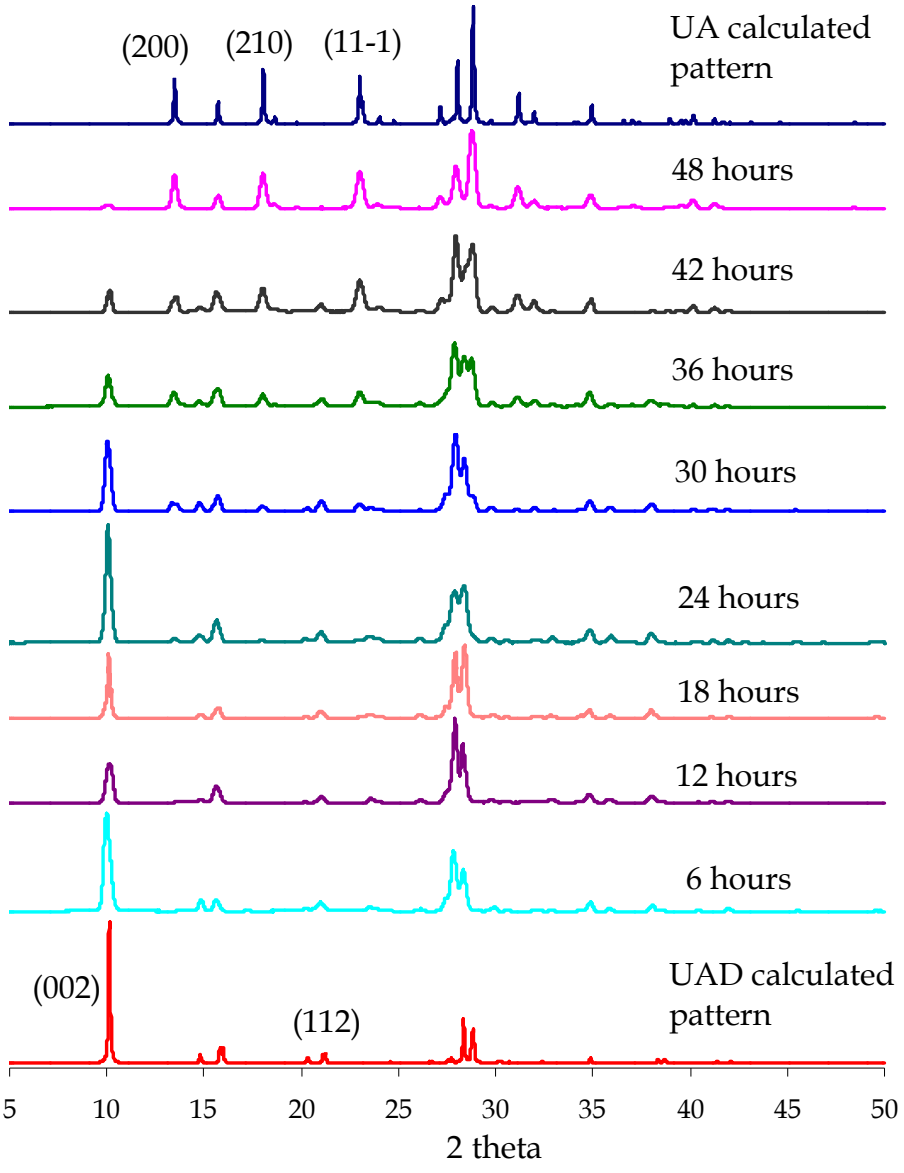

Figure 5.6. PXRD of the transformation of **UAD-urine**$^{25°C}_{pH5}$ in pH 5 McIlvaine buffer at 37 ° C.

The extent of the conversion of **UAD-urine** crystals to UA in pH 5 McIlvaine buffer at 37° C was determined by TGA and is summarized in Figure 5.7. The transformation of UAD grown from distilled water, **UAD$^{25°C}_{pH4}$**, (black curve, data from Chapter 4) is included in the graph for comparison. All **UAD-urine** crystals transform slower than **UAD$^{25°C}_{pH4}$**.

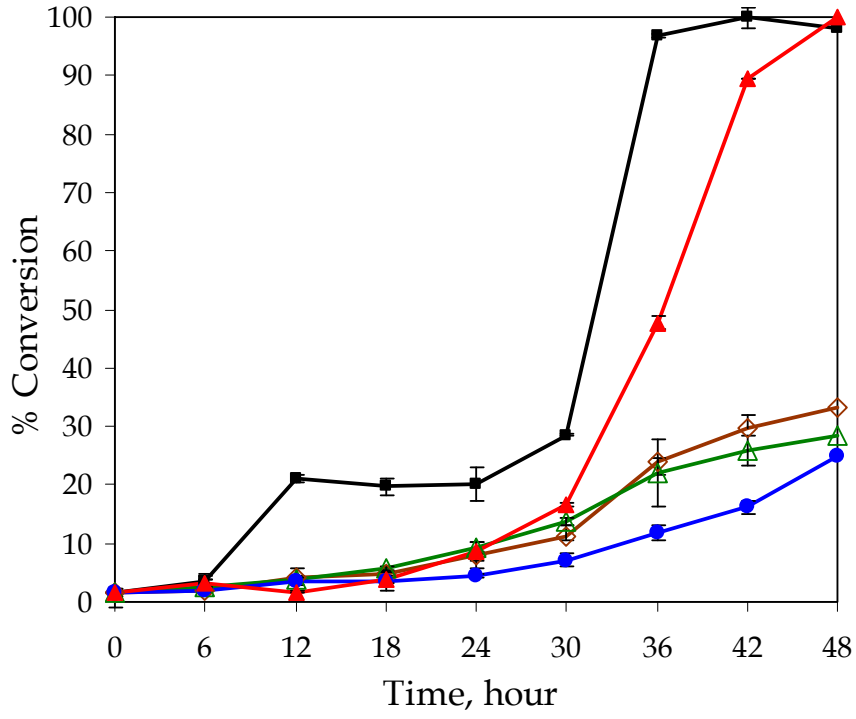

Figure 5. 7. Summary of the conversion of **UAD-urine** to UA in pH 5 McIlvaine buffer at 37° C. (Red) UAD-urine$^{25°C}_{pH5}$, (Brown) UAD-urine$^{37°C}_{pH4}$, (Green) UAD-urine$^{37°C}_{pH5}$, (Blue) UAD-urine$^{25°C}_{pH4}$. (Black) UAD$^{25°C}_{pH4}$ is shown for comparison.

UAD$^{25°C}_{pH4}$ (black) transforms to UA in pH 5 McIlvaine buffer at 37^{o} C in ~42 hours. The only **UAD-urine** sample to approach this transformation rate was **UAD-urine$^{25°C}_{pH5}$** (red). At 42 hours, roughly ~90% of UAD was converted to UA. None of the other **UAD-urine** crystals transformed completely to UA within 48 hours. At 48 hours, **UAD-urine$^{37°C}_{pH4}$** (brown) and

UAD-urine$^{37°C}_{pH5}$ (green) are only 33% and 29% transformed, respectively. **UAD-urine**$^{25°C}_{pH4}$ (blue) is only 25% transformed at 48 hours.

The observed transformation phenomena exhibited by **UAD-urine** crystals can be attributed to factors such as crystal size, solubility, and the presence of impurities in the crystals. The smallest **UAD-urine** crystals completely transformed to UA in 48 hours while the largest crystals transformed only by 25 %. However, size differences alone cannot explain this result. As described in section 3.3.5.3, varying concentrations of Na^+, K^+, and Mg^{2+} are included in **UAD-urine** crystals depending on their initial growth conditions. For all the cations studied, higher dopant levels were observed at higher pH. Inclusions of ions in the UAD matrix seem to significantly lower the rate of the transformation process. The higher inclusion of cations in **UAD-urine**$^{37°C}_{pH5}$ is therefore presumed to significantly lower the rate of the transformation process, which explains its conversion of only 29% within 48 hours.

While we did not determine the solubility of **UAD-urine** crystals in pH 5 McIlvaine buffer, it is apparent that solubility is a factor in the transformation process. As mentioned, solution-mediated phase transformation occurs in stages in which the metastable phase undergoes dissolution and subsequent nucleation and growth of the stable phase. Impurities or additives can alter the solubility of a crystal thereby affecting its dissolution rate.[15] The **UAD-urine** crystals are hypothesized to be less soluble than the pure UAD in pH 5 McIlvaine buffer regardless of the crystal size. This is presumably due to the higher lattice energy of doped UAD which must exchange hydrogen-bonding interactions in the pure crystals for electrostatic interactions in the doped versions. A complete transformation of **UAD-urine** to UA is presumed to occur if the transformation is monitored for longer than 48 hours. A longer transformation time would likely

allow the dissolution and recrystallization process to continue until all the **UAD-urine** crystals are dissolved, and only the stable UA remains.

5.4.2 Transformation in Artificial Urine Solution at 37° C

Figure 5.8 shows microscopic images of the transformation of different **UAD-urine** crystals in artificial urine solution at 37° C for 48 hours. The morphology of the crystals remained the same during the course of the transformation. As discussed previously, microscopy and conoscopy cannot unambiguously differentiate between UAD and UA. The smooth albeit small crystals indicated by the red circles are surmised to be the newly nucleated UA crystals. UA crystals that are grown epitaxially on UAD surface are also evident at 36-48 hours into the transformation as depicted in Figure 5.8c. Qualitative examination of the phase composition of the solid phase by PXRD showed that only the **UAD-urine**$^{25°C}_{pH5}$ completely transformed to UA within 48 hours. This result is similar to the transformation in pH 5 McIlvaine buffer discussed in section 5.4.1. Representative diffraction data of the transformation of **UAD-urine**$^{25°C}_{pH5}$ in artificial urine at 37° C are presented in Figure 5.9.

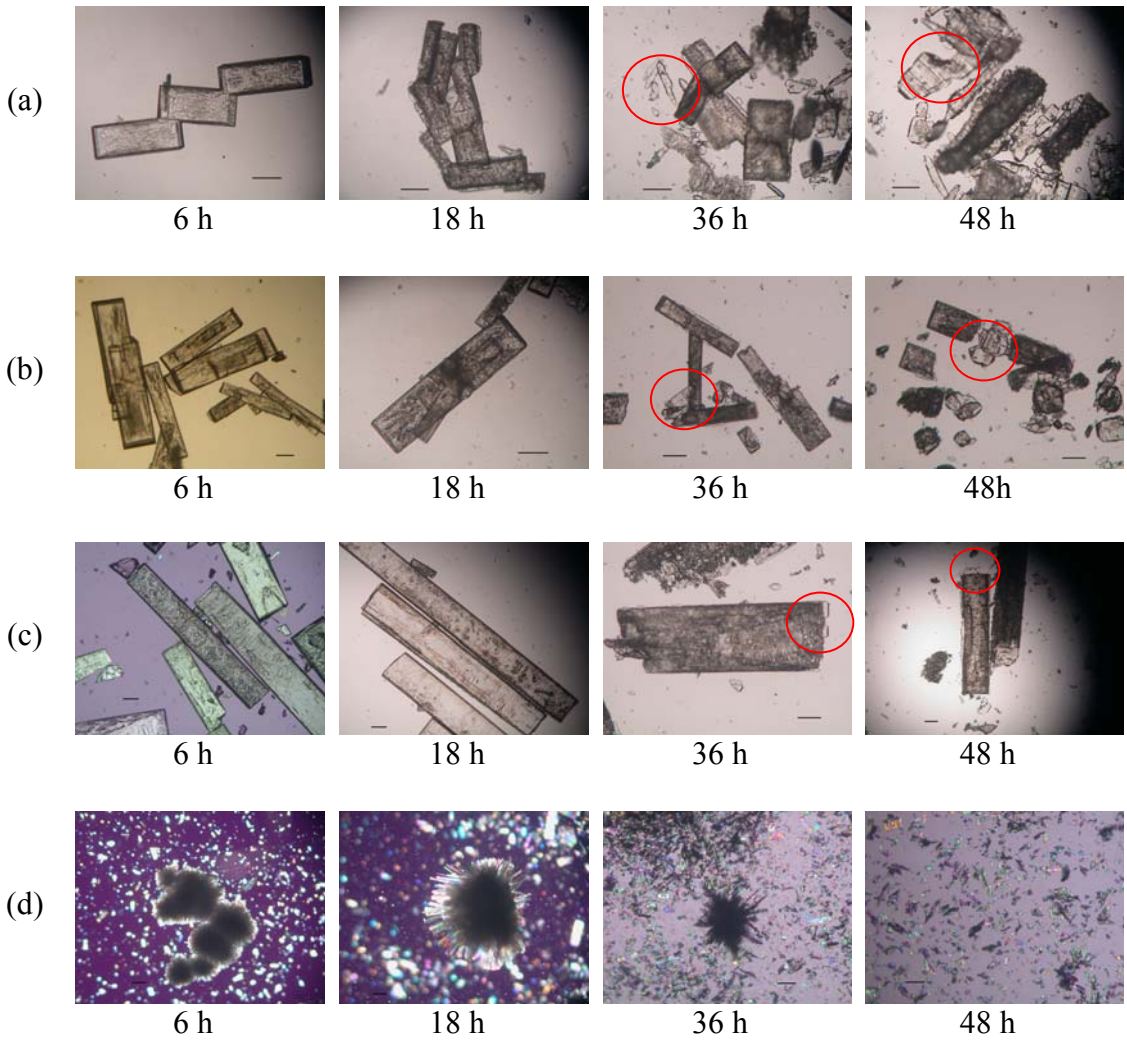

Figure 5.8. Photomicrographs of the transformation of **UAD-urine** in artificial urine solution at 37° C. (a) UAD-urine$^{37°C}_{pH4}$, (b) UAD-urine$^{37°C}_{pH5}$, (c) UAD-urine$^{25°C}_{pH4}$, and (d) UAD-urine$^{25°C}_{pH5}$. Scale bar = 100 µm. Red circles indicate the newly nucleated UA crystals.

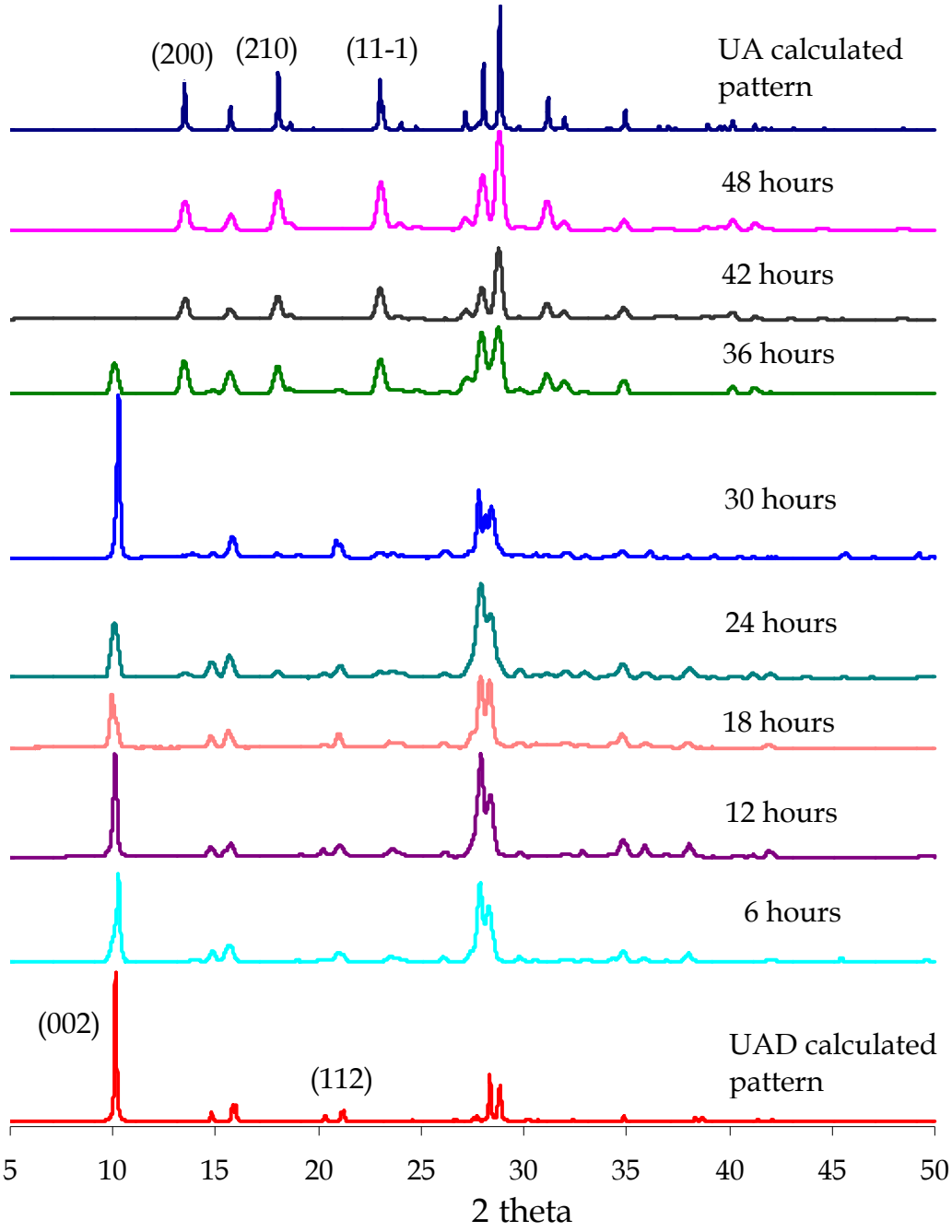

Figure 5.9. PXRD of the transformation of **UAD-urine**$^{25°C}{}_{pH5}$ in artificial urine at 37° C.

The % conversion of the **UAD-urine** crystals to UA in artificial urine at 37° C was determined by TGA and is summarized in Figure 5.10. The transformation of UAD grown from distilled water, **UAD**$^{25°C}_{pH4}$, (black curve, data from Chapter 4) is included in the graph for comparison. All **UAD-urine** crystals transform slower than UAD grown from distilled water. Notably, the trends are similar to what was observed in McIlvaine buffer (Figure 5.7).

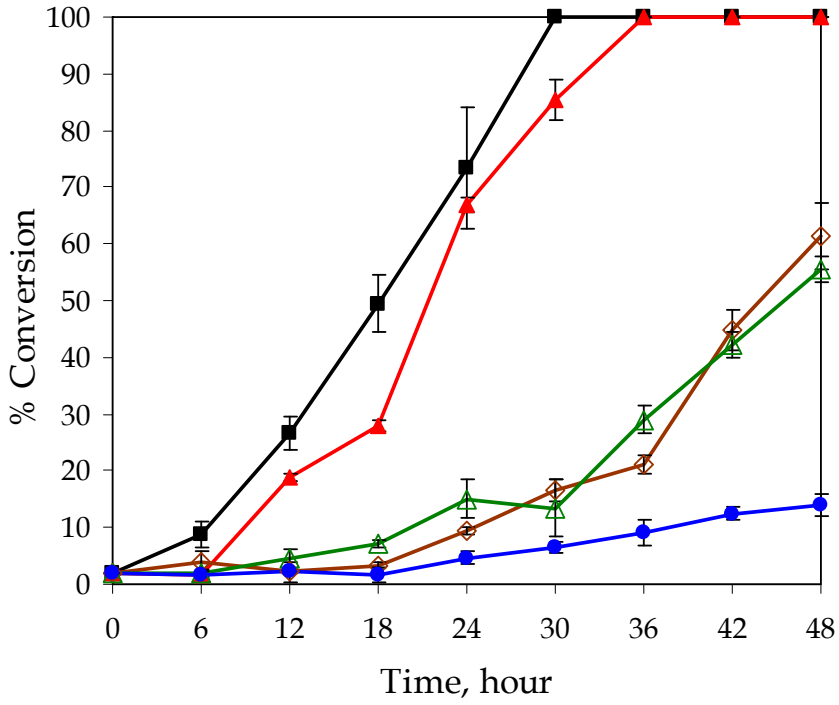

Figure 5. 10. Summary of the conversion of **UAD-urine** in artificial urine solution at 37° C. (Red) UAD-urine$^{25°C}_{pH5}$, (Brown) UAD-urine$^{37°C}_{pH4}$, (Green) UAD-urine$^{37°C}_{pH5}$, (Blue) UAD-urine$^{25°C}_{pH4}$. (Black) UAD$^{25°C}_{pH4}$ is shown for comparison.

UAD-urine$^{25°C}_{pH5}$ (red curve) was the only sample that completely transformed within 48 hours. The % conversion at 30 hours was 15 % lower than that observed for **UAD**$^{25°C}_{pH4}$. After 48 hours, **UAD-urine**$^{37°C}_{pH4}$ (brown curve) and **UAD-urine**$^{37°C}_{pH5}$ (green curve) shows

comparable conversion of 61% and 56% at 48 hours, respectively. Only 14 % **UAD-urine**$^{25°C}_{pH4}$ (blue curve) was transformed after 48 hours.

While only the smallest **UAD-urine** crystals were completely transformed to UA in 48 hours, size differences alone cannot explain the transformation rates observed in this experiment. UAD crystals grown from distilled water and **UAD-urine** crystals are fundamentally different. Apart from morphological differences, inclusions of cations in UAD crystals significantly lower the rate of the transformation process.

It is noteworthy to mention that UA can also include Na^+, K^+, Mg^{2+} impurities when grown from solutions containing up to 0.12 M salts.[8] The resulting crystals showed inclusion levels of 8-12 Na^+, 5-13 K^+, and 11-15 Mg^{2+} was found for every 10^4 uric acid molecules. This is higher than the levels seen in **UAD-urine**, but not unexpectedly so since the solution salt concentration was higher. Whether the starting UAD is doped or undoped, transformation in artificial urine should result in similar dopant levels in the final UA product.

5.5 Transformation of Dye-doped Uric Acid Dihydrate Crystals

The solution-mediated transformation of **UAD-dye** crystals was studied in artificial urine solution. The UAD:UA composition was analyzed every 6 hours for a total of 48 hours in artificial urine solution at 37° C. As described in section 5.3, the inclusion of dye molecules in the UAD host matrix was ~1-2 CG dyes and 2-42 BBY dyes per 10^4 uric acid molecules. Higher % dye dopant level is observed relative to the inorganic dopants in the last section.

5.5.1 UAD-Bismarck Brown Y Crystals

Figure 5.11 follows the transformation of UAD-BBY in artificial urine solution at 37° C. Figures 5.11a and b correspond to the transformation of UAD crystals grown from solution with 5 μM BBY and 25 μM BBY, respectively. Dopant loading in UAD crystals grown in the presence of BBY generally increased with increasing $[BBY]_{sol'n}$, and ranged from 2-42 dye molecules per 10^4 uric acid molecules. BBY was included in all sectors of the crystal and also changed the morphology; the extent of change depends on the $[dye]_{sol'n}$. As the concentration was increased, the entire crystal became darkly colored and the morphology approached a diamond shape.

During the course of the transformation, UAD-BBY crystals in Figure 5.11a turned opaque (6-30 h) and more transparent crystals presumed to be UA are formed at 42 hours. The final UA crystals appeared slightly colored, which we attribute to the incorporation of the dye released from the starting UAD-BBY material. In contrast, the UAD-BBY crystal morphology in Figure 5.11b remains the same over the 42 hour time period.

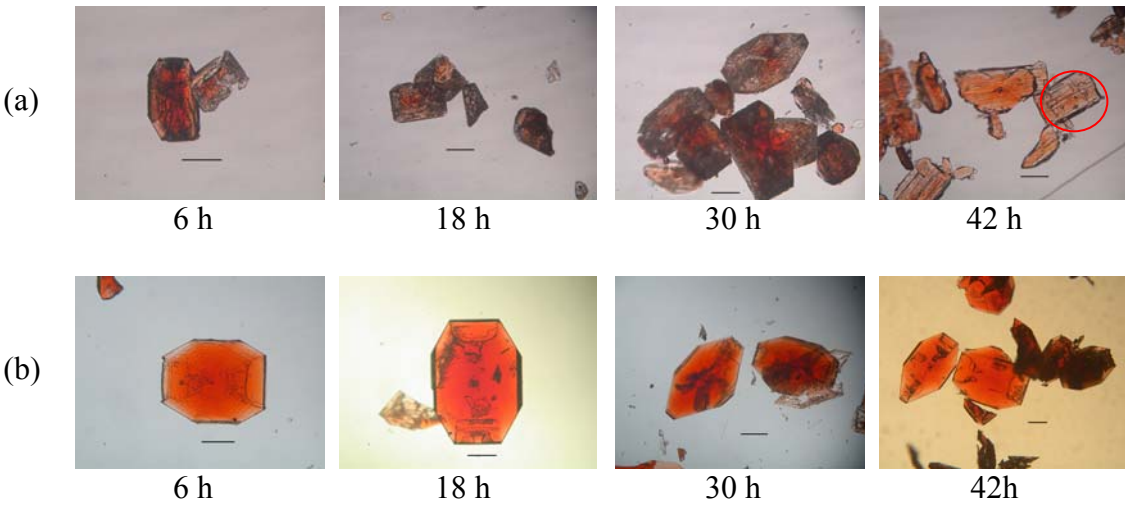

Figure 5. 11. Photomicrographs of the transformation of **UAD-dye** artificial urine solution at 37° C. (a) UAD-BBY$^{25°C}_{(5\mu M)}$ and (b) UAD-BBY$^{25°C}_{(25\mu M)}$. Scale bar = 100 µm.

The phase composition of UAD-BBY samples that were removed from suspensions at defined time intervals was examined by PXRD and TGA. TGA of the **UAD-BBY$^{25°C}_{(5\mu M)}$** shows ~23% conversion to UA after 24 hours and essentially complete conversion to UA after 48 hours. In contrast, **UAD-BBY$^{25°C}_{(25\mu M)}$** was only ~6% and ~7% at 24 hours and 48 hours, respectively. This is consistent with the diffraction data of the transformation **UAD-BBY$^{25°C}_{(25\mu M)}$** presented in Figure 5.12. Throughout the transformation time of 48 hours, the diffraction patterns at 6-48 hours show reflections corresponding mostly to UAD. Evidently, UAD with higher BBY inclusion hardly transformed to UA.

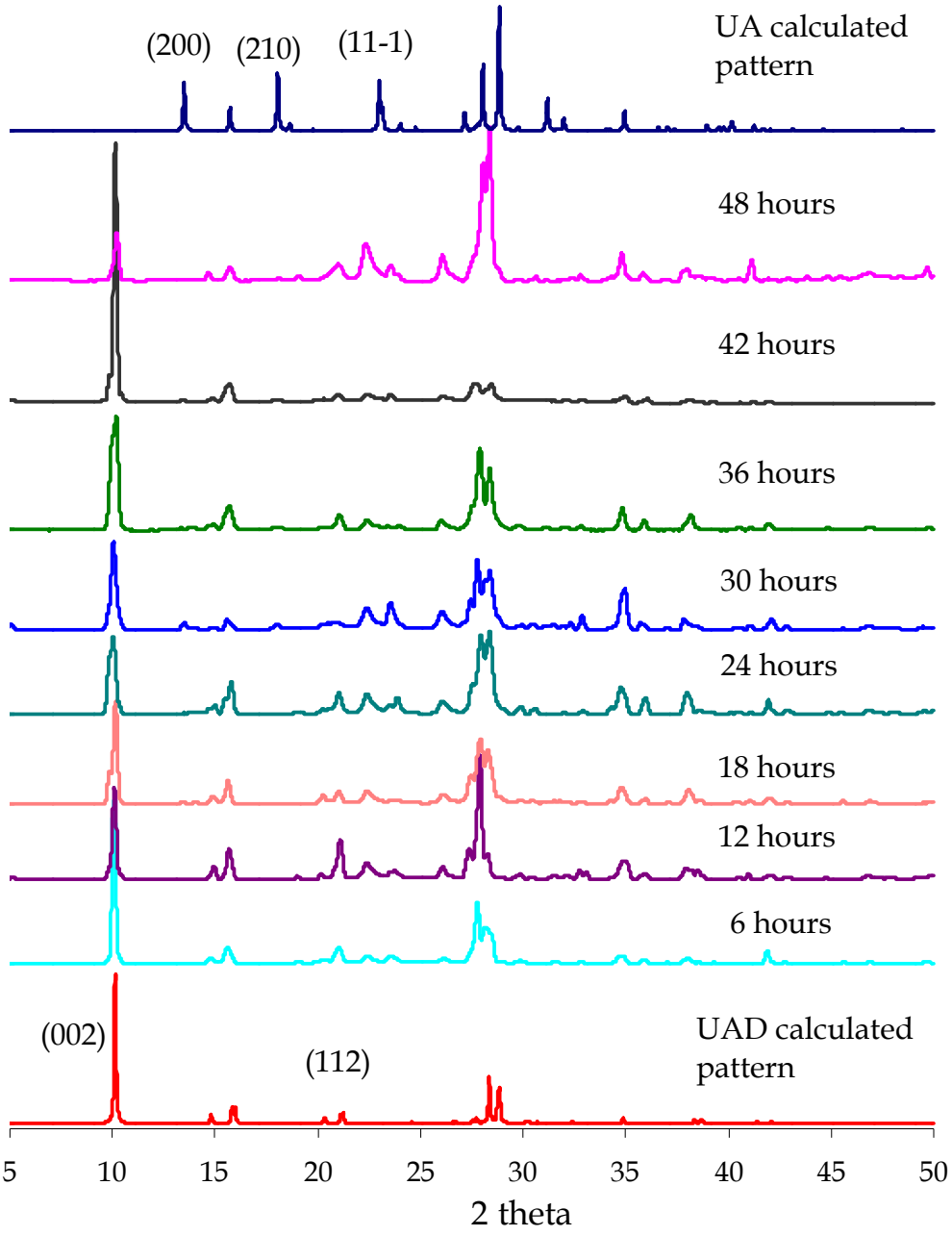

Figure 5. 12. Transformation of **UAD-BBY**$^{25°C}_{(25\mu M)}$ in artificial urine at 37° C.

5.5.2 UAD-Chrysoidin G Crystals

The dopant level of CG molecules in UAD was independent of the $[CG]_{sol'n}$ over the range 100-300 µM, with an average of 1-2 CG molecules included per 10^4 UA molecules.[7] This dopant level is lower than in UAD-BBY. Figure 5.13 follows the transformation of **UAD-CG$^{25°C}_{(200\ \mu M)}$** in artificial urine solution at 37° C. **UAD-CG$^{25°C}_{(200\mu M)}$** crystals undergo dissolution to produce supersaturation for the UA crystals to nucleate and grow. At 24 hours, UA crystals (indicated by red circle) start to nucleate on the surface of UAD. Smooth and tiny crystalline materials are continually produced after **UAD-CG$^{25°C}_{(200\ \mu M)}$** was in contact with the artificial urine solution for 48 hours. UA crystals that were produced at the end of the transformation were faintly colored which is attributed to the inclusion of CG molecules (released from UAD) in the UA formed. Previous work has shown that CG molecules can include in the UA crystal matrix, ~1-2 dyes per 10^4 uric acid molecules when grown from solutions containing $[CG]_{sol'n}$ = 1-400 µM.[8]

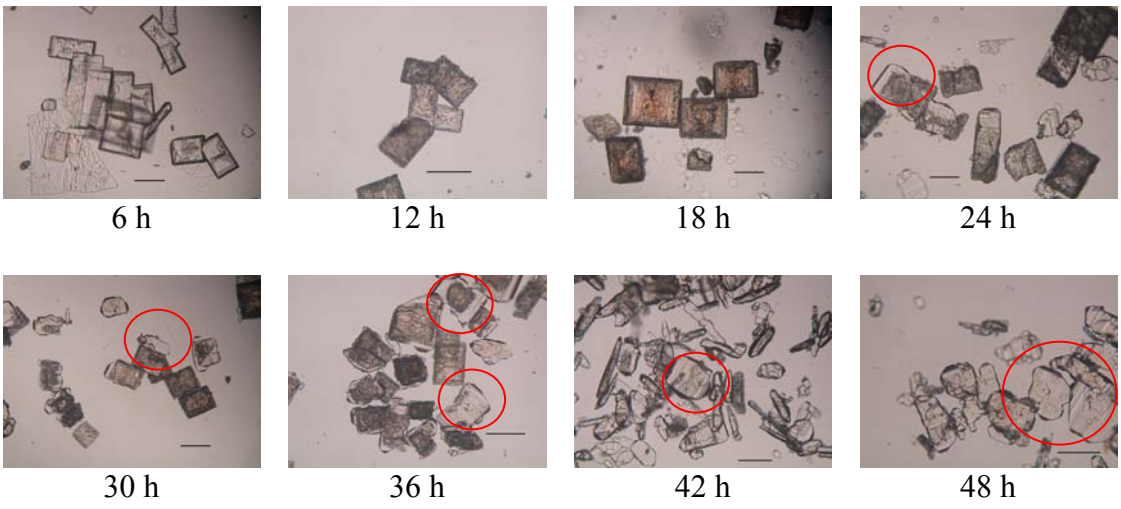

Figure 5. 13. Photomicrographs of the transformation of UAD-CG in artificial urine solution at 37° C. Scale bar = 100 µm. UA crystals are indicated by red circles.

5.5.3 Summary of the Dye-doped UAD Transformations in Artificial Urine

A summary of the transformation of **UAD-dye** crystals in artificial urine at 37° C is shown in Figure 5.14. The transformation of $\mathbf{UAD^{25°C}_{pH4}}$ (black curve, data from Chapter 4) is included in the graph for comparison. All **UAD-dyes** samples transformed slower than $\mathbf{UAD^{25°C}_{pH4}}$. The rate of UAD-CG transformation was faster than in UAD-BBY. At 24 hours, over 50 % of $\mathbf{UAD\text{-}CG^{25°C}_{(200\ \mu M)}}$ had converted, while only 9-15 % UAD-BBY converted (red and blue curves). $\mathbf{UAD\text{-}BBY^{25°C}_{(5\mu M)}}$ (red curve) transformed much faster than $\mathbf{UAD\text{-}BBY^{25°C}_{(25\mu M)}}$ (blue curve). For example at 42 hours, $\mathbf{UAD\text{-}BBY^{25°C}_{(5\mu M)}}$ had converted 7x as much as $\mathbf{UAD\text{-}BBY^{25°C}_{(25\mu M)}}$. It can be inferred that the presence of impurities/dopants in the crystal decreased the solubility of UAD, and therefore decreased the driving force of the solution-mediated transformation. We next examined the transformation of pure UAD ($\mathbf{UAD^{25°C}_{pH4}}$) in artificial urine containing dye to assess the extent to which these dopants affect the nucleation and growth of UA.

The inhibitory effects of the presence of dye impurities in the UAD transformation are due to several factors including the molecular size, functionality and charge of the dye, its relative and absolute ability to include in the matrix of the crystal, and the associations between uric acid and dyes in solution. CG exhibited lower inclusion in the UAD crystal than BBY. It is therefore not surprising to observe lower inhibitory effect of CG than BBY. With UAD-BBY, the inhibitory effect of BBY on the transformation of UAD to UA increased as the dye inclusion in the crystals increases. The association of the released dyes during the transformation process with the growing UA is also a factor in the rate of the transformation of **UAD-dye** crystals. Previous work has shown that uric acid molecules interact with BBY[8, 30] and CG[8] in solution. Visible absorption spectra for UA-BBY show a λ_{max} ranging from 469-479 nm. In aqueous BBY solutions, the λ_{max}

is shifted to 465 nm. Similarly, the λ_{max} of UA-CG is at 474-498 nm and is shifted to 453 nm in aqueous CG solutions.

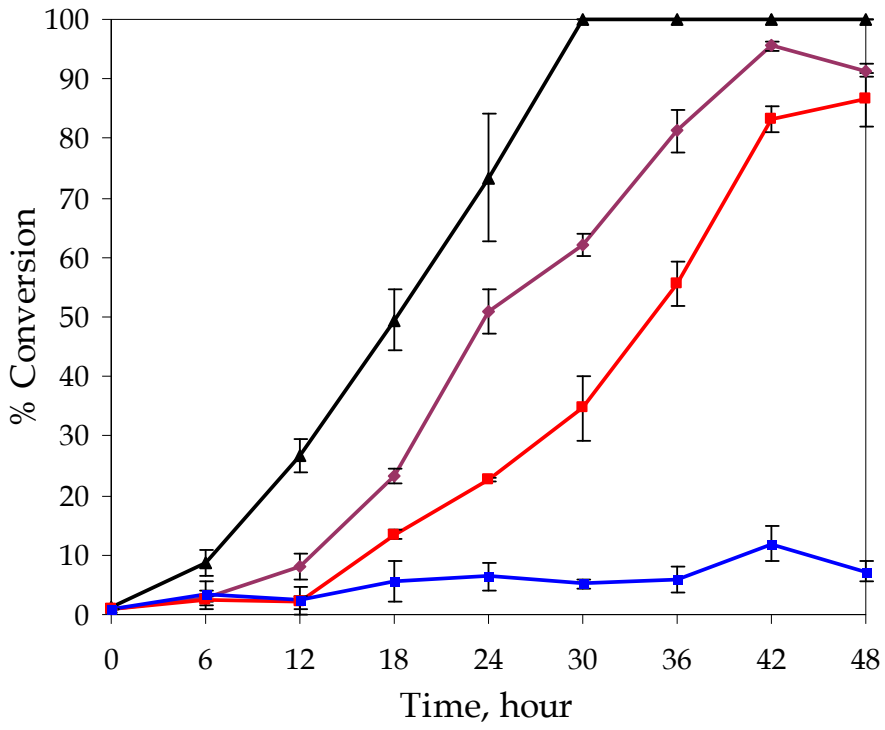

Figure 5. 14. Summary of the conversion of **UAD-dye** in artificial urine solution at 37° C. (Purple) UAD-$CG^{25°C}_{(200\ \mu M)}$, (Red) UAD-$BBY^{25°C}_{(5\ \mu M)}$, (Blue) UAD- $BBY^{25°C}_{(25\ \mu M)}$. (Black) The transformation of $UAD^{25°C}_{pH4}$ is shown for comparison.

5.6 Transformation of UAD in Artificial Urine Solution with Dyes

The solution-mediated transformation of $\mathbf{UAD^{25°C}_{pH4}}$ crystals was studied in model urine solution containing molecular dyes. Solid samples of $\mathbf{UAD^{25°C}_{pH4}}$ in artificial urine solutions containing BBY or CG dyes at 37° C were analyzed every 6 hours for a total of 48 hours.

5.6.1 UAD in Artificial Urine with BBY

The transformation of **UAD$^{25°C}_{pH4}$** in artificial urine containing BBY at 37° C is shown in Figure 5.15. The smooth albeit colored crystals seen at 30-42 hours indicates growth of UA crystals. The crystals appeared colored which is due to the inclusion of BBY dye molecules in the UA matrix. Previous work[8] has shown the inclusion of BBY in UA matrix. About 0.5-20 dyes per 10^4 uric acid molecules were included in the UA crystals when grown from aqueous solutions with $[BBY]_{so'n}$ = 2-50 µM. The absorption spectroscopy on single crystals showed a λ_{max} range indicative of multiple orientations and/or conformations of trapped dyes.

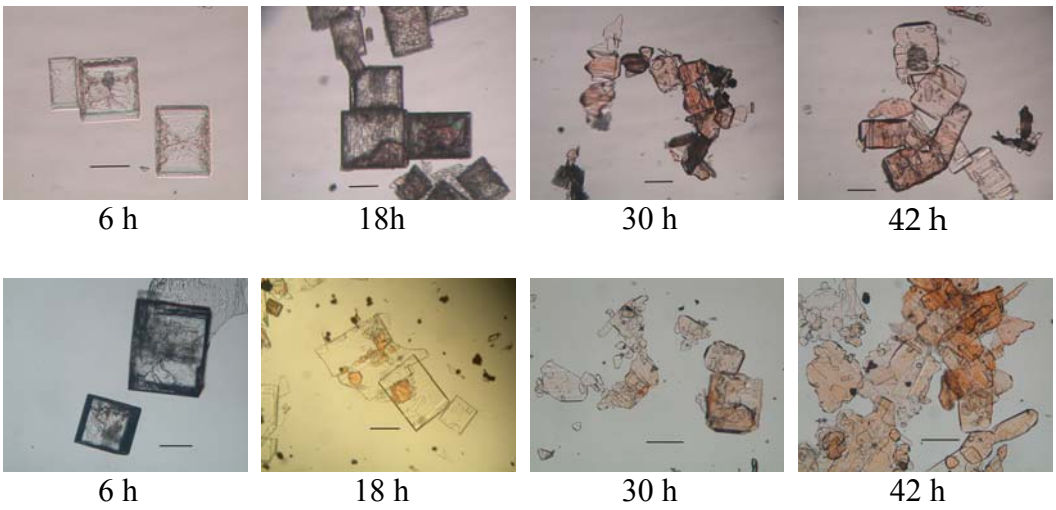

Figure 5. 15. Photomicrographs of the transformation of **UAD$^{25°C}_{pH4}$** in artificial urine containing (a) 5 µM BBY and (b) 25 µM BBY. Scale bar = 100 µm.

Similar to other transformation experiments discussed previously, the phase composition of samples removed from suspensions at defined time interval was examined by PXRD and TGA. The diffraction data of the transformation of pure UAD in artificial urine solution with 25 µM

BBY appears in Figure 5.16. At 24 hours, only diffraction lines corresponding to UA were apparent, indicating complete conversion of UAD to UA. The rate of conversion was similar to that seen in model urine in the absence of dye (black curve, Figure 5.14). From this we conclude that the dye asserts a much greater effect on the dissolution of UAD than the growth of UA.

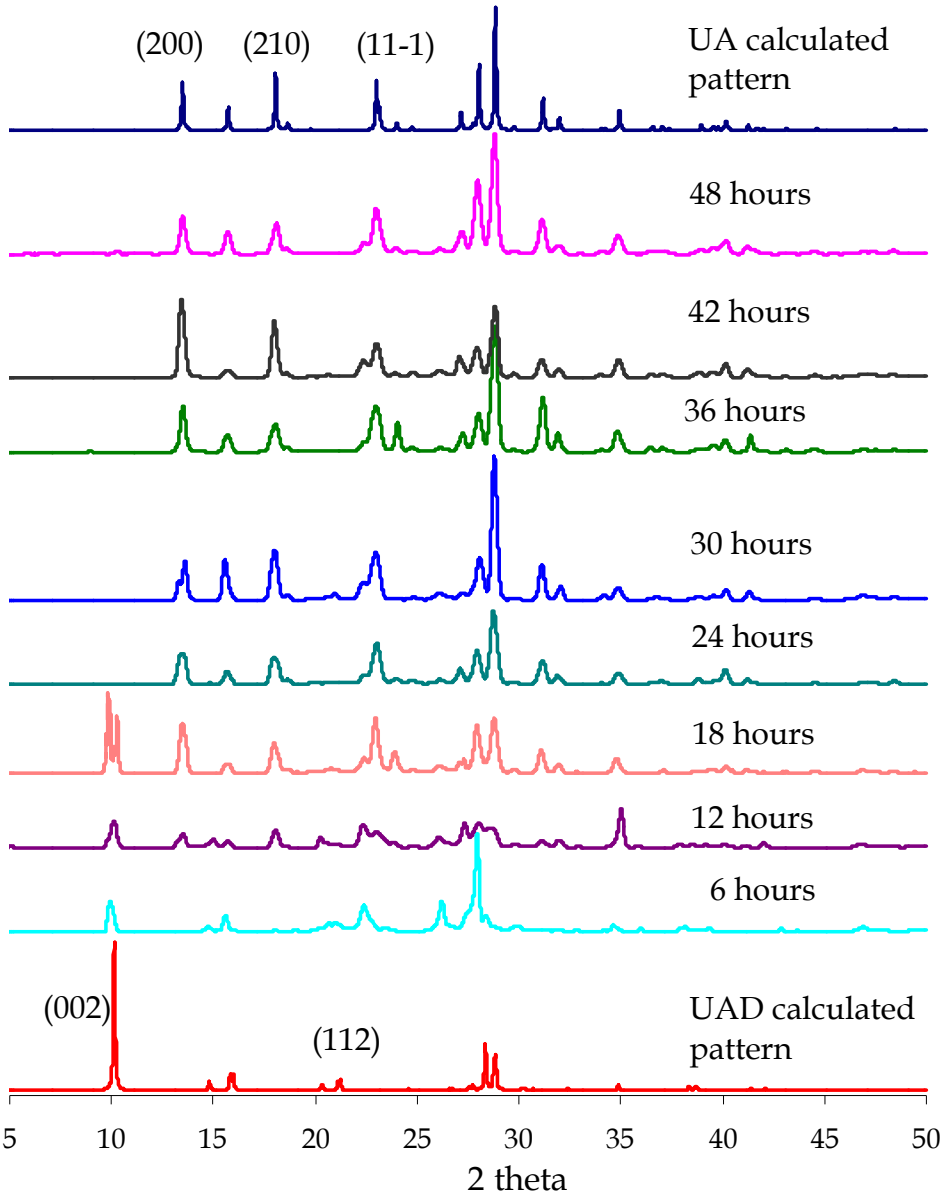

Figure 5. 16. Transformation of $\mathbf{UAD^{25°C}_{pH4}}$ in artificial urine solution containing 25 μM BBY.

5.6.2 UAD in Artificial Urine with CG

The transformation of **UAD**$^{25°C}_{pH4}$ in artificial urine containing 200 µM CG at 37° C is shown in Figure 5.17. The disappearance of colorless UAD and appearance of colored UA crystals at 30-48 hours illustrates the transformation. UA is known to include CG impurities, ~1-2 dyes per 10^4 uric acid molecules when grown from $[CG]_{sol'n}$ = 1-400 µM.[8]

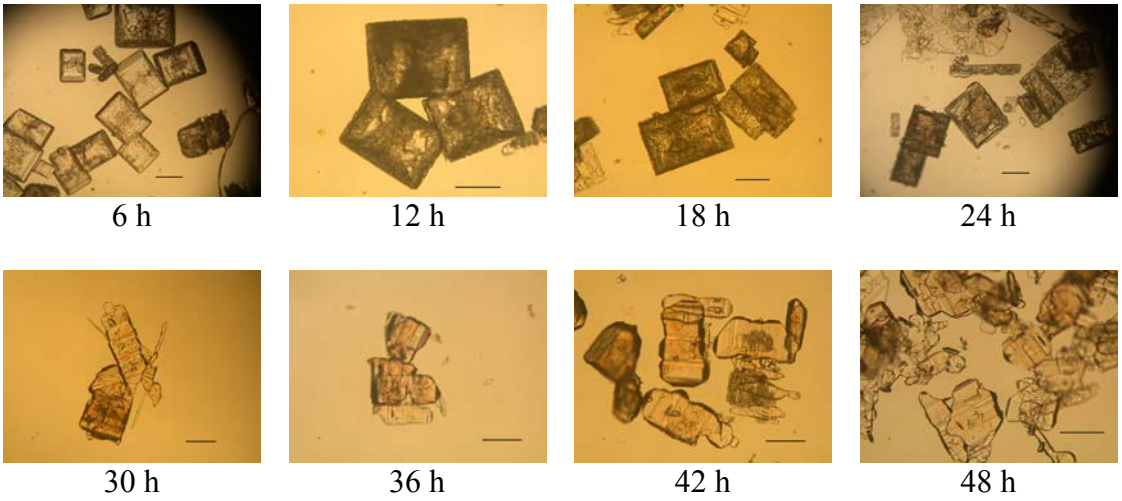

Figure 5. 17. Photomicrographs of the transformation of **UAD**$^{25°C}_{pH4}$ in artificial urine containing 200 µM CG. Scale bar = 100 µm.

5.6.3 Summary of the UAD Transformations in Artificial Urine With Dyes

A summary of the transformation of **UAD**$^{25°C}_{pH4}$ in artificial urine containing molecular dyes at 37° C is shown in Figure 5.18. The transformation of **UAD**$^{25°C}_{pH4}$ in artificial urine solution free of dyes (black curve) is included in the graph for comparison.

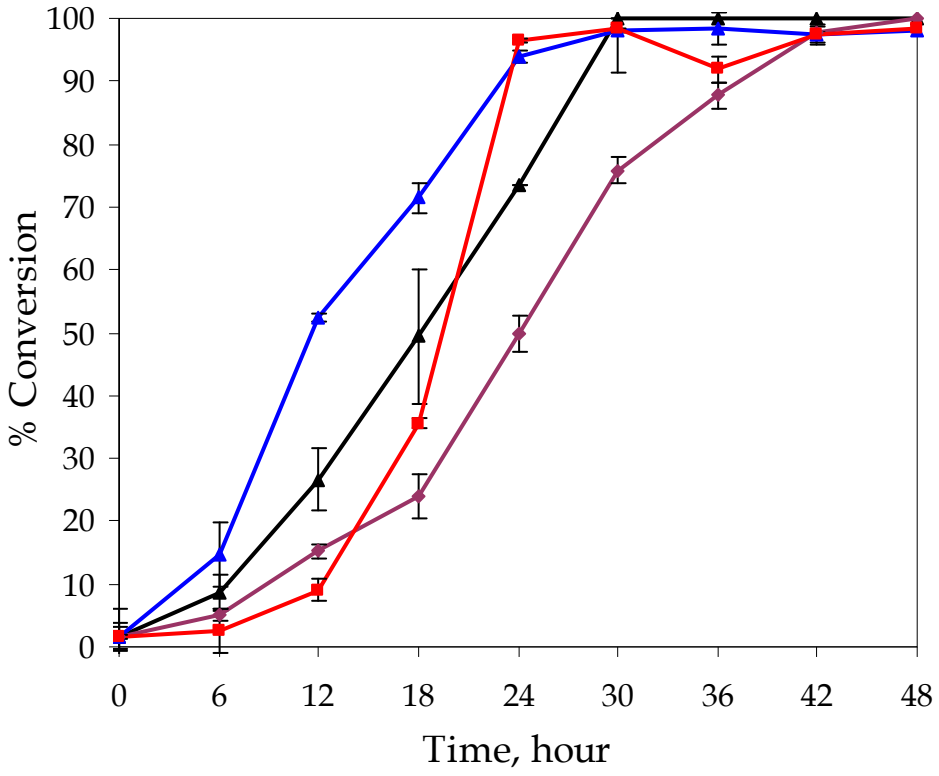

Figure 5. 18. Summary of the conversion of **UAD$^{25°C}_{pH4}$** in artificial urine containing dyes at 37° C. (Purple) artificial urine with 200 µM CG; (Red) artificial urine with 5 µM BBY; (Blue) artificial urine with 25 µM BBY. (Black) **UAD$^{25°C}_{pH4}$** in artificial urine solution without dyes is shown for comparison.

The complete transformation of **UAD$^{25°C}_{pH4}$** in artificial urine containing BBY was slightly faster than in pure artificial urine or artificial urine containing CG. The rate was consistently faster in artificial urine with [BBY] = 25 µM solution. By 24 hours, 94-96 % **UAD$^{25°C}_{pH4}$** to UA conversion occured in both $[BBY]_{sol'n}$ compared to only 73% in artificial urine without dye. When $[BBY]_{sol'n}$ = 5 µM, the % conversion was actually lower than in artificial urine (no dyes) up until 18 hours, however fast conversion occurred in $[BBY]_{so'n}$ = 5 µM between 18 and 24 hours. Complete conversion was observed at 30 hours which is similar to the transformation rate

of $\mathbf{UAD^{25°C}_{pH4}}$ in pure artificial urine solution. In artificial urine solution with [CG] = 200 μM, 50 % conversion was observed at 24 hours and complete conversion by 42 hours. This result suggests that the presence of molecular dyes in the transforming solution only modestly affects the UAD-UA transformation rate, presumably by changing the nucleation/growth rate of UA. Impurity loading in the initial UAD has a more pronounced effect on the transformation rates, presumably by changing the UAD solubility. This indicates that UAD dissolution is the rate determining step in the transformation.

5.7 Conclusions

Solution-mediated transformation of doped UAD has been studied in model aqueous solution and model urine solution. Trace amounts of impurities exerted significant effects on the dissolution of UAD and more modest effects on the subsequent nucleation and crystallization of UA.

UAD doped with physiologically relevant cations transformed to UA slower than pure UAD. The change in the transformation rate is attributed to crystal size, solubility, different defect densities, and the presence of cations included in the crystal matrix. UAD doped with molecular dyes also showed reduction of the rate of UAD transformation relative to pure UAD. The inhibitory effects of impurities used in the UAD transformation studies reveal a complicated dependence on the exact nature and concentration of the impurities included in the UAD matrix. In UAD-CG crystals grown in solution with [CG] = 100-300 μM, only 1-2 dye molecules were included per 10^4 uric acid molecules.[7] The inclusion of dyes seemed independent of the $[CG]_{sol'n}$. In contrast, the included dye in UAD-BBY crystals grown in solution with [BBY] = 2-50μM

generally increased with solution concentration and were found to be 2-42 dye molecules per 10^4 uric acid molecules.[7] CG exhibited lower inclusion levels in UAD crystals than BBY. It is therefore not surprising to observe a lower inhibitory effect of CG than BBY on the transformation rate of UAD. Although the % impurity included in the UAD is important, the specific type of impurity seemingly has a more pronounced effect in the transformation kinetics of the doped UAD crystals.

Our study on the transformation of synthetic UAD crystals in the presence of impurities has shown that organic molecules and physiologically relevant cations stabilize the UAD. This *in vitro* study provides insight into how UAD is stabilized in physiologic solution and how impurities can affect the transformation kinetics.

5.8 References

1. Zellelow, A. Z.; Kim, K.-H.; Sours, R. E.; Swift, J. A., "Solid-State Dehydration of Uric Acid Dihydrate." *Cryst. Growth. Des.* **2010,** 10, 418-425.

2. Kleeberg, J.; Kedar, G. S.; Dobler, M., "Studies on the Morphology of Human Uric Acid Stones." *Urol. Res.* **1981,** 9, 259-261.

3. Herring, L. C., *http://www.herringlab.com/a.html*.

4. Sours, R. E.; Fink, D. A.; Swift, J. A., "Dyeing Uric Acid Crystals with Methylene Blue." *J. Am. Chem. Soc.* **2002,** 124, 8630-8636.

5. Sours, R. E.; Fink, D. A.; Cox, K. A.; Swift, J. A., "Uric Acid Dye Inclusion Crystals." *Mol. Cryst. Liq. Cryst.* **2005,** 440, 187-193.

6. Fink, D. A.; Sours, R. E.; Swift, J. A., "Modulated Uric Acid Crystal Growth in the Presence of Acridine Dyes." *Chem. Mater.* **2003,** 15, 2718-2723.

7. Zellelow, A. Z.; Abiye, M.; Fink, D. A.; Ford, C. E.; Kim, K.-H.; Sours, R. E.; Yannette, C. M.; Swift, J. A., "Doping Uric Acid Crystals. 1. Uric Acid Dihydrate." *Cryst. Growth. Des.* **2010,** 10, 3340-3347.

8. Zellelow, A. Z.; Cox, K. A.; Fink, D. A.; Ford, C. E.; Kim, K.-H.; Sours, R. E.; Swift, J. A., "Doping Uric Acid Crystals. 2. Anhydrous Uric Acid." *Cryst. Growth. Des.* **2010,** 10, 3348-3354.

9. Gaubert, P., "Modifications du facies des cristaux d'acide urique per les matieres colorants ajoutees a l'eau mere." *C. R. Hebd. Seances Acad. Sci.* **1936,** 202, 1192-1194.

10. Kleeberg, J., "Farbung vom Harnsaurekstallen mit Methylenblau." *Zeitschrift fur Urologie* **1972,** 8, 619-629.

11. Kleeberg, J.; Warski, E.; Shalitin, J., "Significance of Staining Uric Acid Crystals with Natural and Synthetic Dyes." *Adv. Exp. Med. Biol.* **1974**, (41B), 821-833.

12. Kleeberg, J., "A Simple Method for Detecting Uric Acid in Snake Excrement by Staining." *Lab. Pract.* **1975,** 24, 87-88.

13. Kleeberg, J., "Relationship between Beet Root Pigment and Uric Acid Crystals." *Isreal. J. Med. Sci.* **1976,** 12, (1), 73-76.

14. Zellelow, A. Z. Crystallization and Phase Transformation of Uric Acids. Georgetown University, Washington, DC, 2010.

15. Mukuta, T.; Lee, A. Y.; Kawakami, T.; Myerson, A. S., "Influence of Impurities on the Solution-Mediated Phase Transformation of an Active Pharmaceutical Ingredient." *Cryst. Growth. Des.* **2005,** 5, (4), 1429-1436.

16. Mohan, R.; Koo, K.-K.; Strege, C.; Myerson, A. S., "Effect of Additives on the Transformation Behaviour of L-Phenylalanine in Aqueous Solution." *Ing. Eng. Chem. Res.* **2001,** 40, 6111-6117.

17. Yang, X.; Lu, J.; Wang, X.-J.; Ching, C.-B., "Effect of sodium chloride on the nucleation and polymorphic transformation of glycine." *J. Crystal Growth* **2008,** 310, 604-611.

18. Gu, C.-H.; Chatterjee, K.; Young, V. J.; Grant, D. J. W., "Stabilization of a metastable polymorph of sulfamerazine by structurally related additives." *J. Crystal Growth* **2002,** 235, 471-481.

19. Qu, H.; Louhi-Kultanen, M.; Kallas, J., "Additive Effects on the Solvent-Mediated Anhydrate/Hydrate Phase Transformation in a Mixed Solvent." *Cryst. Growth. Des.* **2007,** 7, (4), 724-729.

20. Gong, Y.; Collman, B. M.; Mehrens, S. M.; Lu, E.; Miller, J. M.; Blackburn, A.; Grant, D. J. W., "Stable-Form Screening: Overcoming Trace Impurities That Inhibit Solution-Mediated Phase Transformation to the Stable Polymorph of Sulfamerazine." *J. Pharm. Sci.* **2008,** 97, (6), 2130-2144.

21. Garti, N.; Zour, H., "The effect of surfactants on the crystallization and polymorphic transformation of glutamic acid." *J. Crystal Growth* **1997,** 172, 486-498.

22. Brečević, L.; Kralj, D., "The Influence of Some Amino Acids on Calcium Oxalate Dihydrate Transformation." *J. Crystal Growth* **1986,** 79, 178-184.

23. Sikirić, M.; Filipović-Vinceković, N.; Babić-Ivančić, V.; Vdović, N.; Füredi-Milhofer, H., "Interactions in Calcium Oxalate Hydrate/Surfactant Systems." *J. Colloid and Interface Sci.* **1999,** 212, 384-389.

24. Rodriguez-Hornedo, N.; Murphy, D., "Surfactant-Facilitated Crystallization of Dihydrate Carbamazepine During Dissolution of Anhydrous Polymorph." *J. Pharm. Sci.* **2004,** 93, 449-459.

25. Isaacson, L. C., "Urinary composition in calcific nephrolithiasis." *Invest. Urol.* **1969,** 6, (4), 356-363.

26. Perrin, D. D.; Dempsey, B., *Buffers for pH and Metal Ion Control*. John Wiley & Sons: New York, 1974.

27. Lovette, M. A.; Browning, A. R.; Griffin, D. W.; Sizemore, J. P.; Snyder, R. C.; Doherty, M. F., "Crystal Shape Engineering." *Ind. Eng. Chem. Res.* **2008,** 47, 9812-9833.

28. Weissbuch, I.; Popovitz-Biro, R.; Lahav, M.; Leiserowitz, L., "Understanding and Control of Nucleation, Growth, Habit, Dissolution and Structure of Two- and Three-Dimensional Crystals Using 'Tailor-Made' Auxiliaries." *Acta Cryst.* **1995,** B51, 115-148.

29. Thompson, C.; Davies, M. C.; Roberts, C. J.; Tendler, S. J. B.; Wilkinson, M. J., "The effects of additives on the growth and morphology of paracetamol (acetaminophen) crystals." *Int. J. Pharm.* **2004,** 280, 137-150.

30. Sours, R. E. Uric Acid Crystal Growth. Georgetown University, Washington, DC, 2004.

CHAPTER 6 CRYSTAL GROWTH AND CHARACTERIZATION OF CALCIUM URATE HEXAHYDRATE

6.1 Introduction

Uric acid is a weak diprotic acid with a pK_{a1} of 5.5.[1] At pH values above 5.5, the majority of uric acid is ionized to urate by loss of a proton at the N3 position (Figure 6.1). In strong base, uric acid can lose a second proton at N9, though this species is not significant under normal physiological conditions.

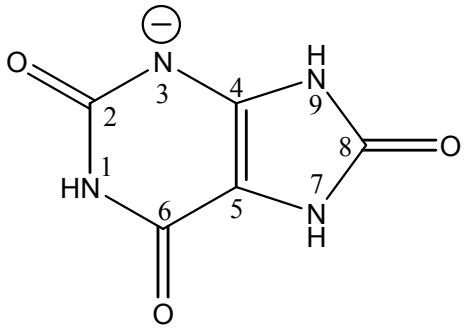

Figure 6.1. Molecular structure of urate, $C_5H_3N_4O_3$. Atoms are numbered according to Fischer.[2]

In the presence of appropriate counterions, urate can crystallize as a salt. The most common salt is monosodium urate monohydrate (MSU), which plays a distinctive role in gout formation and is a minor phase found in kidney stones.[3, 4] Ammonium acid urate is also found as a minor component in human kidney stones, but is a common stone components in renal deposits in domestic pets.[4-6] Other analyses of stones have reported presence of calcium and potassium urates, or "complex urates" which are mixtures of Ca, K, Na.[7] A number of trace elements have also been extracted from renal deposits which presumably can associate with urate in solution and may or may not crystallize as a salt.

The interaction between uric acid anions and different mono and divalent cations has been the subject of theoretical calculations, [8, 9] but only limited structural data is available to support these calculations. The syntheses of various metal salts of uric acid have been attempted in the past decades,[3, 10-20] however, the urate salts are often polycrystalline powder. A recent search of the Cambridge Structural Database (CSD) version 5.3.3, (Nov 2011) for metal urate structures identified single crystal structures for the sodium (NAURAT), magnesium (BADTEX), and lead (DITKEX) salts. Two molecular complexes with guanidinium ions (XANDEV) and methylene blue (UGEXIN) were also found. Dubler *et al.*[11] studied the complexes of Mg^{2+} and urate and they found two different polymorphs of $Mg(C_5H_3N_4O_3)_2{\cdot}8H_2O$ both containing a hexahydrated cation $[Mg(H_2O)_6]^{2+}$, urate anions, and two water molecules per formula unit. This structure is quite different from the previous ones since no direct coordination between the magnesium and urate ions is observed. Both magnesium complexes are monoclinic $P2_1/c$ space group. Monosodium urate monohydrate (MSU), crystallizes in a triclinic space group P-1 where sodium cation coordinates to the urate anion through short Na···O contacts (with all 3 O atoms 3.35-3.53

Å).[3] The urate molecules are also hydrogen bonded to one another and to water molecules. In 2008, Sattar *et al.* reported a crystal structure of a lead salt complex consisting of two urate molecules, a Pb^{2+} ion and a water molecule with a space group of P-1.[19] In this complex, each lead cation is directly coordinated to 5 urate anions. Two urates coordinate through the N3 and O2 positions, 2 through the O6 position, and one through the O2. The interesting part in the synthesis of metal urate complexes is how the metal bonds to urate since there are various positions where it could coordinate or bicoordinate as shown in Figure 6.2.

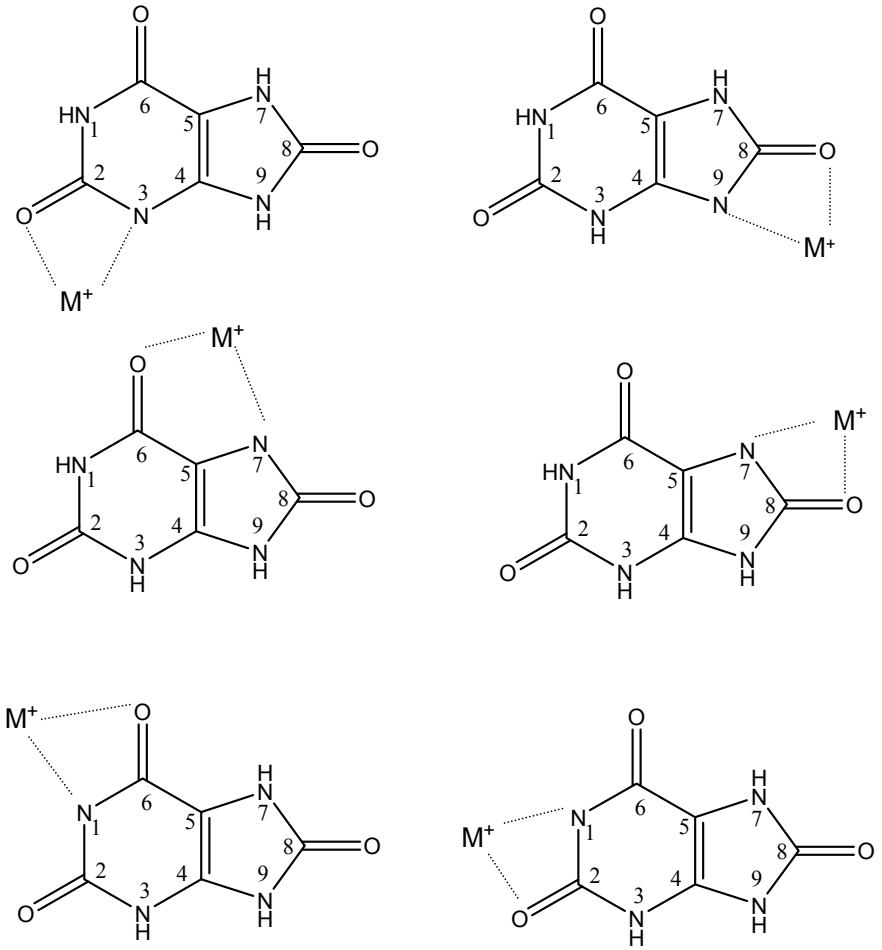

Figure 6.2. Structures of urate complexes showing possible coordination of metal cations (M^+ or M^{2+}) with urate molecules.

Interest in the synthesis of calcium urate dates back as early as 1897 (or urate of calcium as it was called then) when Delépine observed small acicular crystals in urine which differed from calcium oxalate and other known urates at the time.[21] He synthesized calcium urate from uric acid and pure hydrate of calcium, and the crystals appeared the same as the acicular crystals he observed in the urine of two gouty subjects. However, he did not discount the presence of other salts in the acicular crystals since the needle-like appearance was identical to MSU.

In recent years, several researchers have reported the preparation and characterization of calcium urate complexes.[12-15] These studies have resulted in powder X-ray diffraction data, however, no single crystal structure is available in the literature to date. We revisited the growth of calcium urate and this paper reports the first single crystal structure. Understanding the interactions of calcium ions with urates can help elucidate its possible role in pathological biomineralization processes. A recent analysis of urates in ten spontaneously passed uric acid renal calculi revealed a near-pure calcium urate in two cases and a calcium-enriched urate zone in all of the samples.[7]

6.2 Experimental Methods and Materials

6.2.1 Materials

All chemical reagents were used as received: Uric acid (99%, Aldrich), $CaCl_2$ (93%, Aldrich), and NaOH Pellets (EM). Water used was purified by passage through two Barnstead deionizing cartridges followed by distillation.

6.2.2 Crystal Growth

A solution of 10 mM uric acid, 30 mM $CaCl_2$, and 15 mM NaOH was heated and stirred vigorously until all solids dissolved. The solution was filtered, the pH adjusted to 10.5 with 1 M NaOH, and stored at 25° C or 37° C for at least 2 days.

6.2.3 Optical Microscopy

All micrographs were taken using an Olympus BX-50 polarizing microscope fitted with a Nikon COOLPIX995 digital camera operated with krinnicam_v1-03 software (Nikon Corp). The needle-like morphologies of the crystals grown at 25° C or 37° C (Figure 6.3) are identical. Based on previous reports, we initially assumed this to be a calcium urate.

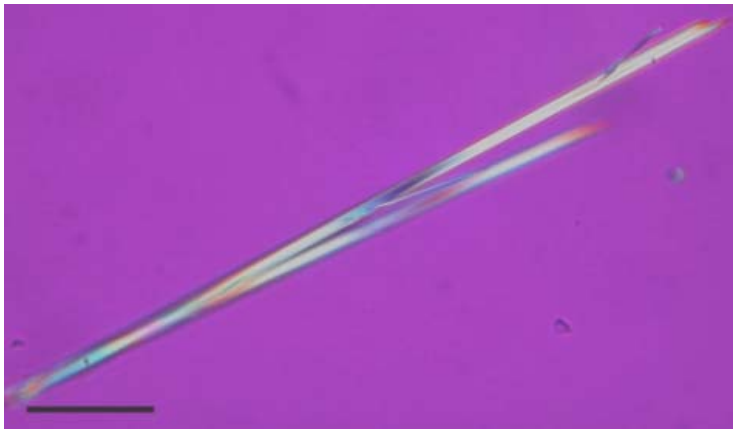

Figure 6.3. Photomicrograph of calcium urate crystals grown at 37° C. Scale bar = 100 μm.

6.2.4 Thermal Analysis

Thermogravimetric analysis was performed on a SDT Q600 TA instrument (New Castle, DE). About 5 mg of sample was heated in an alumina pan from room temperature to 350° C at

10°C/min under a stream of nitrogen. A nitrogen flow rate of 50 mL/min was used and each set of experiments was performed in triplicate. All the experiments were conducted using open 90 µL alumina pans (TA instruments), and the samples were used without sieving or grinding. All experimental curves were analyzed with TA's Universal Analysis Software.

A single endothermic curve was seen when the compound was heated from room temperature to 350° C. A weight loss of 22.11% observed at ~137°C (Figure 6.4) corresponds to loss of six water molecules, close to the theoretical % weight loss of 22.4 % for a hexahydrate. This weight loss was in agreement with the first reported synthesis of calcium urate hexahydrate by Carmona.[12]

(6.1) $$Ca(C_5H_3O_3N_4)_2 \cdot 6H_2O \longrightarrow Ca(C_5H_3O_3N_4)_2 + 6H_2O$$

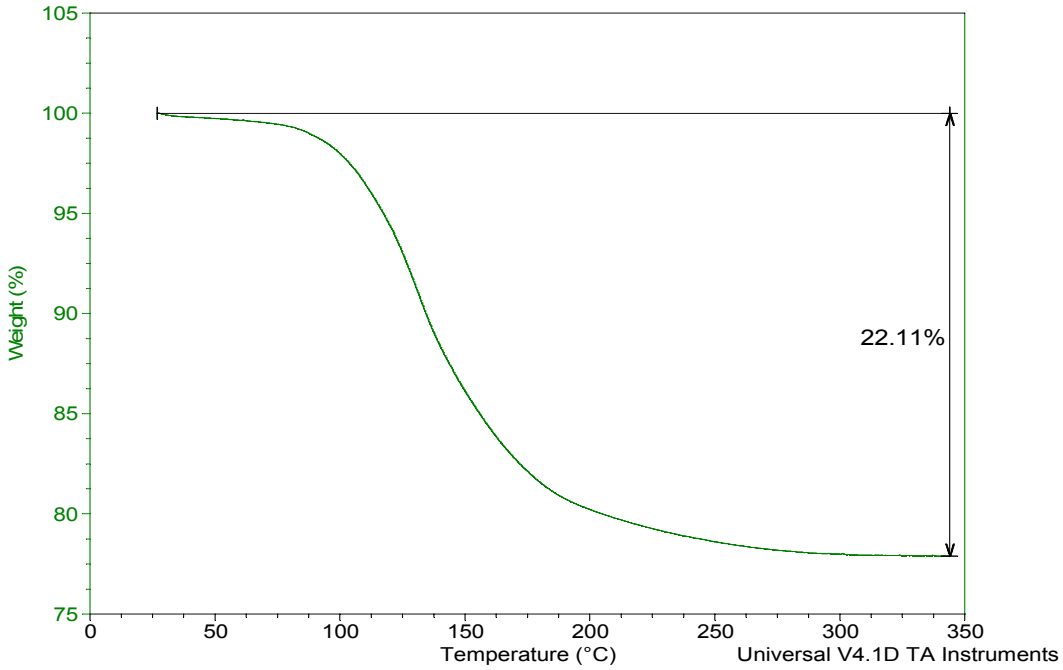

Figure 6.4. Thermal curve of calcium urate (heating rate=10°C/min; sample mass=5.09 mg, weight loss at 350° C = 22.11%).

6.2.5 Powder X-ray Diffraction

All powder X-ray diffraction analyses were performed at room temperature using a Rigaku R-AXIS RAPID-S X-ray diffractometer under the following conditions: tube voltage of 40kV, tube current of 30 mA, and Cu Kα radiation. Samples were prepared in 0.5mm glass capillaries (Charles Super Company). Using a 0.3mm collimator, the data was collected for 1 hour with a Phi spin rate of 1° per second. The diffraction pattern was integrated over a 2θ range from 4° to 50° with a step size of 0.01 degrees. Data analysis was performed using Rigaku RAPID/XRD Version 2.3.3, AreaMax software and Jade v5.035 software (Material Data Inc.).

6.2.6 Single Crystal X-ray Diffraction

A single crystal X-ray structure of crystals grown at 37^{o} C was collected on a Bruker SMART or APEX2 Platform CCD diffractometer at 100 K using Mo Kα radiation (λ = 0.710713). Intensity data was corrected for absorption and decay in SADABS. Structure was solved in SHELXS and refined using SHELXL using XSEED v2.0 using direct methods and refined with anisotropic displacement parameters.

6.3 Crystal Structure

The structure of $CaU_2{\cdot}6H_2O$ was determined by single crystal X-ray diffraction (See Figure 6.5 and Appendix A). $CaU_2{\cdot}6H_2O$ crystals are monoclinic with a space group of $P2_1/n$, Z=4 and cell parameters a = 12.543 (3), b = 6.6222 (16), c = 22.218 (5) Å, and β = 105.990 (3)°, and R = 0.0492. The Ca (II) ion in $CaU_2{\cdot}6H_2O$ fulfills its 8-coordinate geometry through short contacts with a pyrimidine ring of a neighboring urate molecule and six water molecules. The urate

molecule is bonded in a bidentate manner to Ca^{2+} through the N3 and O2 positions (Ca···N 2.508 Å, Ca···O 2.528 Å). All other Ca coordination sites are occupied by water (O_w···Ca 2.503 Å, 2.666 Å, 2.390 Å, 2.388 Å, 2.385 Å, 2.341 Å).

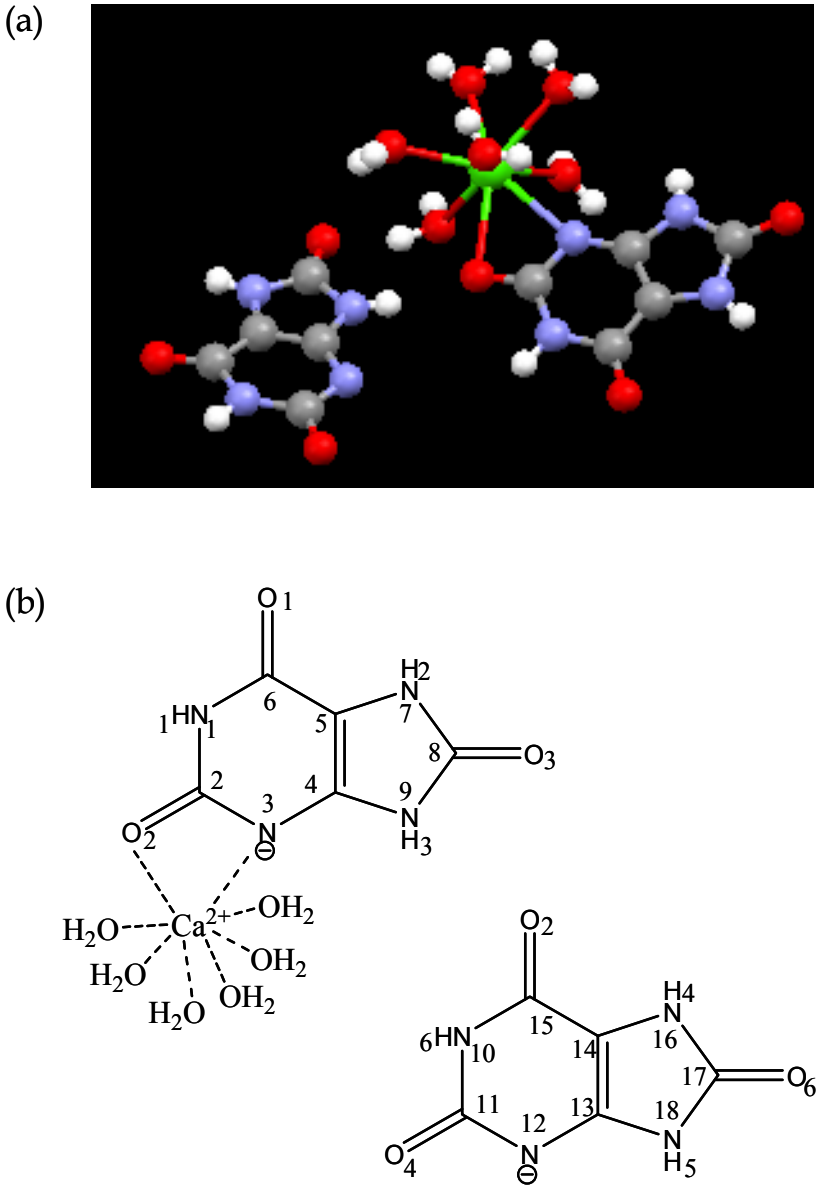

Figure 6.5. (a) Crystal structure of $CaU_2 \cdot 6H_2O$. Each Ca ion in $CaU_2 \cdot 6H_2O$ is coordinated to 1 urate molecule and 6 water molecules. See text for bond distances. (b) Molecular structure of $CaU_2 \cdot 6H_2O$ with all atoms labeled.

The packing diagram of $CaU_2 \cdot 6H_2O$ viewed along the *b* axis is depicted in Figure 6.6. Complex hydrogen bonding exists between urate molecules as well as with urate and water molecules. The urate molecule that is coordinated to the Ca^{2+} ion is hydrogen bonded via O3 and H2 (imidazole ring) to H4 (imidazole ring) and O5 (pyrimidine ring) of the second urate molecule. Another hydrogen bonding interactions occurs between O2 (pyrimidine ring) to H5 (imidazole ring) between neighboring urate molecule. Hydrogen bonding also occurs between O3 and O6 (imidazole ring) and the water molecules that are coordinated to Ca^{2+} ion.

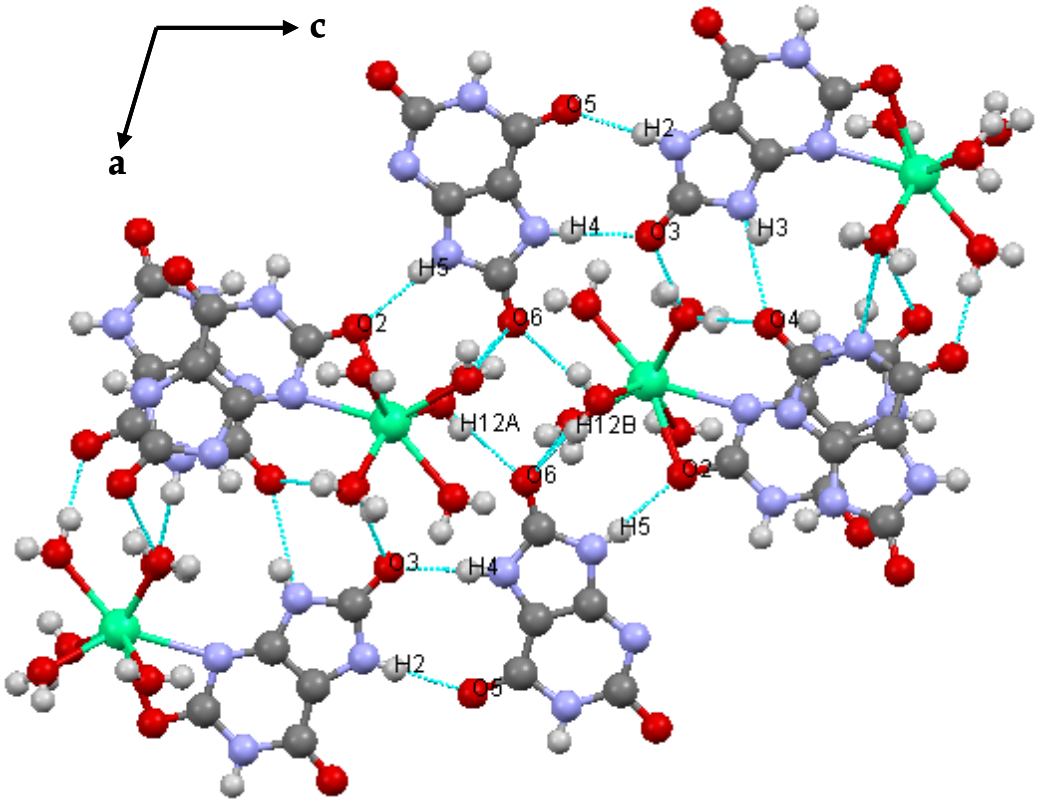

Figure 6.6. Crystal structure of $CaU_2 \cdot 6H_2O$ viewed along the *b* axis showing hydrogen bonding between molecules. Crystallographic axes are indicated.

Figure 6.7 illustrates the packing diagram of $CaU_2 \cdot 6H_2O$ viewed along the *a* axis. The molecules between layers are connected through hydrogen bonding with water molecules that are coordinated to the Ca^{2+} ion. Urate molecules participating in the coordination with Ca^{2+} ion are nearly perpendicular to the (001) plane at 86.67°.

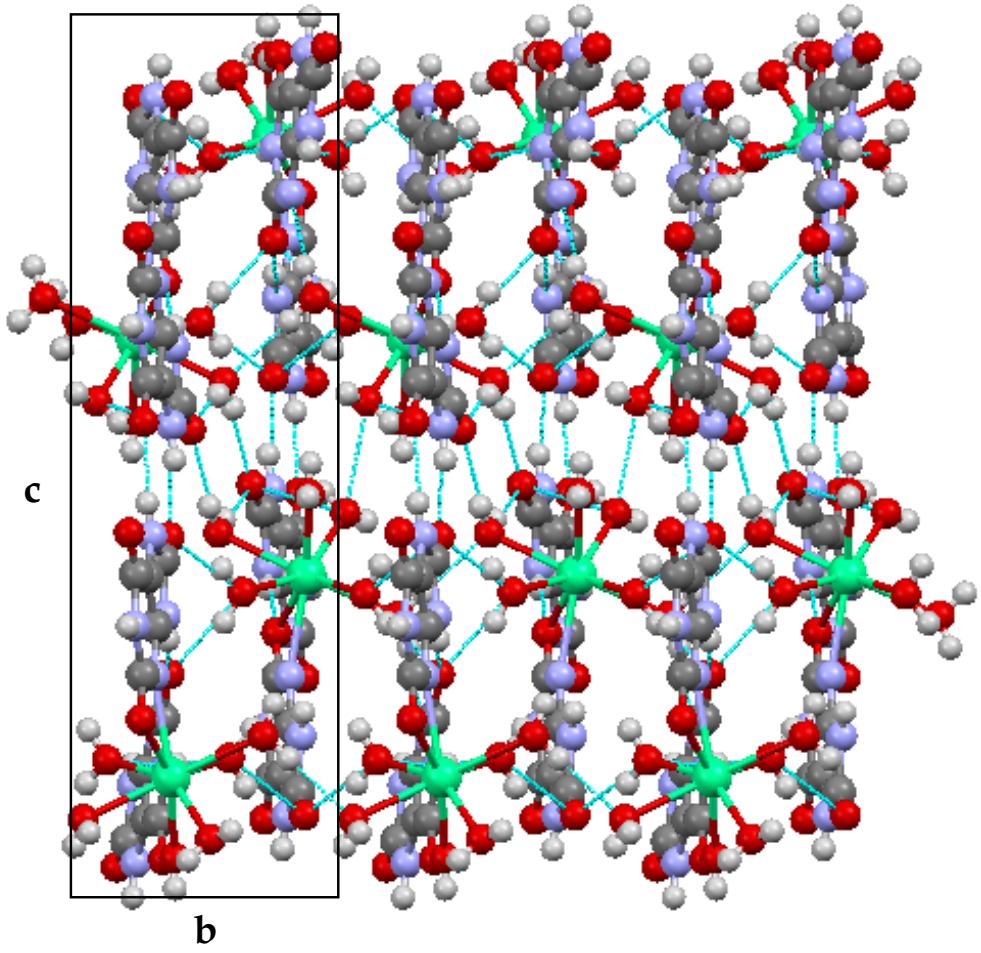

Figure 6.7. Packing diagram of $CaU_2 \cdot 6H_2O$ viewed along the *a* axis. Molecules within a layer are hydrogen bonded with one another and with molecules in adjacent layers. Crystallographic axes are indicated.

The calculated pattern from single crystal data was compared against powder X-ray diffraction data collected for the bulk precipitate from uric acid aqueous solutions. The powder diffraction patterns for $CaU_2 \cdot 6H_2O$ grown at 37° C and 25° C and the calculated pattern from single crystal data is shown in Figure 6.8. Characteristic diffraction lines of (100), (002), (101), (102), (200), (004), (210), (212), (020), and (120) are observed in all powder data suggesting phase purity of the bulk precipitate. Diffraction lines are broad due to low instrument resolution.

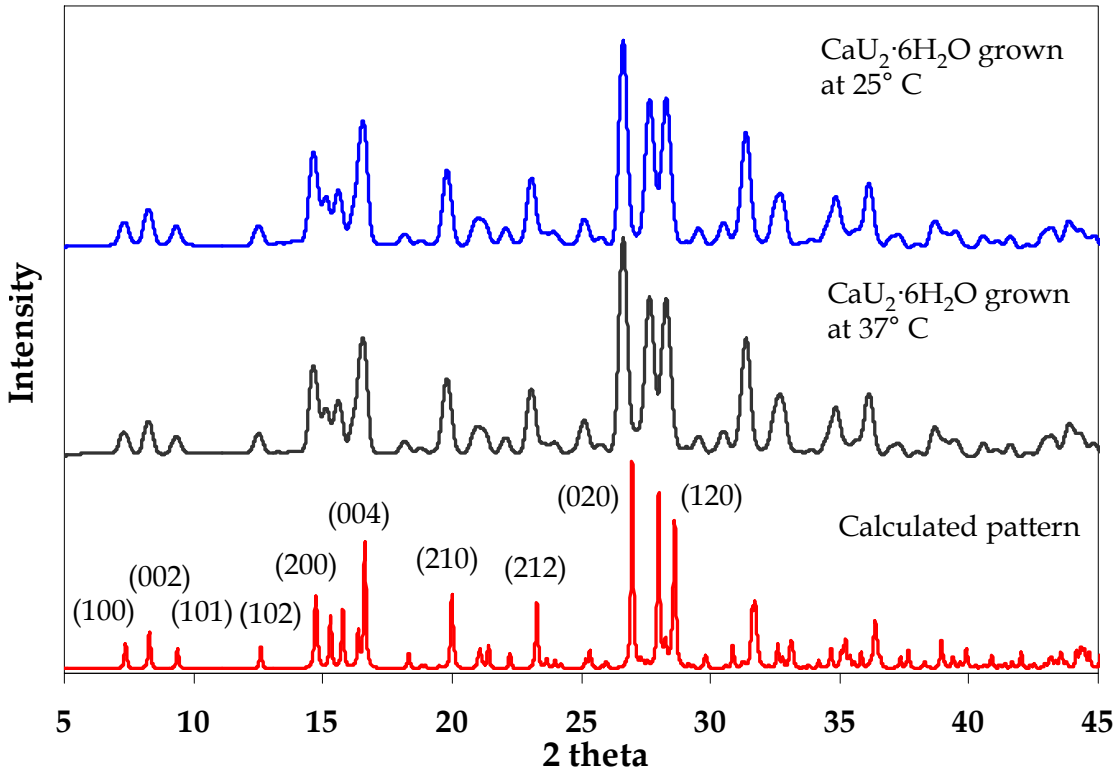

Figure 6.8. PXRD of $CaU_2 \cdot 6H_2O$. (Red) Calculated pattern, (Black) $CaU_2 \cdot 6H_2O$ grown at 37° C, (Blue) $CaU_2 \cdot 6H_2O$ grown at 25° C.

6.4 Conclusions

$CaU_2 \cdot 6H_2O$ crystals grown in basic aqueous solution at 25° C or 37° C are of identical phase as determined by optical microscopy, thermogravimetry, and powder X-ray diffractometry. The single crystal structure collected for crystals grown at 37° C confirms the presence of 6 water molecules measured from thermogravimetric analysis. $CaU_2 \cdot 6H_2O$ indicates interaction sites for the divalent calcium to be the N3 and O2 positions of the urates. This is in agreement with the theoretical calculation of Allen *et al*. in which N3 and O2 positions are the energetically favored binding sites for Ca^{2+} and Mg^{2+} in water solution.[8] The single crystal structure of $CaU_2 \cdot 6H_2O$ exhibit extensive intermolecular hydrogen bonding network between molecules in a layer and with molecules in adjacent layers. As with other urate salts previously reported, the urate anion in $CaU_2 \cdot 6H_2O$ is deprotonated at the N3 position.

6.5 References

1. Smith, R. C.; Gore, J. Z.; McKee, M.; Howard, H., "The First Dissociation Constant of Uric Acid." *Microchem. J.* **1988,** 38, 118-124.

2. Fisher, E., "Ueber die Constitution des Caffeins, Xanthins, Hypoxanthins und Verwandeter Basen." *Ber. Dtsch. Chem. Ges.* **1897,** 30, 549-559.

3. Mandel, N. S.; Mandel, G. S., "Monosodium Urate Monohydrate, the Gout Culprit." *J. Am. Chem. Soc.* **1976,** 98, 2319-2323.

4. Delatte, L. C.; Bellanato, J.; Santos, M.; Rodriguez-Miñon, J. L., "Monosodium urate in urinary calculi." *Eur. Urol.* **1978,** 4, (6), 441-447.

5. Pichette, V.; Bonnardeaux, A.; Cardinal, J.; Houde, M.; Nolin, L.; Boucher, A.; Ouimet, D., "Ammonium Acid Urate Crystal Formation in Adult North American Stone-Formers." *Am. J. Kidney Diseases* **1997,** 30, (2), 237-242.

6. Kruger, J. M.; Osborne, C. A., "Etiopathogenesis of uric acid and ammonium urate uroliths in non-Dalmatian dogs." *Vet. Clin. North. Am.* **1986,** 16, 87-126.

7. Bellanato, J.; Cifuentes, J.-L. R.-M.; Salvador, E.; Medina, J.-A., "Urates in uric acid renal calculi." *International Journal of Urology* **2009,** 16, 318-322.

8. Allen, R. N.; Shukla, M. K.; Burda, J. V.; Leszczynski, J., "Theoretical Study of Interaction of Urate with Li^+, K^+, Be^{2+}, Mg^{2+}, and Ca^{2+} Metal Cations." *J. Phys. Chem. A* **2006,** 110, 6139-6144.

9. Allen, R. N.; Lipkowski, P.; Shukla, M. K.; Leszczynski, J., "Vibrational analysis of complexes of urate with IA group metal cations (Li^+, Na^+ and K^+)." *Spectrichim. Acta, Part A* **2007,** 68, 639-645.

10. Davies, K. J. A.; Sevanian, A.; Muakkassah-Kelly, S. F.; Hochstein, P., "Uric acid-iron ion complexes." *Biochem. J.* **1986,** 235, 747-754.

11. Dubler, R.; Jameson, G. B.; Kopajtić, Z., "Uric Acid Salts of Magnesium: Crystal and Molecular Structures and Thermal Analysis of Two Phases of $Mg(C_5H_3N_4O_3)_2 \cdot 8H_2O$." *J. Inorg. Biochem.* **1986,** 26, 1-21.

12. Carmona, P., "$Ca(C_5H_3O_3N_4)_2 \cdot 6H_2O$: A New Hydrate of Calcium Urate." *J. Solid State Chem.* **1984,** 55, 293-298.

13. Brničević, N.; Babić-Ivančić, V.; Füredi-Milhofer, H., "Calcium Hydrogenurate Complexes of the Type $Ca(C_5H_3N_4O_3)_2L_3$ With L = $(CH_3)_2SO$ or $(CH_3)_2NCHO$." *J. Inorg. Biochem.* **1991,** 43, 771-778.

14. Babić-Ivančić, V.; Füredi-Milhofer, H.; Brničević, N., "Precipitation and Solubility of Calcium Hydrogenurate Hexahydrate." *J. Res. Natl. Inst. Stand. Technol.* **1992,** 97, 365-372.

15. Babić-Ivančić, V.; Brničević, N.; Trojko, R.; Füredi-Milhofer, H., "$Ca(C_5H_3N_4O_3)_2(H_2O)_3$ - Mixed-Coordinated Calcium Hydrogenurate Hydrate." *J. Inorg. Biochem.* **1995,** 57, 33-42.

16. Venkata Ramana, V.; Thyagaraju, V. J.; Sivarama Sastry, K., "Chromium Complexes of Uric Acid - Synthesis, Structure, and Properties." *J. Inorg. Biochem.* **1992,** 48, 85-93.

17. Moawad, M. M., "Complexation and Thermal Studies of Uric Acid with Some Divalent and Trivalent Metal Ions of Biological Interest in the Solid State." *J. Coord. Chem.* **2002,** 55, (1), 61-78.

18. Koksharova, T. V., "Synthesis and Properties of Acidic 3*d*-Metal Urates." *Russ. J. Coord. Chem.* **2002,** 28, (7), 505-509.

19. Sattar, S.; Carroll, M. J.; Sargeant, A. A.; Swift, J. A., "Structure of a lead urate complex and its effect on the nucleation of monosodium urate monohydrate." *CrystEngComm* **2008,** 10, 155-157.

20. Babić-Ivančić, V.; Jendrić, M.; Šoštarić, N.; Opačak-Bernardi, T.; Zorić, S. T.; Sikirić, M. D., "Influence of pH, Temperature and Common Ion on Magnesium Hydrogenurate Octahydrate Solubility." *Coll. Antropol.* **2010,** 34, 259-266.

21. Delépine, S. In Proceedings of the Physiological Society, King's College, January 15, 1887; King's College, 1887; pp i-vi.

APPPENDIX A CRYSTAL DATA FOR CALCIUM URATE HEXAHYDRATE

Table A.1. Crystal data and structure refinement for **$CaU_2 \cdot 6H_2O$**.

Formula	C10 H18 CaN8 O12
Formula weight	482.40
Wavelength	0.71073 Å
Crystal system	Monoclinic
Space group	P 2_1/n
a (Å)	12.543 (3)
b (Å)	6.6222 (16)
c Å	22.210 (5)
α (^{o})	90
β (^{o})	105.990 (3)°
γ (^{o})	90°
Volume [$Å^3$]	1774.0 (7)
Z	4
Density (calc) [g/cm**3]	1.806
Mu(MoKα) [/mm]	0.443
F(000)	1000
Crystal size	0.48 x 0.06 x 0.02 mm^3
Temperature	100 (2) K
Radiation [Angstrom]	MoKα 0.71073
Theta Min-Max [Deg]	1.91, 28.0
Dataset	-16: 16 ; -8: 8 ; -29: 29
Tot., Uniq. Data, R(int)	15188, 4212, 0.089
Observed data [I > 2.0 sigma (I)]	2488
Nref, Npar	4212, 338
R, wR2, S	0.0492, 0.1024, 0.915
w=1/[\s^2^(Fo^2^)+(0.0438P)^2^]	where P=(Fo^2^+2Fc^2^)/3'
Max. and Av. Shift/Error	0.00, 0.00
Min. and Max. Resd. Dens. [e/Ang^3]	-0.46, 0.37

Table A.2. Final Coordinates and Equivalent Isotropic Displacement Parameters of the non-Hydrogen atoms for **$CaU_2 \cdot 6H_2O$.**

Atom	x	y	z	U(eq) [Å]
Ca1	0.95842(5)	0.68553(9)	0.13450(3)	0.00959(15)
O1	1.26316(16)	0.8401(3)	0.41384(9)	0.0167(5)
O2	1.14762(16)	0.7959(3)	0.20025(9)	0.0129(4)
O3	0.83385(15)	0.6918(3)	0.40890(8)	0.0120(4)
O4	1.65712(15)	0.6924(3)	0.25209(8)	0.0124(4)
O5	1.58800(16)	0.7128(3)	0.04048(9)	0.0163(5)
O6	1.15956(16)	0.8878(3)	0.03187(9)	0.0152(5)
O7	0.80614(18)	0.6731(4)	0.04238(9)	0.0209(5)
O8	1.04436(18)	0.5400(4)	0.06390(10)	0.0187(5)
O9	1.06108(17)	0.3445(3)	0.18139(10)	0.0150(5)
O10	0.82128(17)	0.4694(3)	0.15658(9)	0.0146(5)
O11	0.82815(18)	0.9219(3)	0.15409(10)	0.0141(5)
O12	0.99661(18)	1.0098(3)	0.08639(9)	0.0145(5)
N1	1.2013(2)	0.8203(4)	0.30730(10)	0.0123(5)
N3	1.0154(2)	0.7474(3)	0.25035(11)	0.0105(5)
N7	1.0167(2)	0.7569(4)	0.41003(11)	0.0109(6)
N9	0.8960(2)	0.7059(4)	0.31862(11)	0.0096(5)
N10	1.6131(2)	0.6987(4)	0.14655(10)	0.0113(5)
N12	1.47543(19)	0.7557(3)	0.19944(10)	0.0107(5)
N16	1.34318(19)	0.8158(4)	0.03682(11)	0.0116(5)
N18	1.2977(2)	0.8266(4)	0.12549(11)	0.0112(5)
C2	1.1215(2)	0.7885(4)	0.25132(13)	0.0112(6)
C4	0.9965(2)	0.7423(4)	0.30693(13)	0.0100(6)
C5	1.0729(2)	0.7743(4)	0.36405(13)	0.0115(6)
C6	1.1836(2)	0.8127(5)	0.36632(13)	0.0127(6)
C8	0.9088(2)	0.7160(4)	0.38258(12)	0.0090(6)
C11	1.5813(2)	0.7163(4)	0.20100(13)	0.0105(6)
C13	1.4089(2)	0.7816(4)	0.14100(13)	0.0104(6)

C14	1.4384(2)	0.7727(4)	0.08562(13)	0.0114(6)
C15	1.5472(2)	0.7286(4)	0.08582(13)	0.0113(6)
C17	1.2570(2)	0.8477(4)	0.06118(13)	0.0121(6)

U(eq) = 1/3 of the trace of the orthogonalized U Tensor

Table A.3. Hydrogen Atom Positions and Isotropic Displacement Parameters for **$CaU_2{\cdot}6H_2O$**.

Atom	x	y	z	U(iso) [Å]
H1	1.273(3)	0.845(5)	0.3065(14)	0.019(9)
H2	1.038(3)	0.773(5)	0.4477(15)	0.020(9)
H3	0.839(3)	0.697(6)	0.2915(17)	0.043(12)
H4	1.342(3)	0.827(5)	-0.0028(15)	0.026(9)
H5	1.261(3)	0.826(5)	0.1498(14)	0.018(9)
H6	1.684(3)	0.668(5)	0.1497(14)	0.024(9)
H7A	0.737(3)	0.679(5)	0.0453(15)	0.029
H7B	0.796(3)	0.671(5)	0.0072(16)	0.029
H8A	1.102(3)	0.464(5)	0.0728(15)	0.029
H8B	1.068(3)	0.623(5)	0.0397(15)	0.029
H9A	1.055(3)	0.306(5)	0.2176(15)	0.029
H9B	1.041(3)	0.251(5)	0.1555(16)	0.029
H10	0.7857	0.4114	0.1235	0.017
H10A	0.832(3)	0.385(5)	0.1898(15)	0.029
H11A	0.779(3)	0.999(5)	0.1274(15)	0.029
H11B	0.839(3)	0.990(5)	0.1883(16)	0.029
H12A	0.945(3)	1.043(5)	0.0561(16)	0.029
H12B	1.059(3)	0.988(5)	0.0711(15)	0.029

The Temperature Factor has the Form of Exp(-T) Where

T=8*(Pi**2)*U*(Sin(Theta)/Lambda)** for Isotropic Atoms

Table A.4. (An)isotropic Displacement Parameters for **$CaU_2.6H_2O$**.

Atom	U(1,1) or U	U(2,2)	U(3,3)	U(2,3)	U(1,3)	U(1,2)
Ca1	0.0089(3)	0.0131(3)	0.0065(3)	-0.0006(2)	0.0016(2)	0.0001(3)
O1	0.0119(11)	0.0289(13)	0.0076(10)	-0.0006(9)	-0.0001(8)	-0.0092(10)
O2	0.0088(10)	0.0221(12)	0.0078(10)	0.0022(9)	0.0023(8)	-0.0005(9)
O3	0.0108(10)	0.0171(11)	0.0083(10)	0.0000(9)	0.0029(8)	-0.0013(9)
O4	0.0115(11)	0.0161(11)	0.0083(10)	0.0017(9)	0.0007(8)	0.0017(9)
O5	0.0119(11)	0.0292(13)	0.0085(10)	0.0000(9)	0.0041(9)	0.0004(10)
O6	0.0104(11)	0.0239(12)	0.0095(10)	0.0028(9)	0.0000(9)	0.0021(9)
O7	0.0120(11)	0.0446(15)	0.0055(10)	0.0004(11)	0.0014(9)	0.0034(12)
O8	0.0183(13)	0.0254(14)	0.0125(11)	0.0021(10)	0.0043(10)	0.0086(10)
O9	0.0167(12)	0.0164(13)	0.0134(11)	-0.0006(9)	0.0068(10)	-0.0007(10)
O10	0.0155(12)	0.0163(12)	0.0097(11)	0.0028(9)	-0.0002(9)	-0.0007(9)
O11	0.0151(12)	0.0156(12)	0.0100(11)	-0.0003(9)	0.0006(9)	0.0048(9)
O12	0.0098(11)	0.0211(12)	0.0117(11)	0.0024(9)	0.0016(9)	0.0019(10)
N1	0.0087(13)	0.0195(14)	0.0086(12)	-0.0003(11)	0.0024(10)	-0.0028(12)
N3	0.0120(13)	0.0125(13)	0.0061(11)	0.0016(9)	0.0010(10)	0.0005(10)
N7	0.0137(14)	0.0132(14)	0.0062(13)	-0.0016(10)	0.0032(11)	-0.0003(10)
N9	0.0088(13)	0.0131(14)	0.0057(12)	-0.0006(10)	-0.0001(10)	0.0003(11)
N10	0.0091(13)	0.0175(14)	0.0079(12)	0.0025(11)	0.0033(10)	0.0033(11)
N12	0.0127(13)	0.0124(13)	0.0067(12)	0.0016(9)	0.0022(10)	0.0014(10)
N16	0.0111(13)	0.0162(13)	0.0072(12)	0.0006(11)	0.0021(10)	0.0019(11)
N18	0.0114(13)	0.0170(14)	0.0065(12)	0.0018(11)	0.0046(10)	0.0016(11)
C2	0.0126(15)	0.0092(16)	0.0117(14)	-0.0022(12)	0.0029(12)	-0.0012(12)
C4	0.0083(15)	0.0098(15)	0.0103(14)	0.0004(11)	-0.0002(12)	-0.0001(11)
C5	0.0137(16)	0.0111(16)	0.0101(14)	-0.0003(12)	0.0039(12)	0.0004(12)
C6	0.0150(15)	0.0125(15)	0.0097(14)	0.0000(13)	0.0019(12)	-0.0021(13)
C8	0.0108(15)	0.0060(15)	0.0082(14)	-0.0006(11)	-0.0005(12)	0.0013(12)
C11	0.0103(15)	0.0110(16)	0.0099(14)	-0.0005(12)	0.0024(12)	0.0007(12)
C13	0.0103(15)	0.0084(15)	0.0126(15)	-0.0017(12)	0.0034(12)	0.0018(12)

C14	0.0130(16)	0.0116(16)	0.0084(14)	-0.0001(11)	0.0007(12)	-0.0005(12)
C15	0.0116(15)	0.0115(16)	0.0099(14)	0.0001(12)	0.0016(12)	-0.0015(12)
C17	0.0134(16)	0.0117(16)	0.0104(14)	-0.0002(12)	0.0020(12)	0.0004(12)

The Temperature Factor has the Form of Exp(-T) Where

T=8*(Pi**2)*U*(Sin(Theta)/Lambda)** for Isotropic Atoms

T = 2*(Pi**2)*Sumij(h(i)*h(j)*U(i,j)* Astar(i)*Astar(j), for Anisotropic Atoms. Astar(j) are Reciprocal Axial Lengths and h(i) are the Reflection Indices.

Table A.5. Bond Distances (Å) for **$CaU_2 \cdot 6H_2O$**.

Ca1	-O2	2.528(2)
Ca1	-O7	2.385(2)
Ca1	-O8	2.341(2)
Ca1	-O9	2.666(2)
Ca1	-O10	2.390(2)
Ca1	-O11	2.388(2)
Ca1	-O12	2.503(2)
Ca1	-N3	2.508(2)
Ca1	-C2	2.908(3)
O1	-C6	1.250(3)
O2	-C2	1.266(3)
O3	-C8	1.247(3)
O4	-C11	1.274(3)
O5	-C15	1.254(3)
O6	-C17	1.245(3)
O7	-H7A	0.89(3)
O7	-H7B	0.76(3)
O8	-H8A	0.86(3)
O8	-H8B	0.88(3)
O9	-H9A	0.87(3)
O9	-H9B	0.84(3)
O10	-H10	0.8400
O10	-H10A	0.91(3)
O11	-H11A	0.89(3)
O11	-H11B	0.86(3)
O12	-H12B	0.95(3)
O12	-H12A	0.82(4)
N1	-H1	0.91(3)
N1	-C2	1.381(3)

N1	-C6	1.390(3)
N3	-C2	1.352(4)
N3	-C4	1.342(4)
N7	-H2	0.81(3)
N7	-C5	1.397(4)
N7	-C8	1.349(4)
N9	-H3	0.80(4)
N9	-C4	1.376(4)
N9	-C8	1.387(3)
N10	-H6	0.90(3)
N10	-C11	1.380(3)
N10	-C15	1.389(3)
N12	-C11	1.344(4)
N16	-H4	0.88(3)
N16	-C14	1.403(3)
N16	-C17	1.352(4)
N18	-H5	0.80(3)
N18	-C17	1.385(3)
C4	-C5	1.380(4)
C5	-C6	1.399(4)
C13	-N12	1.347(3)
C13	-N18	1.375(4)
C13	-C14	1.380(4)
C14	-C15	1.394(4)

Table A.6. Bond angles [°] for **$CaU_2 \cdot 6H_2O$**.

Ca1	-O7	-H7A	120(2)
Ca1	-O7	-H7B	139(3)
Ca1	-O8	-H8A	127(2)
Ca1	-O8	-H8B	117(2)
Ca1	-O9	-H9A	117(2)
Ca1	-O9	-H9B	110(2)
Ca1	-O10	-H10	109.5
Ca1	-O10	-H10A	125(2)
Ca1	-O11	-H11A	130(2)
Ca1	-O11	-H11B	124(2)
Ca1	-O12	-H12A	112(2)
Ca1	-O12	-H12B	107(2)
O1	-C6	-N1	119.6(3)
O1	-C6	-C5	127.6(3)
O2	-C2	-N1	119.9(3)
O2	-C2	-N3	119.4(3)
O3	-C8	-N7	127.3(2)
O3	-C8	-N9	125.8(3)
O4	-C11	-N12	122.5(3)
O4	-C11	-N10	116.4(2)
O5	-C15	-N10	120.2(3)
O5	-C15	-C14	129.1(3)
O6	-C17	-N16	127.0(3)
O6	-C17	-N18	126.2(3)
O7	-Ca1	-O9	119.50(8)
O7	-Ca1	-O10	72.78(8)
O7	-Ca1	-O11	75.68(8)
O7	-Ca1	-O12	82.26(8)
O8	-Ca1	-O7	79.55(8)

O8	-Ca1	-O9	69.59(8)
O8	-Ca1	-O10	112.42(8)
O8	-Ca1	-O11	148.90(8)
O8	-Ca1	-O12	83.64(8)
O10	-Ca1	-O9	73.14(7)
O10	-Ca1	-O12	146.57(8)
O11	-Ca1	-O9	139.94(7)
O11	-Ca1	-O10	77.75(8)
O11	-Ca1	-O12	74.72(8)
O12	-Ca1	-O9	139.91(7)
C2	-N1	-H1	118.7(19)
C2	-N1	-C6	125.5(3)
C4	-C5	-C6	119.5(3)
C4	-C5	-N7	107.3(3)
C4	-N3	-C2	114.7(2)
C4	-N9	-H3	123(3)
C4	-N9	-C8	109.4(2)
C5	-N7	-H2	130(2)
C6	-N1	-H1	115.8(19)
C8	-N7	-H2	120(2)
C8	-N7	-C5	109.4(2)
C8	-N9	-H3	127(3)
C11	-N10	-H6	118(2)
C11	-N10	-C15	126.9(3)
C11	-N12	-C13	113.2(2)
C13	-C14	-C15	120.5(3)
C13	-C14	-N16	107.5(3)
C13	-N18	-H5	124(2)
C13	-N18	-C17	109.9(2)
C14	-N16	-H4	124(2)
C15	-C14	-N16	132.0(3)

C15	-N10	-H6	115(2)
C17	-N16	-H4	126(2)
C17	-N16	-C14	109.1(2)
C17	-N18	-H5	126(2)
N1	-C6	-C5	112.8(3)
N3	-C2	-N1	120.7(2)
N3	-C4	-N9	126.1(3)
N3	-C4	-C5	126.9(3)
N7	-C5	-C6	133.2(3)
N7	-C8	-N9	106.9(2)
N9	-C4	-C5	107.1(2)
N10	-C15	-C14	110.7(3)
N12	-C11	-N10	121.1(2
N12	-C13	-N18	125.8(3)
N12	-C13	-C14	127.4(3)
N16	-C17	-N18	106.8(2
N18	-C13	-C14	106.8(2)
H7A	-O7	-H7B	101(3)
H8A	-O8	-H8B	96(3)
H9A	-O9	-H9B	109(3)
H10	-O10	-H10A	110.8
H11B	-O11	-H11A	102(3)
H12B	-O12	-H12A	107(3)

Table A.7. Torsion angles [°] for **$CaU_2 \cdot 6H_2O$**.

Ca1	-N3	-C2	-N1	-174.3(2)
Ca1	-N3	-C2	-O2	5.0(3)
Ca1	-N3	-C4	-C5	168.9(3)
Ca1	-N3	-C4	-N9	-11.9(6)
Ca1	-O2	-C2	-N1	174.4(2)
Ca1	-O2	-C2	-N3	-5.0(3)
O2	-Ca1	-C2	-N1	-91(2)
O2	-Ca1	-N3	-C2	-2.71(15)
O2	-Ca1	-N3	-C4	-172.5(4)
O2	-Ca1	-C2	-N3	175.0(3)
O7	-Ca1	-C2	-N1	160(2)
O7	-Ca1	-C2	-N3	66.7(4)
O7	-Ca1	-C2	-O2	-108.2(4)
O7	-Ca1	-O2	-C2	148.9(2)
O7	-Ca1	-N3	-C2	-158.52(18)
O7	-Ca1	-N3	-C4	31.7(5)
O8	-Ca1	-C2	-N1	-60(2)
O8	-Ca1	-C2	-O2	31.82(19)
O8	-Ca1	-C2	-N3	-153.20(16)
O8	-Ca1	-N3	-C2	36.3(2)
O8	-Ca1	-N3	-C4	-133.5(4)
O8	-Ca1	-O2	-C2	-150.45(18)
O9	-Ca1	-O2	-C2	-81.18(17)
O9	-Ca1	-N3	-C2	78.65(17)
O9	-Ca1	-N3	-C4	-91.1(4)
O9	-Ca1	-C2	-N1	0(2)
O9	-Ca1	-C2	-N3	-93.68(17)
O9	-Ca1	-C2	-O2	91.33(17)
O10	-Ca1	-O1	-C2	-31.1(2)

O10	-Ca1	-C2	-N1	65(2)
O10	-Ca1	-C2	-N3	-29.01(18)
O10	-Ca1	-C2	-O2	156.00(16)
O10	-Ca1	-N3	-C2	152.58(17)
O10	-Ca1	-N3	-C4	-17.2(4)
O11	-Ca1	-O2	-C2	57.17(18)
O11	-Ca1	-C2	-O2	-126.33(17)
O11	-Ca1	-N3	-C2	-128.62(18)
O11	-Ca1	-N3	-C4	61.6(4)
O11	-Ca1	-C2	-N1	142(2)
O11	-Ca1	-C2	-N3	48.66(17)
O12	-Ca1	-C2	-O2	-51.59(17)
O12	-Ca1	-C2	-N3	123.39(17)
O12	-Ca1	-N3	-C2	-59.95(18)
O12	-Ca1	-N3	-C4	130.3(4)
O12	-Ca1	-C2	-N1	-143(2)
O12	-Ca1	-O2	-C2	125.74(18)
C2	-Ca1	-N3	-C4	-169.8(5)
C2	-N1	-C6	-O1	178.5(3)
C2	-N1	-C6	-C5	-1.8(4)
C2	-N3	-C4	-C5	0.1(4)
C2	-N3	-C4	-N9	179.3(3)
C4	-N9	-C8	-O3	179.5(3)
C4	-N9	-C8	-N7	-0.4(3)
C4	-C5	-C6	-N1	2.1(4)
C4	-C5	-C6	-O1	-178.2(3)
C4	-N3	-C2	-O2	179.7(3)
C4	-N3	-C2	-N1	0.4(4)
C4	-N3	-C2	-Ca1	174.7(3)
C5	-N7	-C8	-O3	-179.5(3)
C5	-N7	-C8	-N9	0.4(3)

C6	-N1	-C2	-O2	-178.8(3)
C6	-N1	-C2	-N3	0.5(5)
C6	-N1	-C2	-Ca1	-90(2)
C8	-N7	-C5	-C4	-0.2(3)
C8	-N7	-C5	-C6	-179.3(3)
C8	-N9	-C4	-N3	-179.0(3)
C8	-N9	-C4	-C5	0.3(3)
C11	-N10	-C15	-O5	178.0(3)
C11	-N10	-C15	-C14	-2.6(4)
C13	-C14	-C15	-N10	0.0(4)
C13	-C14	-C15	-O5	179.3(3)
C13	-N12	-C11	-O4	178.1(3)
C13	-N12	-C11	-N10	-2.2(4)
C13	-N18	-C17	-O6	179.8(3)
C13	-N18	-C17	-N16	0.0(3)
C14	-C13	- N12	-C11	-0.3(4)
C14	-C13	-N18	-C17	-0.5(3)
C14	-N16	-C17	-O6	-179.3(3)
C14	-N16	-C17	-N18	0.5(3)
C15	-N10	-C11	-O4	-176.4(3)
C15	-N10	-C11	-N12	3.9(5)
C17	-N16	-C14	-C13	-0.8(3)
C17	-N16	-C14	-C15	179.8(3)
N3	-Ca1	-C2	-O2	-175.0(3)
N3	-Ca1	-C2	-N1	94(2)
N3	-Ca1	-O1	-C2	2.90(16)
N3	-C4	-C5	-C6	-1.5(5)
N3	-C4	-C5	-N7	179.3(3)
N7	-C5	-C6	-N1	-178.9(3)
N7	-C5	-C6	-O1	0.8(6)
N9	-C4	-C5	-C6	179.2(3)

N9	-C4	-C5	-N7	-0.1(3)
N12	-C13	-C14	-C15	1.5(5)
N12	-C13	-C14	-N16	-178.0(3)
N12	-C13	-N18	-C17	178.3(3)
N16	-C14	-C15	-N10	179.3(3)
N16	-C14	-C15	-O5	-1.3(5)
N18	-C13	-C14	-C15	-179.8(3)
N18	-C13	-C14	-N16	0.8(3)
N18	-C13	-N12	-C11	-178.9(3)

APPPENDIX B COPYRIGHT PERMISSIONS

American Chemical Society's Policy on Theses and Dissertations

If your university requires a signed copy of this letter see contact information below.

Thank you for your request for permission to include **your** paper(s) or portions of text from **your** paper(s) in your thesis. Permission is now automatically granted; please pay special attention to the implications paragraph below. The Copyright Subcommittee of the Joint Board/Council Committees on Publications approved the following:

> Copyright permission for published and submitted material from theses and dissertations
> ACS extends blanket permission to students to include in their theses and dissertations their own articles, or portions thereof, that have been published in ACS journals or submitted to ACS journals for publication, provided that the ACS copyright credit line is noted on the appropriate page(s).
>
> Publishing implications of electronic publication of theses and dissertation material
> Students and their mentors should be aware that posting of theses and dissertation material on the Web prior to submission of material from that thesis or dissertation to an ACS journal may affect publication in that journal. Whether Web posting is considered prior publication may be evaluated on a case-by-case basis by the journal's editor. If an ACS journal editor considers Web posting to be "prior publication", the paper will not be accepted for publication in that journal. If you intend to submit your unpublished paper to ACS for publication, check with the appropriate editor prior to posting your manuscript electronically.

If your paper has **not** yet been published by ACS, we have no objection to your including the text or portions of the text in your thesis/dissertation in **print and microfilm formats**; please note, however, that electronic distribution or Web posting of the unpublished paper as part of your thesis in electronic formats might jeopardize publication of your paper by ACS. Please print the following credit line on the first page of your article: "Reproduced (or 'Reproduced in part') with permission from [JOURNAL NAME], in press (or 'submitted for publication'). Unpublished work copyright [CURRENT YEAR] American Chemical Society." Include appropriate information.

If your paper has already been published by ACS and you want to include the text or portions of the text in your thesis/dissertation in **print or microfilm formats**, please print the ACS copyright credit line on the first page of your article: "Reproduced (or 'Reproduced in part') with permission from [FULL REFERENCE CITATION.] Copyright [YEAR] American Chemical Society." Include appropriate information.

Submission to a Dissertation Distributor: If you plan to submit your thesis to UMI or to another dissertation distributor, you should not include the unpublished ACS paper in your thesis if the thesis will be disseminated electronically, until ACS has published your paper. After publication of the paper by ACS, you may release the entire thesis (**not the individual ACS article by itself**) for electronic dissemination through the distributor; ACS's copyright credit line should be printed on the first page of the ACS paper.

Use on an Intranet: The inclusion of your ACS unpublished or published manuscript is permitted in your thesis in print and microfilm formats. If ACS has published your paper you may include the manuscript in your thesis on an intranet that is not publicly available. Your ACS article cannot be posted electronically on a publicly available medium (i.e. one that is not password protected), such as but not limited to, electronic archives, Internet, library server, etc. The only material from your paper that can be posted on a public electronic medium is the article abstract, figures, and tables, and you may link to the article's DOI or post the article's author-directed URL link provided by ACS. This paragraph does not pertain to the dissertation distributor paragraph above.

Questions? Call +1 202/872-4368/4367. Send e-mail to copyright@acs.org or fax to +1 202-776-8112. 10/10/03, 01/15/04, 0